Reduction of Low-Thrust Continuous Controls for Trajectory Dynamics and Orbital Targeting

by

Jennifer S. Hudson

A dissertation submitted in partial fulfillment
of the requirements for the degree of
Doctor of Philosophy
(Aerospace Engineering)
in The University of Michigan
2010

Doctoral Committee:

Professor Daniel J. Scheeres, University of Colorado, Co-Chair
Professor N. Harris McClamroch, Co-Chair
Professor Dennis S. Bernstein
Professor Anthony M. Bloch

To my husband, Paul, my daughter, Sarah, and my baby-to-be.

ACKNOWLEDGEMENTS

I am indebted to many people and organizations for their support in completing this dissertation. First, I would like to thank my advisor, Professor Daniel Scheeres, for his invaluable guidance, expertise, and patience. I also thank my co-chair, Professor Harris McClamroch, the rest of my doctoral committee, and the other flight dynamics and control faculty in the Aerospace Engineering department.

I would like to thank the staff and students in the Aerospace Engineering department for their help and encouragement throughout my graduate school experience. I am particularly grateful to Denise Phelps, Amor Menezes, and Eric Gustafson for their assistance in completing this process.

This work was funded by fellowships from the National Science Foundation and the University of Michigan Department of Aerospace Engineering.

I would like to thank all those who made it possible to complete this Ph.D. during the years that I became a parent to two beautiful children. I sincerely thank my parents for their generosity and enthusiasm. Finally, I thank my husband, Paul, and my daughter, Sarah, for their continued support, patience, and sense of humor.

TABLE OF CONTENTS

LIST OF FIGURES

FIGURE

LIST OF TABLES

TABLE

ABSTRACT

A novel method to evaluate the trajectory dynamics of low-thrust spacecraft is developed. Using a two-body Newtonian model, the spacecraft thrust vector components are represented by Fourier series in terms of eccentric anomaly, and Gauss's variational equations are averaged over one orbit to obtain a set of secular equations. These secular equations are a function of 14 of the thrust Fourier coefficients, regardless of the order of the original Fourier series, and are sufficient to determine a low-thrust spiral trajectory with significantly reduced computational requirements as compared with integration of the full Newtonian problem.

This method is applied to orbital targeting problems. The targeting problems are defined as two-point boundary value problems with fixed endpoint constraints. Average low-thrust controls that solve these problems are found using the averaged variational equations and a cost function represented also as a Fourier series. The resulting fuel costs and dynamic fidelity of the targeting solutions are evaluated.

Low-thrust controls with equivalent average trajectory dynamics but different thrust profiles are also studied. Higher-order control coefficients that do not affect the average dynamics are used to reduce fuel costs and transform time-varying controls into controls with constant thrust arcs, which can be implemented more easily by low-thrust propulsion systems.

These methods have applications to low-thrust mission design and space situational awareness. Example problems based on past missions and potential future scenarios demonstrate the effectiveness of these methods.

CHAPTER 1

Introduction

Low-thrust propulsion systems offer an efficient option for many interplanetary and Earth orbit missions. Advances in electric propulsion have made low-thrust engines a growing trend in the spacecraft industry over the past few decades. The Deep Space 1, SMART-1, Hayabusa, and Dawn missions have demonstrated this technology, and it is slated for launch on the LISA Pathfinder and BepiColombo missions, among others. With high specific impulse and long engine lifetimes, low-thrust propulsion is well-suited for many applications, including orbit transfers and interplanetary missions.

Trajectory design and control of low-thrust spacecraft, however, remain difficult problems. The general continuous-thrust problem requires integration of the Newtonian equations of motion for the trajectory, which may comprise hundreds of orbits and is highly sensitive to small changes in the thrust profile. Analytical solutions exist for several special cases of low-thrust orbit transfer problems, such as Forbes's spiral[1], the logarithmic spiral [1, 2, 3], the exponential sinusoid [4], constant radial or circumferential thrust [5, 6, 7], Markopoulos's Keplerian thrust arcs [8], Lawden's spiral [9], and Bishop and Azimov's spiral [10]. The calculus of variations [11] and direct optimization methods [12] have also been used to determine optimal low-thrust control laws within certain constraints. Several methods for open-loop, minimum-time transfers [13, 14, 15] and optimal transfers using Lyapunov feedback control [16, 17] also exist. Averaging methods, in combination with other approaches, have proven

effective in overcoming sensitivities to small variations in initial orbit and thrust profile [18, 19, 20, 21]. Yet all of these solutions remain limited to certain regions of the thrust and orbital parameter space.

The focus of this dissertation is a novel method to evaluate the effect of low-thrust propulsion on spacecraft orbit dynamics with minimal constraints. Using a two-body Newtonian model, we represent each component of the thrust acceleration as a Fourier series in eccentric anomaly, and then average Gauss's variational equations over one orbit to define a set of secular equations. The equations are a function of only 14 of the thrust Fourier coefficients, regardless of the order of the original Fourier series. Thus the continuous control is reduced to a set of 14 parameters.

With the addition of a small correction term to eliminate offsets of the averaged trajectory due to initial conditions, the averaged secular equations are sufficient to determine a low-thrust trajectory. This is verified by comparison of the averaged trajectory dynamics with the fully integrated Newtonian equations of motion for several example acceleration functions.

This method has applications to orbital targeting problems. Two-point boundary value problems are solved using an iterative method that converges to the minimum-norm set of the 14 force Fourier coefficients. Problems involving sequences of target states are also solved by either finding the optimal set of control coefficients between each pair of states or by fitting a single set of control coefficients to the entire orbit transfer using a least-squares approach. The resulting fuel costs and dynamic fidelity of the targeting solutions are evaluated. These methods require significantly reduced computing resources compared to integration of the full Newtonian equations of motion.

We also make use of the acceleration Fourier coefficients that do not appear in the averaged secular equations. These coefficients are of higher order than the 14 key coefficients, and they do not affect the fundamental trajectory dynamics. Thus, they

can be used to modify a calculated control to meet implementation requirements or further reduce fuel costs without altering the trajectory. To demonstrate this concept, several methods are developed to transform a time-varying control into a step control.

Most current low-thrust spacecraft engines are able to operate over a range of thrust levels, but operators of these systems often prefer to minimize switching between throttle points. Therefore a control law based on constant thrust arcs is desirable. We present several methods for selecting higher-order Fourier coefficients to create a constant-thrust control law with average trajectory dynamics equivalent to those of a variable-thrust control. Extensions of these methods to fuel cost reduction are also discussed.

Trajectory analysis using the reduced Fourier coefficients has several potential fields of application, including mission design and space situational awareness (SSA). Mission designers could use the averaged secular equations to efficiently estimate control laws for a large number of potential orbital paths, to compare fuel costs and other trajectory characteristics, and to estimate the feasibility and cost of proposed deviations from a selected path. In SSA applications, observers could reconstruct the orbital path of a suspected low-thrust spacecraft from a few discrete observations to identify the fundamental characteristics of the control law used, estimate fuel consumption, and predict the future trajectory. The different methods developed for solving orbital targeting problems and calculating equivalent control laws have different strengths and weaknesses that make them appropriate, respectively, for these different applications.

The method has certain limits of applicability. The averaged secular equations are developed only for the restricted two-body model; other gravitational perturbations or spacecraft mass effects must be considered separately. The thrust acceleration must be able to be represented by a Fourier series, as is true for almost any physical system. The resulting controls are periodic in eccentric anomaly, unless the control

Fourier coefficients are changed from orbit to orbit. Trajectories that include circular orbits present analytical challenges that are also discussed.

1.1 Contributions

The primary contributions of this research are:

- Development of a method to evaluate the average trajectory dynamics of low-thrust spacecraft with minimal constraints on the thrust and orbital parameter space.
- Development of efficient methods to find average solutions to low-thrust orbital targeting problems and evaluate the resulting fuel costs.
- Development of methods to transform time-varying trajectory controls into controls with lower fuel costs or constant thrust arcs for better implementation by existing low-thrust propulsion systems.

1.2 Relevant Publications

The following publications are related to the subject matter of this dissertation.

- J. Hudson, D. Scheeres, "Reduction of Low-Thrust Continuous Controls for Trajectory Dynamics," Journal of Guidance, Control, and Dynamics, Vol. 32, No. 3, pp. 780-787, 2009.
- J. Hudson, D. Scheeres, "Orbital Targeting and Trajectory Optimization using the Reduced Eccentric Anomaly Low-Thrust Coefficients," submitted to Journal of Guidance, Control, and Dynamics.
- J. Hudson, D. Scheeres, "Equivalent Average Trajectory Dynamics using the Reduced Low-Thrust Coefficients," AIAA/AAS Astrodynamics Specialist Conference, Toronto, ON, August 2010, AIAA-2010-7829.

- J. Hudson, D. Scheeres, "Determination of Fundamental Low-Thrust Control Frequencies for Fitting Sequences of Orbital States," AIAA/AAS Space Flight Mechanics Meeting, San Diego, CA, February 2010, AAS 10-213.

- J. Hudson, D. Scheeres, "Trajectory Optimization Using the Reduced Eccentric Anomaly Low-Thrust Coefficients," AIAA/AAS Astrodynamics Specialist Conference, Honolulu, HI, August 2008, AIAA-2008-6617.

- J. Hudson, D. Scheeres, "Reduction of Low Thrust Continuous Controls for Trajectory Dynamics," AIAA/AAS Astrodynamics Specialist Conference, Mackinac Island, MI, August 2007, AAS 07-345.

CHAPTER 2

Averaged Variational Equations

2.1 Variational Equations

We consider a spacecraft of negligible mass in orbit about a central body, which is assumed to be a point mass. The spacecraft is subject to a continuous thrust acceleration of potentially varying magnitude and direction. The spacecraft trajectory can be described by the Newtonian equations of motion

$$\dot{\vec{r}} = \vec{v}, \tag{2.1}$$

$$\dot{\vec{v}} = -\frac{\mu}{r^3}\vec{r} + \vec{F}, \tag{2.2}$$

where $\vec{r}$ is the position vector, $\vec{v}$ is the velocity vector, and μ is the standard gravitational parameter of the central body. The thrust acceleration vector $\vec{F}$ can be resolved along the radial, normal, and circumferential directions,

$$\vec{F} = F_R\hat{r} + F_W\hat{w} + F_S\left(\hat{w}\times\hat{r}\right), \tag{2.3}$$

where $\hat{r} = \frac{\vec{r}}{|\vec{r}|}$ and $\hat{w} = \frac{\vec{r}\times\vec{v}}{|\vec{r}\times\vec{v}|}$.

The Newtonian equations can be decomposed into the Lagrange Planetary Equations, which describe the time rate of change of the classical orbit elements of a body subject to the perturbations F_R, F_W, and F_S. The Gauss form of the Lagrange

Planetary Equations [22] is

$$\frac{da}{dt} = 2\sqrt{\frac{a}{\mu}}\left[F_R \frac{ae}{\sqrt{1-e^2}}\sin\nu + F_S \frac{a^2\sqrt{1-e^2}}{a\left(1-e\cos E\right)}\right], \tag{2.4}$$

$$\frac{de}{dt} = \sqrt{\frac{a}{\mu}}\sqrt{1-e^2}\left[F_R \sin\nu + F_S\left(\cos\nu + \cos E\right)\right], \tag{2.5}$$

$$\frac{di}{dt} = \sqrt{\frac{a}{\mu}}\frac{\left(1-e\cos E\right)}{\sqrt{1-e^2}} F_W \cos\left(\nu+\omega\right), \tag{2.6}$$

$$\frac{d\Omega}{dt} = \sqrt{\frac{a}{\mu}}\frac{\left(1-e\cos E\right)}{\sqrt{1-e^2}} F_W \sin\left(\nu+\omega\right)\csc i, \tag{2.7}$$

$$\frac{d\omega}{dt} = \sqrt{\frac{a}{\mu}}\frac{\sqrt{1-e^2}}{e}\left[-F_R\cos\nu + F_S\left(1+\frac{1-e\cos E}{1-e^2}\right)\sin\nu\right] - \cos i\frac{d\Omega}{dt}, \tag{2.8}$$

$$\begin{aligned}\frac{d\epsilon_1}{dt} &= -2\sqrt{\frac{a}{\mu}}\left(1-e\cos E\right)F_R + \left(1-\sqrt{1-e^2}\right)\left(\frac{d\omega}{dt}+\frac{d\Omega}{dt}\right) \\ &\quad +2\sqrt{1-e^2}\sin^2\left(\frac{i}{2}\right)\frac{d\Omega}{dt}.\end{aligned} \tag{2.9}$$

In these equations, a is the semi-major axis, e is the eccentricity, i is the inclination, Ω is the longitude of the ascending node, ω is the argument of periapsis, ν is the true anomaly, and E is the eccentric anomaly. The element ϵ_1 is used to determine the mean anomaly, M,

$$M = \int n\, dt + \epsilon_1 - \left(\Omega+\omega\right), \tag{2.10}$$

where n is the mean motion.

In the modeling and simulation of low-thrust spacecraft orbits, both the Newtonian equations and the Gauss equations provide identical results. The Gauss equations are often preferred for clear visualization of the orbit over time.

2.2 Fourier Series Expansion of Control

Given an arbitrary thrust acceleration vector $\vec{F}$, each of its components can be represented as a Fourier series over an arbitrary, finite time interval. The properties

of Fourier series are described in Appendix A. This representation is reasonable for almost any low-thrust spacecraft control, as the Fourier series of a function converges to the periodic extension of the function itself for nearly all physical systems.

The Fourier series of the acceleration vector components can be expanded in time or in a time-varying orbital parameter, such as true anomaly, eccentric anomaly, or mean anomaly. Letting θ represent this arbitrary parameter, the acceleration component Fourier series on the interval $(0, L)$ are

$$F_R \sim \sum_{k=0}^{\infty} \left[\alpha_k^{R,\theta} \cos\left(\frac{2\pi k\theta}{L}\right) + \beta_k^{R,\theta} \sin\left(\frac{2\pi k\theta}{L}\right) \right], \tag{2.11}$$

$$F_W \sim \sum_{k=0}^{\infty} \left[\alpha_k^{W,\theta} \cos\left(\frac{2\pi k\theta}{L}\right) + \beta_k^{W,\theta} \sin\left(\frac{2\pi k\theta}{L}\right) \right], \tag{2.12}$$

$$F_S \sim \sum_{k=0}^{\infty} \left[\alpha_k^{S,\theta} \cos\left(\frac{2\pi k\theta}{L}\right) + \beta_k^{S,\theta} \sin\left(\frac{2\pi k\theta}{L}\right) \right]. \tag{2.13}$$

The acceleration function $\vec{F}$ is thus defined by the coefficients $\alpha_k^{(R,W,S),\theta}$ and $\beta_k^{(R,W,S),\theta}$.

2.3 Averaged Variational Equations

We begin the first-order averaging analysis by assuming a thrust acceleration vector that is specified over one orbit period ($L = 2\pi$) with a sufficiently low magnitude that the size and shape of the orbit do not change significantly over one orbit. Therefore, we can average the Gauss equations over one orbit period with respect to mean anomaly to find equations for the mean orbit elements,

$$\overline{\dot{o}} = \frac{1}{2\pi} \int_0^{2\pi} \dot{o}\, dM, \tag{2.14}$$

where o represents any orbit element. The 2π periodic acceleration slightly simplifies the Fourier series and coefficient definitions,

$$F_R \sim \sum_{k=0}^{\infty} \left[\alpha_k^{R,\theta} \cos k\theta + \beta_k^{R,\theta} \sin k\theta \right], \tag{2.15}$$

$$F_W \sim \sum_{k=0}^{\infty} \left[\alpha_k^{W,\theta} \cos k\theta + \beta_k^{W,\theta} \sin k\theta \right], \tag{2.16}$$

$$F_S \sim \sum_{k=0}^{\infty} \left[\alpha_k^{S,\theta} \cos k\theta + \beta_k^{S,\theta} \sin k\theta \right], \tag{2.17}$$

where

$$\alpha_0^{(R,W,S),\theta} = \frac{1}{2\pi} \int_0^{2\pi} F(\theta)\, d\theta, \tag{2.18}$$

$$\alpha_k^{(R,W,S),\theta} = \frac{1}{\pi} \int_0^{2\pi} F(\theta) \cos(k\theta)\, d\theta, \tag{2.19}$$

$$\beta_k^{(R,W,S),\theta} = \frac{1}{\pi} \int_0^{2\pi} F(\theta) \sin(k\theta)\, d\theta. \tag{2.20}$$

At this point, the choice of orbital parameter for the thrust acceleration vector components' Fourier series expansion becomes significant. If the acceleration components are expanded as Fourier series in true anomaly and the independent parameter for the averaging is likewise transformed to true anomaly, the resulting secular equa-

tions become quite lengthy. For example, the equation for semi-major axis becomes

$$\begin{aligned}
\bar{\dot{a}} &= \frac{1}{2\pi}\int_0^{2\pi} \dot{a}dM \\
&= \frac{1}{2\pi}\left(1-e^2\right)^{\frac{3}{2}}\int_0^{2\pi}\frac{\dot{a}}{\left(1+e\cos\nu\right)^2}d\nu \\
&= \frac{1}{\pi}\sqrt{\frac{a}{\mu}}\left(1-e^2\right)\int_0^{2\pi}\left[F_R\frac{ae\sin\nu}{\left(1+e\cos\nu\right)^2}+F_S\frac{a}{1+e\cos\nu}\right]d\nu \\
&= \frac{1}{\pi}\sqrt{\frac{a}{\mu}}\left(1-e^2\right)\int_0^{2\pi}\Bigg[\left(\sum_{k=0}^{\infty}\alpha_k^{R,\nu}\cos k\nu+\beta_k^{R,\nu}\sin k\nu\right)\frac{ae\sin\nu}{\left(1+e\cos\nu\right)^2} \\
&\quad +\left(\sum_{k=0}^{\infty}\alpha_k^{S,\nu}\cos k\nu+\beta_k^{S,\nu}\sin k\nu\right)\frac{a}{1+e\cos\nu}\Bigg]d\nu. \qquad (2.21)
\end{aligned}$$

Note that the denominator $\left(1+e\cos\nu\right)^k$ can be expanded as the cosine series

$$\frac{1}{\left(1+e\cos\nu\right)^k}=\sum_{i=0}^{\infty}b_i^k\left(e\right)\cos i\nu. \qquad (2.22)$$

Thus in the true anomaly expansion, each averaged equation contains integrals of products of sine and cosine series. Resolved into secular equations, each equation contains the full Fourier series for each acceleration direction. Even more complicated results are found if the expansion and averaging are carried out in mean anomaly.

However, if the acceleration vector components are expanded as Fourier series in eccentric anomaly and the averaging is carried out with eccentric anomaly as the independent parameter, the problematic denominators are eliminated, as $dM = \left(1-e\cos E\right)dE$. The averaged Gauss equation for any orbital element is thus given by

$$\bar{\dot{o}}=\frac{1}{2\pi}\int_0^{2\pi}\left(1-e\cos E\right)\dot{o}\,dE. \qquad (2.23)$$

Applying this, the averaged Gauss equations with respect to eccentric anomaly can

be stated as

$$\overline{\dot{a}} = \frac{1}{\pi}\sqrt{\frac{a^3}{\mu}}\int_0^{2\pi}\left[F_R e\sin E + F_S\sqrt{1-e^2}\right]dE, \tag{2.24}$$

$$\begin{aligned}\overline{\dot{e}} = {} & \frac{1}{2\pi}\sqrt{\frac{a}{\mu}}\sqrt{1-e^2}\int_0^{2\pi}\Bigg[F_R\sqrt{1-e^2}\sin E \\ & +F_S\left(2\cos E - \frac{3}{2}e - \frac{1}{2}e\cos 2E\right)\Bigg]dE,\end{aligned} \tag{2.25}$$

$$\begin{aligned}\overline{\dot{i}} = {} & \frac{1}{2\pi}\sqrt{\frac{a}{\mu}}\frac{1}{\sqrt{1-e^2}}\int_0^{2\pi}F_W\Bigg[\left(1+e^2\right)\cos\omega\cos E - \frac{3}{2}e\cos\omega - \sqrt{1-e^2}\sin\omega\sin E \\ & -\frac{1}{2}e\cos\omega\cos 2E + \frac{1}{2}e\sqrt{1-e^2}\sin\omega\sin 2E\Bigg]dE,\end{aligned} \tag{2.26}$$

$$\begin{aligned}\overline{\dot{\Omega}} = {} & \frac{1}{2\pi}\sqrt{\frac{a}{\mu}}\frac{\csc i}{\sqrt{1-e^2}}\int_0^{2\pi}F_W\Bigg[\sqrt{1-e^2}\cos\omega\sin E + \left(1+e^2\right)\sin\omega\cos E - \frac{3}{2}e\sin\omega \\ & -\frac{1}{2}e\sqrt{1-e^2}\cos\omega\sin 2E - \frac{1}{2}e\sin\omega\cos 2E\Bigg]dE,\end{aligned} \tag{2.27}$$

$$\begin{aligned}\overline{\dot{\omega}} = {} & \frac{1}{2\pi}\sqrt{\frac{a}{\mu}}\frac{1}{e}\int_0^{2\pi}\Bigg[-F_R\left(\sqrt{1-e^2}\cos E - e\sqrt{1-e^2}\right) \\ & +F_S\left(\left(2-e^2\right)\sin E - \frac{1}{2}e\sin 2E\right)\Bigg]dE - \cos i\overline{\dot{\Omega}},\end{aligned} \tag{2.28}$$

$$\begin{aligned}\overline{\dot{\epsilon_1}} = {} & -\frac{1}{\pi}\sqrt{\frac{a}{\mu}}\int_0^{2\pi}\left(1-e\cos E\right)^2 F_R + \left(1-\sqrt{1-e^2}\right)\left(\overline{\dot{\omega}}+\overline{\dot{\Omega}}\right) \\ & +2\sqrt{1-e^2}\sin^2\left(\frac{i}{2}\right)\overline{\Omega}.\end{aligned} \tag{2.29}$$

Henceforth we do not write the superscript $\theta = E$ for the Fourier coefficients, as all thrust acceleration Fourier series are expanded in eccentric anomaly.

Substituting the Fourier series for the thrust vector components, Equations 2.15

- 2.17, into the averaged Gauss equations leads to the orthogonality conditions,

$$\int_0^L \cos nx \cos mx dx = \begin{cases} 0, & n \neq m, \\ \frac{L}{2}, & n = m \neq 0, \\ L, & n = m = 0, \end{cases} \tag{2.30}$$

$$\int_0^L \sin nx \sin mx dx = \begin{cases} 0, & n \neq m,\ n = 0,\ or\ m = 0, \\ \frac{L}{2}, & n = m \neq 0. \end{cases} \tag{2.31}$$

This orthogonality eliminates all but the 0th, 1st, and/or 2nd order coefficients of each thrust acceleration Fourier series. Therefore, the averaged secular Gauss equations are

$$\overline{\dot{a}} = 2\sqrt{\frac{a^3}{\mu}}\left[\frac{1}{2}e\,\beta_1^R + \sqrt{1-e^2}\,\alpha_0^S\right], \tag{2.32}$$

$$\overline{\dot{e}} = \sqrt{\frac{a}{\mu}}\sqrt{1-e^2}\left[\frac{1}{2}\sqrt{1-e^2}\,\beta_1^R + \alpha_1^S - \frac{3}{2}e\,\alpha_0^S - \frac{1}{4}e\,\alpha_2^S\right], \tag{2.33}$$

$$\begin{aligned}\overline{\dot{i}} = {} & \sqrt{\frac{a}{\mu}}\frac{1}{\sqrt{1-e^2}}\left[\frac{1}{2}\left(1+e^2\right)\cos\omega\,\alpha_1^W - \frac{3}{2}e\cos\omega\,\alpha_0^W - \frac{1}{2}\sqrt{1-e^2}\sin\omega\,\beta_1^W\right. \\ & \left. -\frac{1}{4}e\cos\omega\,\alpha_2^W + \frac{1}{4}e\sqrt{1-e^2}\sin\omega\,\beta_2^W\right],\end{aligned} \tag{2.34}$$

$$\begin{aligned}\overline{\dot{\Omega}} = {} & \sqrt{\frac{a}{\mu}}\frac{\csc i}{\sqrt{1-e^2}}\left[\frac{1}{2}\sqrt{1-e^2}\cos\omega\,\beta_1^W + \frac{1}{2}\left(1+e^2\right)\sin\omega\,\alpha_1^W - \frac{3}{2}e\sin\omega\alpha_0^W\right. \\ & \left. -\frac{1}{4}e\sqrt{1-e^2}\cos\omega\,\beta_2^W - \frac{1}{4}e\sin\omega\,\alpha_2^W\right],\end{aligned} \tag{2.35}$$

$$\begin{aligned}\overline{\dot{\omega}} = {} & \sqrt{\frac{a}{\mu}}\frac{1}{e}\left[-\frac{1}{2}\sqrt{1-e^2}\,\alpha_1^R + e\sqrt{1-e^2}\,\alpha_0^R + \frac{1}{2}\left(2-e^2\right)\,\beta_1^S - \frac{1}{4}e\beta_2^S\right] \\ & -\cos i\,\overline{\dot{\Omega}},\end{aligned} \tag{2.36}$$

$$\begin{aligned}\overline{\dot{\epsilon_1}} = {} & \sqrt{\frac{a}{\mu}}\left[\left(-2-e^2\right)\alpha_0^R + 2e\alpha_1^R - \frac{1}{2}e^2\alpha_2^R\right] + \\ & \left(1-\sqrt{1-e^2}\right)\left(\overline{\dot{\omega}} + \overline{\dot{\Omega}}\right) + 2\sqrt{1-e^2}\sin^2\left(\frac{i}{2}\right)\overline{\dot{\Omega}}.\end{aligned} \tag{2.37}$$

The average rates of change of the orbital elements a, e, i, Ω, ω, and ϵ_1 are only dependent on the 14 Fourier coefficients α_0^R, α_1^R, α_2^R, β_1^R, α_0^S, α_1^S, α_2^S, β_1^S, β_2^S, α_0^W,

α_1^W, α_2^W, β_1^W, and β_2^W, regardless of the order of the original thrust acceleration Fourier series.

The assumption of a thrust acceleration vector specified over only one orbit period is not necessary; the same averaging method can be used with acceleration functions specified over other periods by substituting Equations 2.11 - 2.13 and A.2 - A.4 and averaging the Gauss equations over the full interval. An example of this is presented in Section 2.4. In general, when $L = m\pi$, the 0th, $\frac{m}{2}$-th, and m-th coefficients remain, with fractional indices required in the Fourier series when m is not an even integer. However, the averaging assumption may become less valid for aperiodic controls of long duration, for which the orbit changes significantly from start to finish.

2.4 Agreement with Newtonian Equations

To verify the averaged secular equations, we first consider a simple control: a step acceleration function in the circumferential direction only, with two burns and coast arcs as pictured in Figure 2.1. The Fourier series for this step function is determined

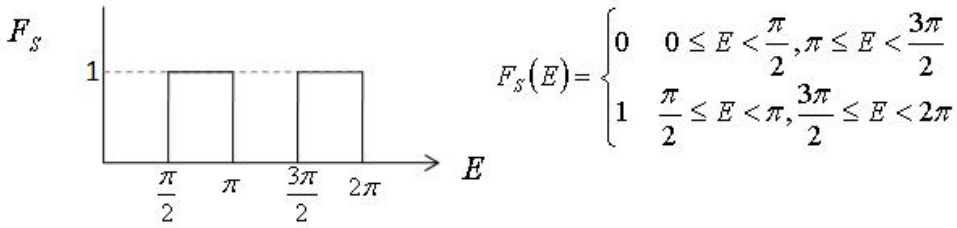

Figure 2.1: Step circumferential acceleration

by Equations 2.18 - 2.20

$$F_S = \sum_{k=0}^{\infty} \alpha_k^S \cos(kE) + \beta_k^S \sin(kE), \tag{2.38}$$

$$\alpha_0^S = \frac{1}{2\pi} \int_0^{2\pi} F_S dE = \frac{1}{2}, \tag{2.39}$$

$$\alpha_k^S = \frac{1}{\pi} \int_0^{2\pi} F_S \cos(kE)\, dE = 0, \tag{2.40}$$

$$\beta_k^S = \frac{1}{\pi} \int_0^{2\pi} F_S \sin(kE)\, dE = \begin{cases} -\frac{4}{k\pi}, & k = 2, 6, 10, ..., \\ 0, & otherwise. \end{cases} \tag{2.41}$$

Figure 2.2 compares this Fourier series, numerically evaluated up to order 100, to the series of only the five terms that appear in the averaged secular equations. There is considerable variation between these two representations of the periodic step acceleration control. In this section, all dimensions are normalized to a standard gravitational parameter $\mu = 1$, so figure units are not stated.

Figure 2.3 describes the osculating orbital elements of an example spacecraft subjected to these thrusts. Equations 2.32 - 2.37 with α_0^S, α_1^S, α_2^S, β_1^S, and β_2^S of the two-step acceleration profile above were integrated using a Runge-Kutta method to estimate the trajectory over 10 orbits. For comparison, the Newtonian equations (Equations 2.1 and 2.2) were also integrated using the Fourier series up to order 100. The two methods determined very similar orbital trajectories.

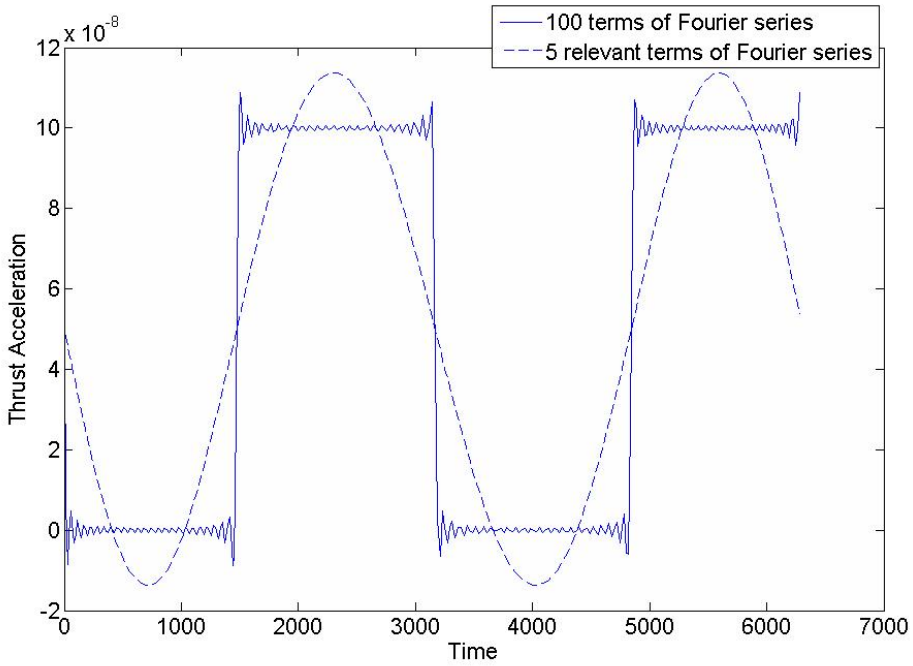

Figure 2.2: Fourier series approximations of step circumferential acceleration

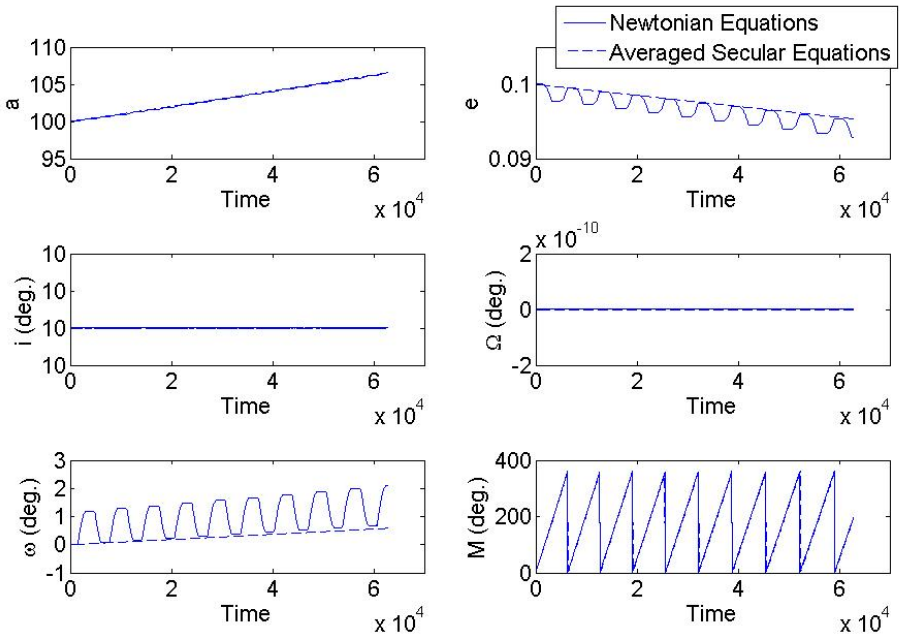

Figure 2.3: Orbital element trajectory due to step circumferential acceleration

Another case of interest is acceleration with constant magnitude but varying direction, as on a spacecraft with one gimbaled thruster. As an example of this case, we consider an acceleration that oscillates sinusiodally between the radial and circumferential directions, as shown in Figure 2.4. The Fourier series for the components of this acceleration vector are immediate: $\alpha_1^R = 1$, $\alpha_0^S = 1$, $\alpha_1^S = -1$, and all other coefficients are zero.

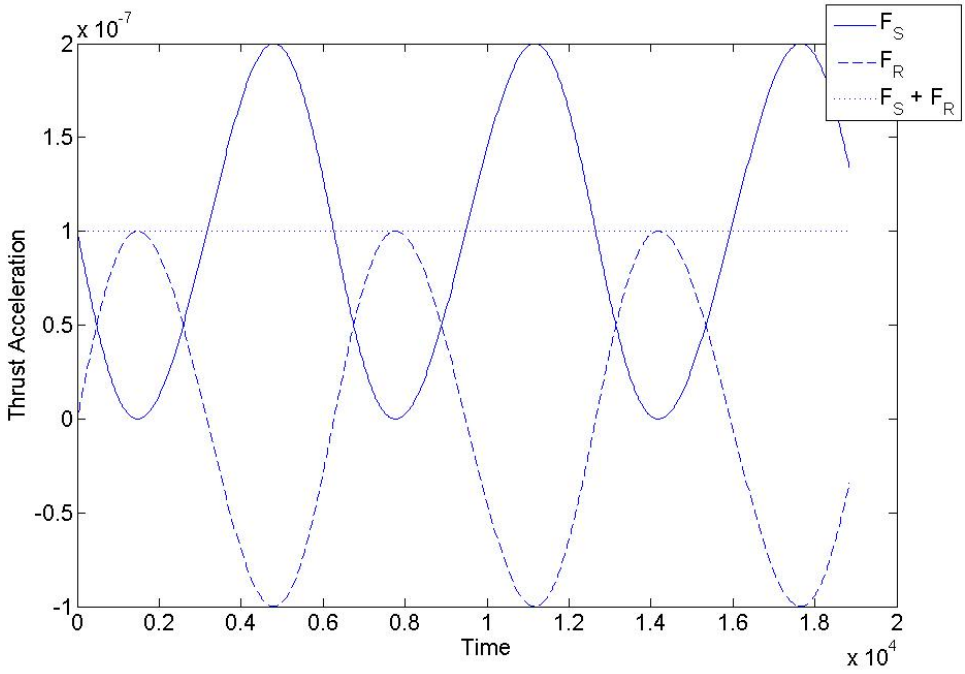

Figure 2.4: Constant-magnitude acceleration

Figure 2.5 shows the trajectory resulting from this acceleration, as determined by both the Newtonian equations and the averaged secular equations. Again, there is close agreement between the two methods.

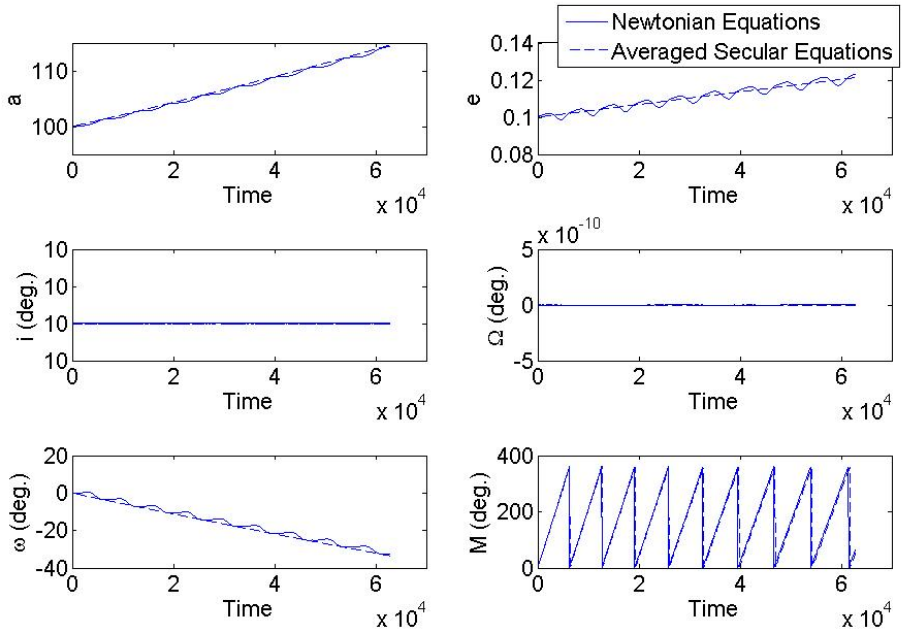

Figure 2.5: Orbital element trajectory due to constant-magnitude acceleration

Next, we consider a more complex control. Figures 2.6 - 2.8 describe the trajectory of a system whose thrust acceleration Fourier coefficients were randomly selected up to order 10 within the range (-2.5e-7, 2.5e-7). Figure 2.6 compares the time histories of the osculating orbital elements as determined by both methods. We note that there is close agreement between the Newtonian equations and the averaged secular equations for the first several orbits. In the later orbits there is some drift, most noticeable in mean anomaly and argument of periapsis, due to higher order effects not captured in the averaging process and to mismatch between the average initial conditions and the secular initial conditions. Correction of this drift is addressed in Section 2.5.

Figure 2.7 compares one component of this acceleration vector over three orbits with the first five terms of its Fourier series expansion, i.e. the terms which appear in the secular equations.

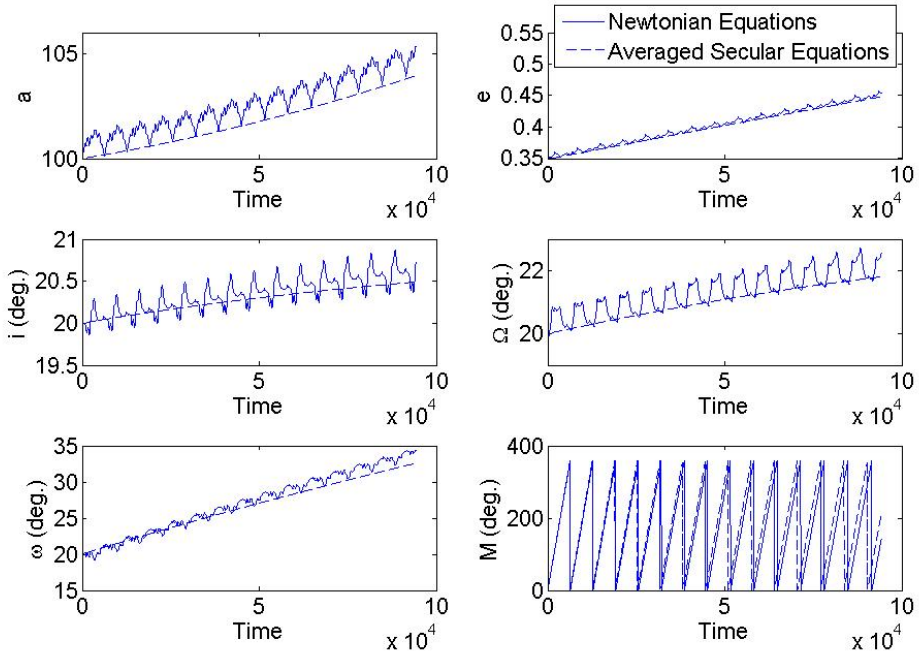

Figure 2.6: Orbital element trajectory due to randomly-generated acceleration

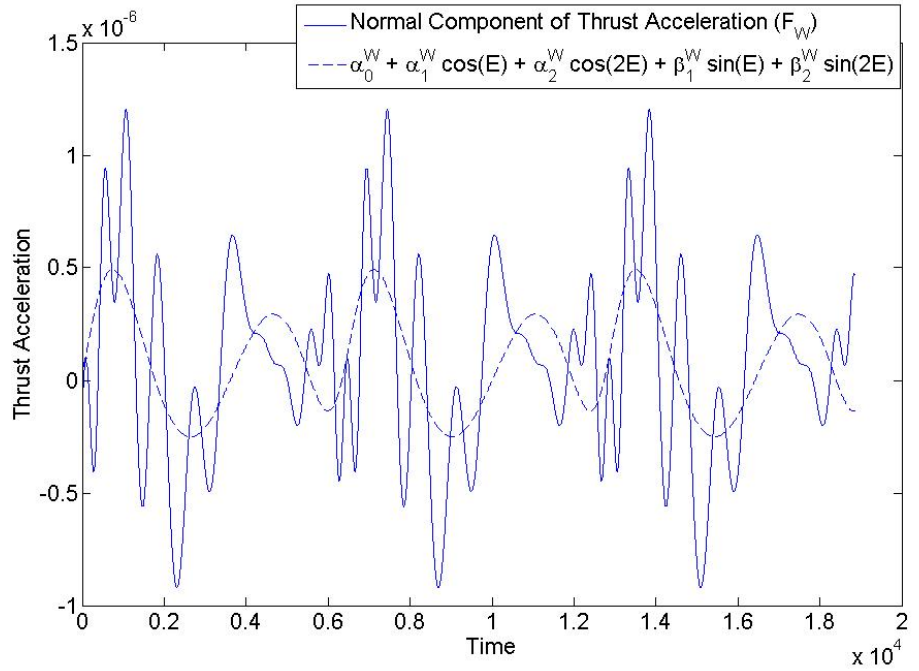

Figure 2.7: Normal component of randomly-generated acceleration

Figure 2.8 shows the eccentric anomaly over the 15-orbit timespan. Note that the eccentric anomaly shifts slightly as the nominal orbit evolves. This implies that the original control has a changing time variation as the orbit evolves, even though the coefficients may stay constant.

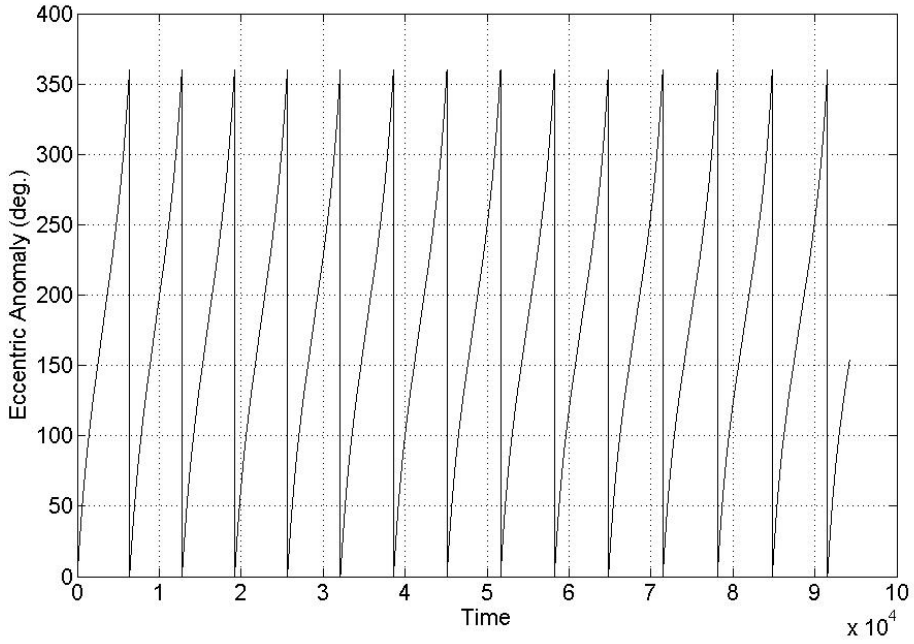

Figure 2.8: Eccentric anomaly of trajectory due to randomly-generated acceleration

Figures 2.9 and 2.10 show an example of the same method applied to a control with a period longer than 2π. In this example, the acceleration function is defined on the interval $(0,\ 6\pi)$, with randomly-selected Fourier coefficients up to order 10 in the range (-2.5e-8, 2.5e-8) and dimensions normalized to $\mu = 1$ as above. The 14 coefficients that remain in the averaged secular equations in this case are α_0^R, α_3^R, α_6^R, β_3^R, α_0^S, α_3^S, α_6^S, β_3^S, β_6^S, α_0^W, α_3^W, α_6^W, β_3^W, and β_6^W. Figure 2.9 shows the osculating orbital elements over 20 orbits. Figure 2.10 shows the normal component of the acceleration vector and the first five terms of its Fourier series over the first nine orbits, or the first three cycles of the periodic acceleration.

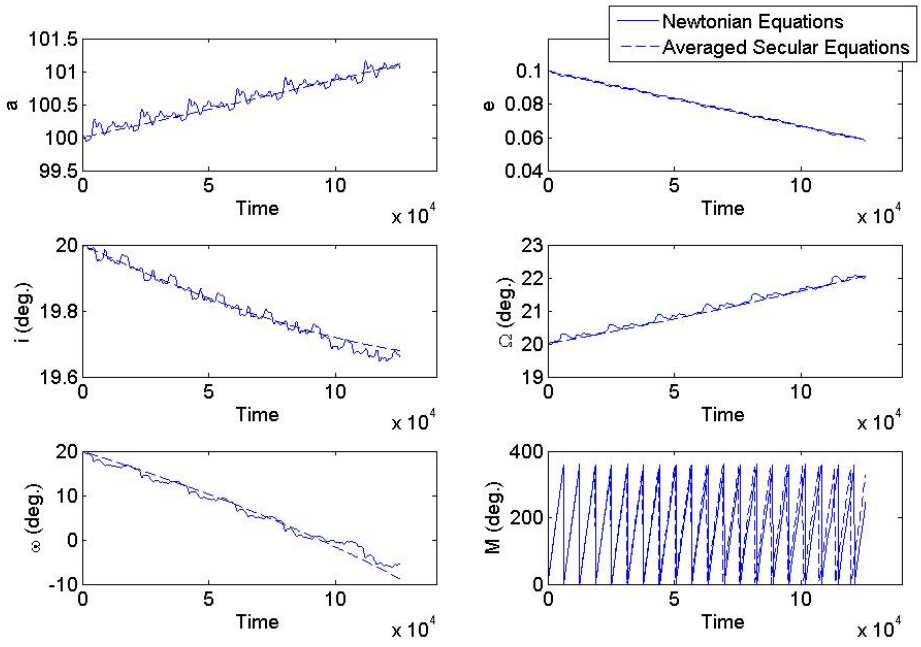

Figure 2.9: Orbital element trajectory due to randomly-generated acceleration with period 6π

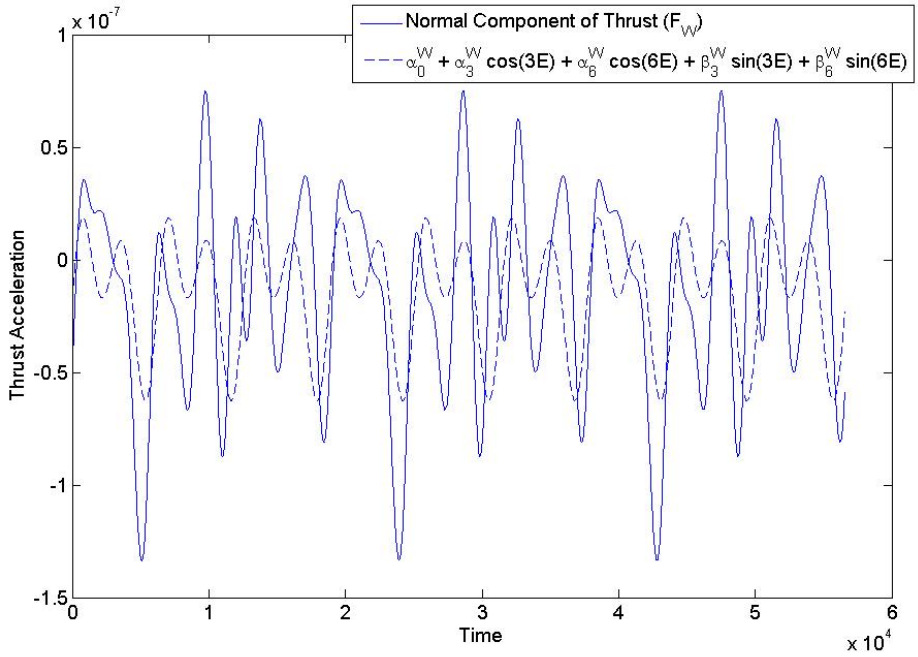

Figure 2.10: Normal component of randomly-generated 6π periodic acceleration vector over nine orbits

2.5 Offset Correction

Average trajectories calculated using Equations 2.32-2.37 show the correct trends in the evolution of the osculating orbital elements, and are reasonable approximations of the true trajectories. However, they may be offset from the true averages and may diverge from true trajectories over many orbits. This may be partially due to higher order effects not captured in the averaging method, but it may also be due to non-trivial periodic components, which can shift the mean value of the state from the initial condition. This initial condition offset can be corrected by the addition of an averaged periodic term to the initial conditions of the averaged secular equation for each orbital element.

At any time t, the true value of any orbital element o, can be expressed as the sum of an initial condition o_0, a secular term $\overline{\dot{o}}t$ and a periodic term $o_p(t)$,

$$o(t) = o_0 + \overline{\dot{o}}t + o_p(t). \tag{2.42}$$

The periodic term repeats itself over each orbit. The average value of the orbital element over one orbit is thus

$$\overline{o} = o_0 + \frac{T}{2}\overline{\dot{o}} + \overline{o}_p, \tag{2.43}$$

where T is the period, $\vec{x}$ is a vector of the six orbital elements, and $\overline{\dot{o}} = \overline{f}(\vec{x})$ represents Equations 2.32-2.37.

The time derivative of Equation 2.42 provides a differential equation for the periodic term,

$$\dot{o}_p = f(\vec{x}, t) - \overline{f}(\vec{x}), \tag{2.44}$$

where $o(t) = f(\vec{x}, t)$. We substitute the nominal inital condition $\vec{x}_0$ for the true orbital element vector, knowing that the corrections are of higher order, and perform

the quadrature for o_p,

$$o_p = \int_0^t f\left(\vec{x}_0, \tau\right) d\tau - \overline{f}\left(\vec{x_0}\right) t. \tag{2.45}$$

This periodic term can be averaged over one orbit,

$$\overline{o}_p = \frac{1}{2\pi} \int_0^{2\pi} \left[\int_0^t f\left(\vec{x}_0, \tau\right) d\tau - \overline{f}\left(\vec{x}_0\right) t \right] dM. \tag{2.46}$$

For compatibility with the form of the Gauss equations above, the independent parameters of the two integrals are shifted to eccentric anomaly,

$$\begin{aligned} \overline{o}_p &= \frac{1}{2\pi} \int_0^{2\pi} \left[\int_{E_0}^{E} \frac{1}{n} \left(1 - e\cos E'\right) f\left(\vec{x_0}, E'\right) dE' \right] \left(1 - e\cos E\right) dE \\ &\quad -\frac{\pi}{n} \overline{f}\left(\vec{x_0}\right), \end{aligned} \tag{2.47}$$

where $n = \sqrt{\frac{\mu}{a^3}}$ is the mean motion. Note that $\frac{\pi}{n} = \frac{T}{2}$. This expression for $\overline{o}_p$ can be substituted into Equation 2.43 to determine the average value of the orbital element over the first period,

$$\overline{o} = o_0 + \frac{1}{2\pi} \int_0^{2\pi} \left[\int_{E_0}^{E} \sqrt{\frac{a^3}{\mu}} \left(1 - e\cos E'\right) f\left(\vec{x_0}, E'\right) dE' \right] \left(1 - e\cos E\right) dE. \tag{2.48}$$

To correct the initial conditions for the averaged secular equations, Equation 2.47 is substituted into Equation 2.42 at $t = 0$. The averaged secular equations, thus initialized, yield a more accurate average of the true periodic trajectory,

$$\begin{aligned} o\left(0\right) &= o_0 + \frac{1}{2\pi} \int_0^{2\pi} \left[\int_{E_0}^{E} \frac{1}{n} \left(1 - e\cos E'\right) f\left(\vec{x}, E'\right) dE' \right] \left(1 - e\cos E\right) dE \\ &\quad -\frac{T}{2} \overline{f}\left(\vec{x}\right). \end{aligned} \tag{2.49}$$

To calculate the averaged periodic correction term, we substitute the Fourier series in eccentric anomaly for the acceleration component terms in the Gauss equations. To avoid infinite series in the solution, we include only the 14 terms of the Fourier series whose coefficients appear in the averaged secular equations, as they have been shown to have the most significant effect on the trajectory dynamics. Assuming zero eccentric anomaly initial conditions, the correction terms are

$$\begin{aligned}
\overline{a}_p &= \frac{a^3}{\mu}\Bigg[e\Big[(2+e)\alpha_0^R + \frac{1}{2}\alpha_1^R - \left(\frac{1}{2}e+\frac{2}{3}\right)\alpha_2^R + \pi\beta_1^R\Big] + \sqrt{1-e^2}\Big[2\pi\alpha_0^S \\
&\quad +(2+e)\beta_1^S + \beta_2^S\Big]\Bigg] - \frac{T}{2}\dot{\overline{a}}(\vec{x}_0), \qquad (2.50)\\
\overline{e}_p &= \frac{1}{2}\frac{a^2}{\mu}\Bigg[(1-e^2)\Big[\,(2+e)\,\alpha_0^R + \frac{1}{2}\alpha_1^R - \left(\frac{1}{2}e+\frac{2}{3}\right)\alpha_2^R + \pi\beta_1^R\Big] \\
&\quad +\sqrt{1-e^2}\Big[-3e\pi\alpha_0^S + 2\pi\alpha_1^S - \frac{1}{2}e\pi\alpha_2^S + \left(1-\frac{5}{4}e^2-\frac{8}{3}e\right)\beta_1^S \\
&\quad +\left(-\frac{5}{8}e+\frac{8}{3}\right)\beta_2^S\Big]\Bigg] - \frac{T}{2}\dot{\overline{e}}(\vec{x}_0), \qquad (2.51)\\
\dot{\overline{i}}_p &= \frac{1}{2}\frac{a^2}{\mu}\frac{1}{\sqrt{1-e^2}}\Bigg[\alpha_0^W\Big[\sqrt{1-e^2}\sin\omega\left(-1-\frac{1}{2}e\right) - 3\pi e\cos\omega\Big] \\
&\quad +\alpha_1^W\Big[\pi\cos\omega\left(1+e^2\right) + \sqrt{1-e^2}\sin\omega\left(\frac{2}{3}e+\frac{1}{4}e^2-\frac{1}{2}\right)\Big] \\
&\quad +\alpha_2^W\Big[\sqrt{1-e^2}\sin\omega\left(\frac{2}{3}+\frac{5}{8}e\right) - \frac{1}{2}\pi e\cos\omega\Big] \\
&\quad +\beta_1^W\Big[\cos\omega\left(\frac{1}{2}-\frac{8}{3}e-\frac{3}{4}e^2\right) - \pi\sqrt{1-e^2}\sin\omega\Big] \\
&\quad +\beta_2^W\Big[\cos\omega\left(\frac{4}{3}-\frac{9}{8}e+\frac{4}{3}e^2+\frac{1}{2}e^3\right) + \frac{1}{2}\pi e\sqrt{1-e^2}\sin\omega\Big]\Bigg] \\
&\quad -\frac{T}{2}\ddot{\overline{i}}(\vec{x}_0), \qquad (2.52)
\end{aligned}$$

$$
\begin{aligned}
\overline{\Omega}_p &= \frac{1}{2}\frac{a^2}{\mu}\frac{\csc i}{\sqrt{1-e^2}}\Bigg[\cos\omega\sqrt{1-e^2}\Big[\alpha_0^W\left(2+\frac{1}{2}e\right)+\alpha_1^W\left(-\frac{1}{4}e^2+\frac{1}{2}-\frac{2}{3}e\right) \\
&\quad +\alpha_2^W\left(-\frac{5}{8}e-\frac{2}{3}\right)+\pi\beta_1^W-\frac{1}{2}e\pi\beta_2^W\Big]+\sin\omega\Big[\pi\alpha_1^W\left(1+e^2\right)-\frac{7}{2}\pi e\alpha_2^W \\
&\quad +\beta_1^W\left(\frac{1}{2}-\frac{8}{3}e-\frac{3}{4}e^2\right)+\beta_2^W\left(\frac{4}{3}-\frac{9}{8}e+\frac{4}{3}e^2+\frac{1}{2}e^3\right)\Big]\Bigg]-\frac{T}{2}\overline{\dot{\Omega}}(\vec{x}_0), \qquad (2.53) \\
\overline{\omega}_p &= \frac{1}{2}\frac{a^2}{\mu}\frac{1}{e}\Bigg[\alpha_0^S\left(4-\frac{3}{2}e-2e^2-e^3\right)+\alpha_1^S\left(\pi-\frac{2}{3}e-\frac{3}{4}e^2\right) \\
&\quad +\alpha_2^S\left(-\frac{4}{3}-\frac{9}{8}e+\frac{2}{3}e^2+\frac{1}{2}e^3\right)\pi\beta_1^S\left(2-e^2\right)-\frac{1}{2}\pi\beta_2^S+2e\pi\sqrt{1-e^2}\alpha_0^R \\
&\quad -\pi\sqrt{1-e^2}\alpha_1^R+\beta_1^R\sqrt{1-e^2}\left(-\frac{1}{2}+2e+e^2\right)\Bigg]-\cos i\overline{\Omega}_p \\
&\quad +\frac{T}{2}\overline{\dot{\Omega}}(\vec{x}_0)-\frac{T}{2}\overline{\dot{\omega}}(\vec{x}_0), \qquad (2.54) \\
\overline{\epsilon_{1p}} &= -\frac{a^2}{\mu}\Bigg[\pi\alpha_0^R\left(2+e^2\right)-2\pi e\alpha_1^R+\frac{1}{2}\pi e^2\alpha_2^R+\beta_1^R\left(2-e+\frac{2}{3}e^2\right)\Bigg] \\
&\quad +\left(1-\sqrt{1-e^2}\right)\left[\omega_p+\Omega_p+\frac{T}{2}\overline{\dot{\omega}}(\vec{x}_0)+\frac{T}{2}\overline{\dot{\Omega}}(\vec{x}_0)\right] \\
&\quad +2\sqrt{1-e^2}\sin^2\frac{i}{2}\left[\Omega_p+\frac{T}{2}\overline{\dot{\Omega}}(\vec{x}_0)\right]-\frac{T}{2}\overline{\dot{\epsilon}_1}(\vec{x}_0). \qquad (2.55)
\end{aligned}
$$

Figure 2.11 shows the effect of these corrections on the system with randomly-selected Fourier coefficients in Figure 2.6. The corrected initial conditions shift the estimated average trajectory to more accurately reflect the true average trajectory. They also can reduce the divergence between the true and average trajectories, most noticeably in the plot of mean anomaly. Some drift remains, however, due to higher order effects. This can be seen in the argument of periapsis; the corrected trajectory closely approximates the average of the Newtonian trajectory over the first few orbits, but diverges as higher-order effects accumulate over several orbits.

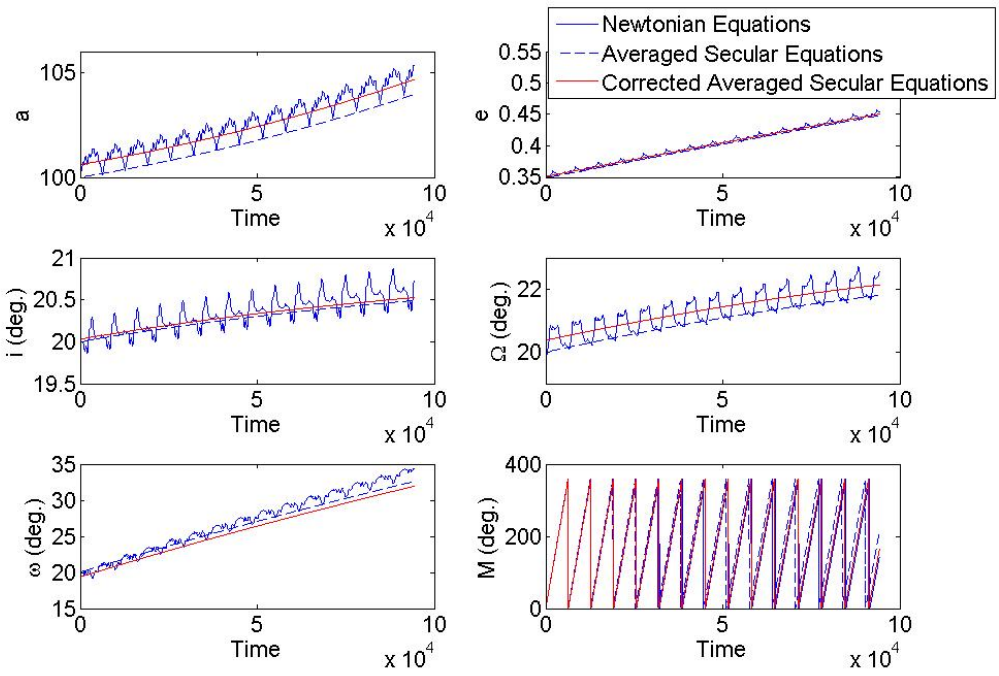

Figure 2.11: Orbital element trajectory due to randomly-generated acceleration with short-period offset correction. The original trajectory is the same as in Figure 2.6

2.6 Nonsingular Equations

Equations 2.32-2.37 contain singularities in the case of zero eccentricity or inclination, due to singularities in the Gauss equations. To avoid these singularities when evaluating trajectories that closely approach circular or equatorial orbits, we substitute the nonsingular variables

$$h_1 = e \sin \tilde{\omega}, \tag{2.56}$$

$$k_1 = e \cos \tilde{\omega}, \tag{2.57}$$

$$h_2 = \sin i \sin \Omega, \tag{2.58}$$

$$k_2 = \sin i \cos \Omega. \tag{2.59}$$

We can return to the classical orbit elements from these variables using the reverse transformations

$$\begin{aligned}
\tilde{\omega} &= \tan^{-1}\left(\frac{h_1}{k_1}\right), && (2.60)\\
e &= \sqrt{h_1^2 + k_1^2}, && (2.61)\\
\Omega &= \tan^{-1}\left(\frac{h_2}{k_2}\right), && (2.62)\\
i &= \sin^{-1}\left(\frac{h_2}{\sin\Omega}\right) = \sin^{-1}\left(\frac{k_2}{\cos\Omega}\right), && (2.63)\\
\omega &= \tilde{\omega} - \Omega. && (2.64)
\end{aligned}$$

We find the averaged differential equations for the nonsingular variables using the same approach as above,

$$\begin{aligned}
\dot{h}_1 &= \dot{e}\sin\tilde{\omega} + \dot{\tilde{\omega}} e\cos\tilde{\omega}\\
&= \frac{1}{2\pi}\int_0^{2\pi} (1 - e\cos E)\,\dot{h}_1 dE. && (2.65)
\end{aligned}$$

The equations for e, i, Ω, and ω are thus replaced by

$$\begin{aligned}
\overline{\dot{h}_1} &= \frac{na^2}{\mu}\Bigg[e\sqrt{1-e^2}\cos\tilde{\omega}\alpha_0^R - \frac{1}{2}\sqrt{1-e^2}\cos\tilde{\omega}\alpha_1^R + \frac{1}{2}\left(1-e^2\right)\sin\tilde{\omega}\beta_1^R \\
&\quad \frac{e}{\sqrt{1-e^2}}\cos\tilde{\omega}\tan\frac{i}{2}\Big[-\frac{3}{2}e\sin\omega\alpha_0^W + \frac{1}{2}\left(1+e^2\right)\sin\omega\alpha_1^W \\
&\quad -\frac{1}{4}e\sin\omega\alpha_2^W + \frac{1}{2}\sqrt{1-e^2}\cos\omega\beta_1^W - \frac{1}{4}e\sqrt{1-e^2}\cos\omega\beta_2^W\Big] \\
&\quad -\frac{3}{2}e\sqrt{1-e^2}\sin\tilde{\omega}\alpha_0^S + \sqrt{1-e^2}\sin\tilde{\omega}\alpha_1^S - \frac{1}{4}e\sqrt{1-e^2}\sin\tilde{\omega}\alpha_2^S \\
&\quad +\frac{1}{2}\cos\tilde{\omega}\left(2-e^2\right)\beta_1^S - \frac{1}{4}e\cos\tilde{\omega}\beta_2^S\Bigg], \qquad (2.66)\\
\overline{\dot{k}_1} &= \frac{na^2}{\mu}\Bigg[-e\sqrt{1-e^2}\sin\tilde{\omega}\alpha_0^R + \frac{1}{2}\sqrt{1-e^2}\sin\tilde{\omega}\alpha_1^R + \frac{1}{2}\left(1-e^2\right)\cos\tilde{\omega}\beta_1^R \\
&\quad \frac{e}{\sqrt{1-e^2}}\sin\tilde{\omega}\tan\frac{i}{2}\Big[\frac{3}{2}e\sin\omega\alpha_0^W - \frac{1}{2}\left(1+e^2\right)\sin\omega\alpha_1^W \\
&\quad +\frac{1}{4}e\sin\omega\alpha_2^W - \frac{1}{2}\sqrt{1-e^2}\cos\omega\beta_1^W + \frac{1}{4}e\sqrt{1-e^2}\cos\omega\beta_2^W\Big] \\
&\quad -\frac{3}{2}e\sqrt{1-e^2}\cos\tilde{\omega}\alpha_0^S + \sqrt{1-e^2}\cos\tilde{\omega}\alpha_1^S - \frac{1}{4}e\sqrt{1-e^2}\cos\tilde{\omega}\alpha_2^S \\
&\quad -\frac{1}{2}\sin\tilde{\omega}\left(2-e^2\right)\beta_1^S + \frac{1}{4}e\sin\tilde{\omega}\beta_2^S\Bigg], \qquad (2.67)\\
\overline{\dot{h}_2} &= \frac{na^2}{\mu\sqrt{1-e^2}}\Bigg[\left(\cos i\sin\Omega\cos\omega + \cos\Omega\sin\omega\right)\Big[-\frac{3}{2}e\alpha_0^W + \frac{1}{2}\left(1+e^2\right)\alpha_1^W \\
&\quad -\frac{1}{4}e\alpha_2^W\Big] + \left(-\cos i\sin\Omega\cos\omega + \cos\Omega\cos\omega\right)\Big[\frac{1}{2}\sqrt{1-e^2}\beta_1^W \\
&\quad -\frac{1}{4}e\sqrt{1-e^2}\beta_2^W\Big]\Bigg], \qquad (2.68)\\
\overline{\dot{k}_2} &= \frac{na^2}{\mu\sqrt{1-e^2}}\Bigg[\left(\cos i\cos\Omega\cos\omega - \sin\Omega\sin\omega\right)\Big[-\frac{3}{2}e\alpha_0^W + \frac{1}{2}\left(1+e^2\right)\alpha_1^W \\
&\quad -\frac{1}{4}e\alpha_2^W\Big] + \left(\cos i\cos\Omega\cos\omega + \sin\Omega\sin\omega\right)\Big[-\frac{1}{2}\sqrt{1-e^2}\beta_1^W \\
&\quad +\frac{1}{4}e\sqrt{1-e^2}\beta_2^W\Big]\Bigg]. \qquad (2.69)
\end{aligned}$$

We can also use the substitution [23]

$$e = \sin\phi, \tag{2.70}$$

$$\frac{1}{e} = \frac{\tan\frac{\phi}{2}}{1-\sqrt{1-e^2}}, \tag{2.71}$$

to rewrite the equation for ϵ_1,

$$\begin{aligned}\overline{\dot{\epsilon_1}} = \frac{na^2}{\mu}\Bigg[& \left(-2-e^2+e\sqrt{1-e^2}\tan\frac{\phi}{2}\right)\alpha_0^R + \frac{1}{2}\left(4e-\sqrt{1-e^2}\tan\frac{\phi}{2}\right)\alpha_1^R \\ & -\frac{1}{2}e^2\alpha_2^R + \frac{\tan\frac{i}{2}}{\sqrt{1-e^2}}\Big[-\frac{3}{2}e\sin\omega\alpha_0^W + \frac{1}{2}\left(1+e^2\right)\sin\omega\alpha_1^W \\ & -\frac{1}{4}e\sin\omega\alpha_2^W + \frac{1}{2}\sqrt{1-e^2}\cos\omega\beta_1^W - \frac{1}{4}e\sqrt{1-e^2}\cos\omega\beta_2^W\Big] \\ & +\tan\frac{\phi}{2}\Big[\frac{1}{2}\left(2-e^2\right)\beta_1^S - \frac{1}{4}e\beta_2^S\Big]\Bigg].\end{aligned} \tag{2.72}$$

These substitutions are effective for near-zero eccentricity and inclination. However, we find innacuracies when integrating trajectories that pass through exactly circular orbits, indicating that the averaging analysis must be reconsidered for this case.

2.7 Circular Orbits

When the method described in Section 2.6 is used to model circular orbits, two problems can occur. First, the eccentricity vector becomes undefined in the exactly circular case, which prevents most of the orbital elements from being calculated correctly. To resolve this, a different coordinate frame can be used to define the eccentricity vector and its normal, such as the line of nodes, its normal in the ecliptic plane, and the vertical, as shown by the vectors $\hat{a}$, $\hat{b}$, and $\hat{z}$ in Figure 2.12.

Second, in highly perturbed problems, as the spacecraft approaches a circular orbit it may be captured at periapsis or apoapsis, causing the eccentric anomaly to

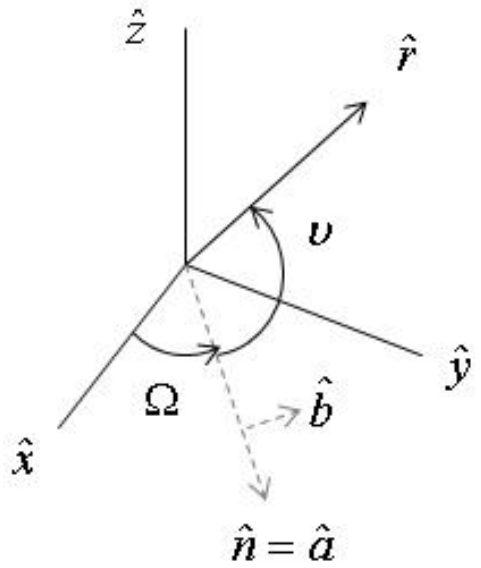

Figure 2.12: Alternate coordinate frame for circular orbits ($\hat{a}$,$\hat{b}$,$\hat{z}$)

enter a period of libration. This phenomenon is shown in Figures 2.13 and 2.14. In these cases, the averaging assumptions described in Section 2.3 are violated, as the eccentric anomaly does not complete a full 360° cycle. To work with these problems, we can perform the averaging over the quantity $E + \omega$, so that the motion of the spacecraft always follows an orbit-like path from an inertial perspective.

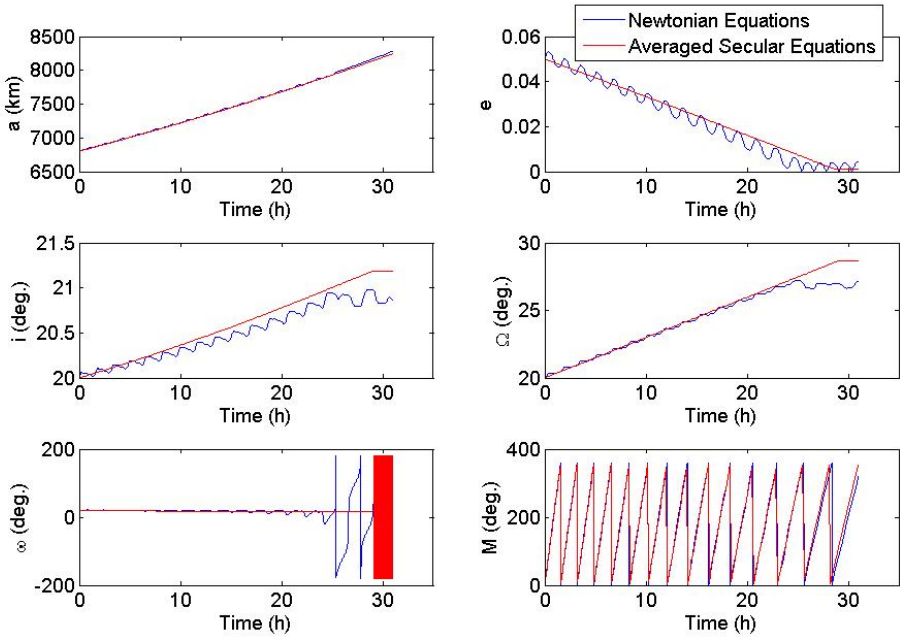

Figure 2.13: Trajectory as orbit approaches circular. The spacecraft stops completing full revolutions after about 14 orbits.

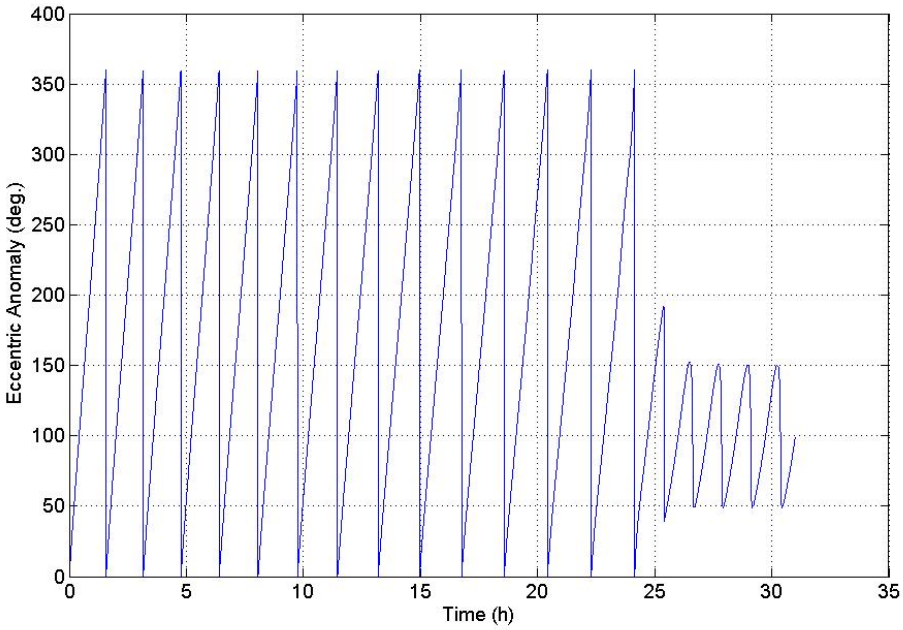

Figure 2.14: Eccentric anomaly as orbit approaches circular. The eccentric anomaly enters a period of libration as the spacecraft stops completing full orbits.

In the following analysis, we implement both of these solutions. We also consider another set of state variables to avoid singularities and simplify the equations of motion. Here we use a state vector with seven elements: the eccentricity vector $\vec{e}$, the angular momentum vector $\vec{h}$, and the scalar energy $\mathscr{E}$. Beginning with the definition of the eccentricity vector,

$$\vec{e} = \frac{1}{\mu}\vec{v} \times (\vec{r} \times \vec{v}) - \frac{\vec{r}}{|\vec{r}|}, \tag{2.73}$$

we find the time derivative such that this equation takes the form of the Gauss equations,

$$\begin{aligned} \dot{\vec{e}} &= \frac{\partial \vec{e}}{\partial \vec{v}} \cdot \vec{F} \\ &= \frac{1}{\mu}\left[2\vec{r}\vec{v} - \vec{v}\vec{r} - (\vec{r} \cdot \vec{v})\, U\right] \cdot \vec{F}. \end{aligned} \tag{2.74}$$

Assuming the orbit is nearly circular, we make the approximations

$$\vec{r} \approx r\hat{R}, \tag{2.75}$$

$$\vec{v} \approx v\hat{S}. \tag{2.76}$$

Therefore, Equation 2.74 can be stated as

$$\dot{\vec{e}} = \frac{rv}{\mu}\left(2F_S\hat{R} - F_R\hat{S}\right). \tag{2.77}$$

To match the averaging variable, we redefine the Fourier series for the thrust vector components,

$$F_R, F_W, F_S = \sum_{i=0}^{\infty}\left[\tilde{\alpha}_i^{(R,W,S)} \cos i\,(E+\omega) + \tilde{\beta}_i^{(R,W,S)} \sin i\,(E+\omega)\right]. \tag{2.78}$$

Using trigonometric identities, it can be shown that these "tilde" Fourier coefficients

are related to the original coefficients by the equations

$$\tilde{\alpha}_i = \alpha_i \cos(i\omega) - \beta_i \sin(i\omega), \tag{2.79}$$

$$\tilde{\beta}_i = \alpha_i \sin(i\omega) + \beta_i \cos(i\omega). \tag{2.80}$$

We then make the circular approximation $E \approx \nu$, so the independent variable of both the averaging and the Fourier series becomes the argument of latitude, $\theta = \nu + \omega$. Thus, the averaged secular equation for the eccentricity vector is

$$\begin{aligned}
\dot{\vec{e}} &= \frac{1}{2\pi} \int_0^{2\pi} \frac{rv}{\mu} \left[2 \sum_{i=0}^{\infty} \left(\tilde{\alpha}_i{}^S \cos i(\theta) + \tilde{\beta}_i{}^S \sin i(\theta) \right) \hat{R} \right. \\
&\quad \left. - \sum_{i=0}^{\infty} \left(\tilde{\alpha}_i{}^R \cos i(\theta) + \tilde{\beta}_i{}^R \sin i(\theta) \right) \hat{S} \right] \\
&= \frac{h}{\mu} \left[\left(\tilde{\alpha}_1^S \cos\Omega - \tilde{\beta}_1^S \cos i \sin\Omega + \frac{1}{2}\tilde{\alpha}_1^R \cos i \sin\Omega + \frac{1}{2}\tilde{\beta}_1^R \cos\Omega \right) \hat{x} \right. \\
&\quad + \left(\tilde{\alpha}_1^S \sin\Omega - + \tilde{\beta}_1^S \cos i \cos\Omega - \frac{1}{2}\tilde{\alpha}_1^R \cos i \cos\Omega + \frac{1}{2}\tilde{\beta}_1^R \sin\Omega \right) \hat{y} \\
&\quad \left. + \left(\tilde{\beta}_1^S \sin i - \frac{1}{2}\tilde{\alpha}_1^R \sin i \right) \hat{z} \right].
\end{aligned} \tag{2.81}$$

The vectors $\hat{x}$ and $\hat{y}$ can be converted to the vectors $\hat{a}$ and $\hat{b}$ shown in Figure 2.12 by the relations

$$\hat{a} = \frac{\hat{z} \times \vec{h}}{|\hat{z} \times \vec{h}|} = \cos\Omega \hat{x} + \sin\Omega \hat{y}, \tag{2.82}$$

$$\hat{b} = \hat{z} \times \hat{a} = -\sin\Omega \hat{x} + \cos\Omega \hat{y}. \tag{2.83}$$

The same process can be used to find the averaged secular equations for the angular

momentum vector and the energy,

$$\dot{\vec{h}} = r\left(F_S\hat{W} - F_W\hat{S}\right), \tag{2.84}$$

$$\begin{aligned}\overline{\dot{\vec{h}}} = r\Bigg[&\left(\tilde{\alpha}_0^S \sin i \sin\Omega + \frac{1}{2}\tilde{\beta}_1^W \cos\Omega + \frac{1}{2}\alpha_1^W \cos i \sin\Omega\right)\hat{x} \\ &+ \left(-\tilde{\alpha}_0^S \sin i \cos\Omega + \frac{1}{2}\tilde{\beta}_1^W \sin\Omega - \frac{1}{2}\alpha_1^W \cos i \cos\Omega\right)\hat{y} \\ &+ \left(\tilde{\alpha}_0^S \cos i - \frac{1}{2}\alpha_1^W \sin i\right)\hat{z}\Bigg],\end{aligned} \tag{2.85}$$

$$\dot{\mathscr{E}} = \frac{h}{r}F_S, \tag{2.86}$$

$$\overline{\dot{\mathscr{E}}} = \frac{h}{r}\tilde{\alpha}_0^S. \tag{2.87}$$

Equations 2.81, 2.85, and 2.87 were used to calculate the trajectory shown in Figures 2.16 - 2.17. The initial state in this example is a circular orbit, which would be problematic for the standard formulation of the averaged secular equations. The dimensions in this example represent a low-thrust spacecraft in low Earth orbit.

Because of the circular orbit assumptions described above, these equations are only appropriate for cases where the eccentricity is close to zero. For long-duration simulations where the orbit is near-circular during part of the trajectory, hand-off between Equations 2.32 - 2.37 and Equations 2.81, 2.85, and 2.87 can be performed as necessary.

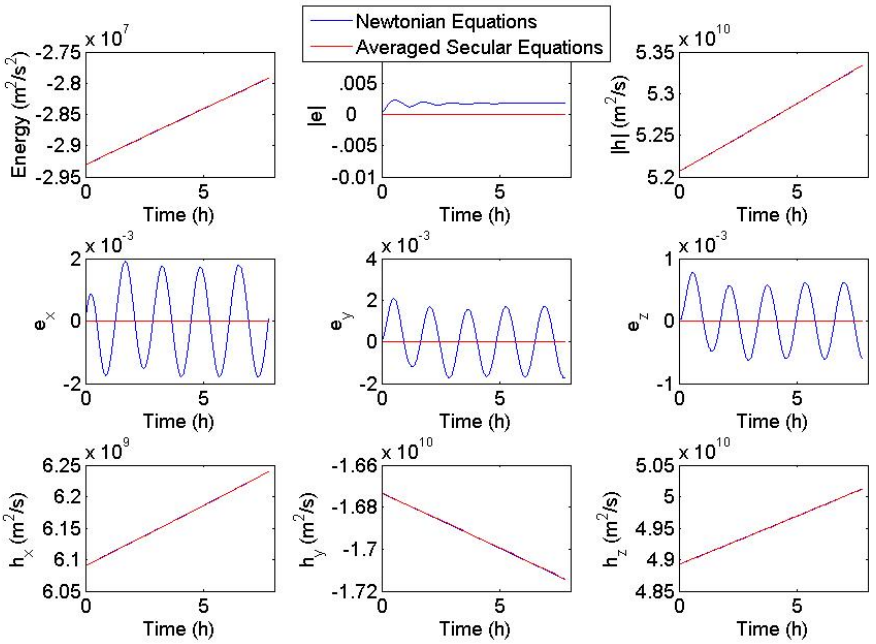

Figure 2.15: Alternate state variable trajectory for initially-circular problem. This example has an initial condition of zero eccentricity, so the averaged secular equations for $\vec{E}$, $\vec{h}$, and $\mathscr{E}$ were used to calculate the trajectory.

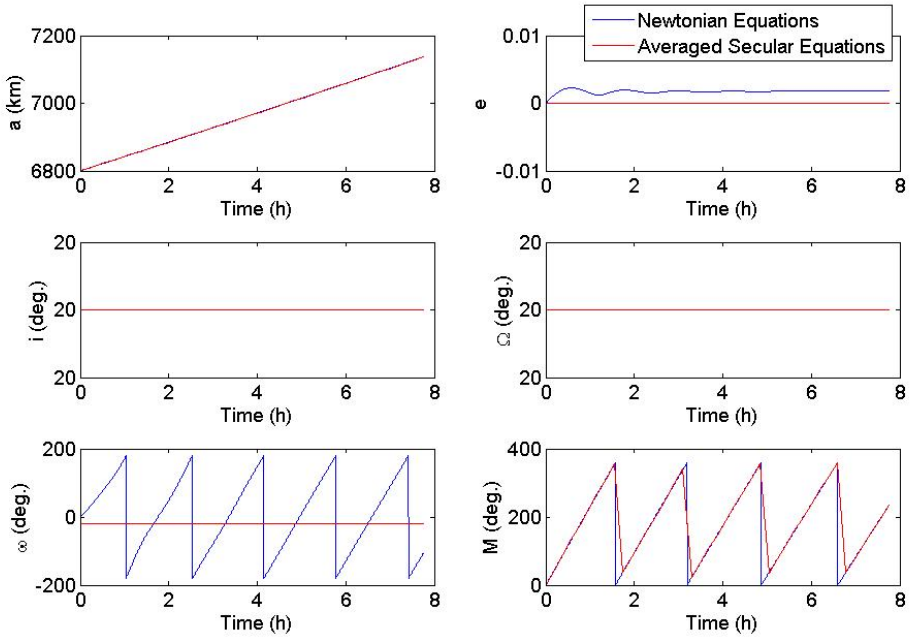

Figure 2.16: Classical orbital element trajectory for initially-circular problem. The average trajectory was calculated using the averaged secular equations for $\vec{E}$, $\vec{h}$, and $\mathscr{E}$, then converted to the classical orbital elements shown.

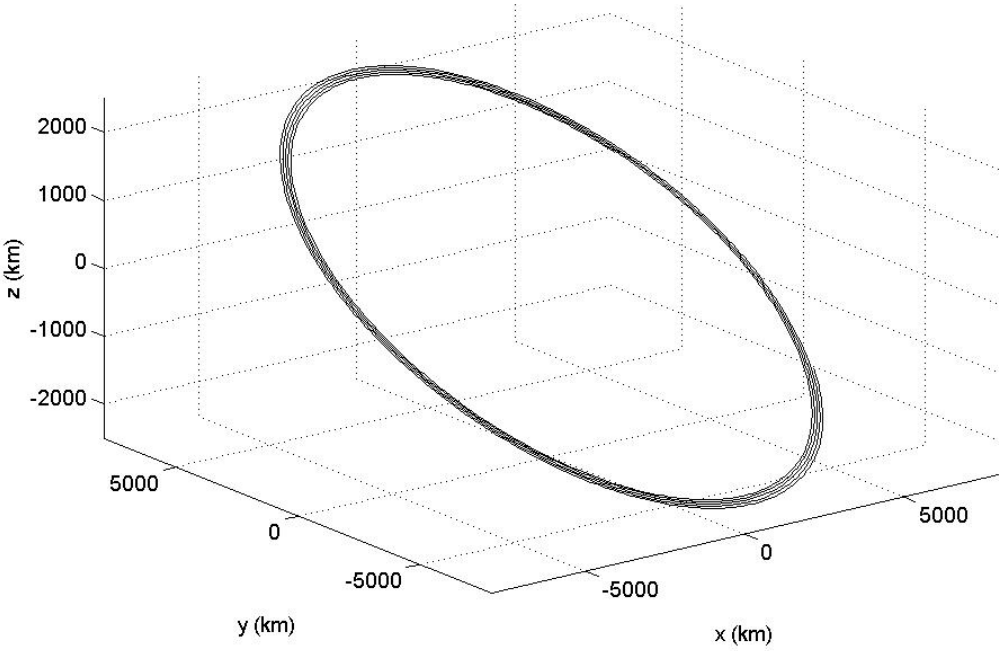

Figure 2.17: 3D trajectory for initially-circular problem

CHAPTER 3

Orbital Targeting

The averaged secular variational equations provide an efficient means of solving low-thrust orbit transfer problems. Any spacecraft targeting problem with a time span sufficient to allow low-thrust transfer can theoretically be solved by numerical integration of the averaged equations and iterative evaluation of the 14 thrust Fourier coefficients.

We primarily consider orbital targeting problems with fixed endpoint constraints. These problems take the form of two-point boundary value problems in which a spacecraft must transfer from an initial state to a final state, each defined by six orbital elements, in a fixed amount of time.

The averaged equations solve these problems for the secular orbital elements. These solutions will not precisely agree with the true spacecraft trajectory, as calculated by the Newtonian equations of motion, due to the short period offsets between them. However the secular solutions are useful approximations, as they represent the average of the full solution. They may be used to estimate flight requirements, such as velocity increment and fuel consumption, or to initialize other optimization methods to determine the true optimal trajectory.

3.1 Two-Point Boundary Value Problems

We approach the targeting problem in the averaged equations as a two-point boundary value problem with given initial state $\vec{x_0}$, final state $\vec{x_f}$, and transfer time

T. The equations of motion have the form

$$\dot{\vec{x}} \;=\; G\left(\vec{x}\right)\vec{\alpha} + F\left(\vec{x}\right), \tag{3.1}$$

where $\vec{x}$ is the state vector of orbital elements, $\vec{\alpha}$ is the 14×1 vector of thrust Fourier coefficients that appear in the averaged secular equations, and $F\left(\vec{x}\right)$ accounts for the additional mean motion term in the differential equation for mean anomaly,

$$\vec{x} = \begin{bmatrix} a \\ e \\ i \\ \Omega \\ \omega \\ M \end{bmatrix}, \quad \vec{\alpha} = \begin{bmatrix} \alpha_0^R \\ \alpha_1^R \\ \alpha_2^R \\ \beta_1^R \\ \alpha_0^S \\ \alpha_1^S \\ \alpha_2^S \\ \beta_1^S \\ \beta_2^S \\ \alpha_0^W \\ \alpha_1^W \\ \alpha_2^W \\ \beta_1^W \\ \beta_2^W \end{bmatrix}, \quad \vec{F} = \begin{bmatrix} 0 \\ 0 \\ 0 \\ 0 \\ 0 \\ n \end{bmatrix}.$$

The term $G\left(\vec{x}\right)\vec{\alpha}$ represents Equations 2.32 - 2.37.

Solutions to these problems involve only the secular orbital elements. The true trajectory, as calculated by the Newtonian equations, does not match these solutions exactly due to the short period offsets. Nonetheless, these secular solutions accurately represent the averaged dynamics of the true trajectory and are thus useful for many

applications.

We assume an initial control that does not meet the targeting objectives,

$$\vec{x}_f \neq \vec{x}\left(T, \vec{\alpha}_0, \vec{x}_0\right). \tag{3.2}$$

We then add a small adjustment to $\vec{\alpha}_0$ to make the state at time T equal to the final state,

$$\vec{x}_f = \vec{x}\left(T, \vec{\alpha}_0 + \delta\vec{\alpha}, \vec{x}_0\right). \tag{3.3}$$

We expand this as its first-order Taylor series approximation,

$$\vec{x}\left(T, \vec{\alpha}, \vec{x_0}\right) \approx \vec{x}\left(T, \vec{\alpha_0}, \vec{x_0}\right) + \frac{\partial \vec{x}}{\partial \vec{\alpha}} \cdot \delta\vec{\alpha}, \tag{3.4}$$

where $\vec{\alpha} = \vec{\alpha}_0 + \delta\vec{\alpha}$, and solve for $\left(\frac{\partial \vec{x}}{\partial \vec{\alpha}}\right)\delta\vec{\alpha}$,

$$\left(\frac{\partial \vec{x}}{\partial \vec{\alpha}}\right)\delta\vec{\alpha} = \left(\vec{x}_f - \vec{x}\left(T, \vec{\alpha_0}, \vec{x_0}\right)\right). \tag{3.5}$$

However, this problem has an infinity of possible solutions as there are 14 free variables in $\vec{\alpha}$ and only 6 constraint equations. We therefore add an additional constraint, imposing that we choose the one solution that minimizes a cost function $J(\vec{\alpha})$.

The problem then becomes a constrained minimization problem, which can be solved by defining a generalized cost function that includes the boundary value constraints multiplied by a Lagrange multiplier vector,

$$\overline{J} = J\left(\vec{\alpha}\right) + \vec{\lambda}\left[\vec{x}\left(T, \vec{\alpha}, \vec{x_0}\right) - \vec{x_f}\right]. \tag{3.6}$$

Here the Langrange multiplier $\vec{\lambda}$ is represented as a six-dimensional row vector. The

necessary condition to minimize $J(\vec{\alpha})$ and satisfy the boundary conditions is

$$\frac{\partial \overline{J}}{\partial\left(\vec{\alpha}, \vec{\lambda}\right)} = [\mathbf{0}]_{20x1} = \begin{bmatrix} \frac{\partial J}{\partial \vec{\alpha}} + \vec{\lambda}\frac{\partial \vec{x}}{\partial \vec{\alpha}} \\ \vec{x}\left(T, \vec{\alpha}, \vec{x_0}\right) - \vec{x_f} \end{bmatrix}. \tag{3.7}$$

We again replace $\vec{x}\left(T, \vec{\alpha}, \vec{x_0}\right)$ with its Taylor series approximation, Equation 3.4. For clarity, let $\frac{\partial \vec{x}}{\partial \vec{\alpha}} = \Psi$. To evaluate this matrix, we take the partial derivative of Equation 3.1 with respect to $\vec{\alpha}$,

$$\frac{\partial}{\partial \vec{\alpha}}\left(\dot{\vec{x}}\right) = \left[\frac{\partial \vec{F}}{\partial \vec{x}} + \vec{\alpha}\frac{\partial G}{\partial \vec{x}}\right]\left(\frac{\partial \vec{x}}{\partial \vec{\alpha}}\right) + G\left(\vec{x}\right). \tag{3.8}$$

We ignore the $\vec{\alpha}\frac{\partial G}{\partial \vec{x}}$ term, which is small compared to $G\left(\vec{x}\right)$, assuming that the perturbing thrust coefficients are small. We then have an equation of the form

$$\dot{\Psi}\left(t\right) = \frac{\partial \vec{F}\left(t\right)}{\partial \vec{x}}\Psi\left(t\right) + G\left(\vec{x}\left(t\right)\right), \tag{3.9}$$

$$\Psi\left(0\right) = 0. \tag{3.10}$$

Noting that the matrix $\frac{\partial \vec{F}}{\partial \vec{x}}$ has only one nonzero element, we solve the homogeneous

system,

$$\dot{\Psi}_h = \begin{bmatrix} 0 & 0 & 0 & 0 & 0 & 0 \\ 0 & 0 & 0 & 0 & 0 & 0 \\ 0 & 0 & 0 & 0 & 0 & 0 \\ 0 & 0 & 0 & 0 & 0 & 0 \\ 0 & 0 & 0 & 0 & 0 & 0 \\ -\frac{3}{2}\frac{n}{a} & 0 & 0 & 0 & 0 & 0 \end{bmatrix} \Psi, \tag{3.11}$$

$$\Psi_h(t) = \begin{bmatrix} 1 & 0 & 0 & 0 & 0 & 0 \\ 0 & 1 & 0 & 0 & 0 & 0 \\ 0 & 0 & 1 & 0 & 0 & 0 \\ 0 & 0 & 0 & 1 & 0 & 0 \\ 0 & 0 & 0 & 0 & 1 & 0 \\ -\frac{3}{2}\frac{n}{a}t & 0 & 0 & 0 & 0 & 1 \end{bmatrix} \Psi_0 = \Phi(t)\Psi_0, \tag{3.12}$$

$$\Phi(0) = I, \tag{3.13}$$

where $\Phi = \frac{\partial \vec{x}}{\partial \vec{x_0}}$ is the orbital element transition matrix.

Using the standard procedure, we find the particular solution, then sum the homogeneous and particular solutions at $t = 0$ to find the general solution,

$$\Psi(t) = \Phi(t) \int_0^t \Phi^{-1}(\tau)\, G(\vec{x}(\tau))\, d\tau. \tag{3.14}$$

This expression for Ψ can be used to find the solution to the necessary conditions (3.7). Beginning with the zero thrust case, we iteratively update the thrust coefficient vector $\vec{\alpha} = \vec{\alpha_0} + \delta\vec{\alpha}$ by solving the two simultaneous vector equations,

$$\left.\frac{\partial J}{\partial \vec{\alpha}}\right|_{\vec{\alpha}+\delta\vec{\alpha}} + \vec{\lambda} \cdot \Psi = 0, \tag{3.15}$$

$$\vec{x}(T, \vec{\alpha_0}, \vec{x_0}) + \Psi \cdot \delta\vec{\alpha} - \vec{x_f} = 0. \tag{3.16}$$

We assume a cost function of the form

$$J\left(\vec{\alpha}\right) = \frac{1}{2\pi}\int_0^{2\pi} f\left(\vec{\mathbf{F}}\right) dM, \tag{3.17}$$

where $\vec{\mathbf{F}}$ represents the force due only to the 14 relevant terms in the component Fourier series. We evaluate this total cost over one orbit, which agrees with the averaging result. Thus, this is proportional to the average cost of the given control.

If the integrand of the cost function is represented as a Fourier series,

$$f\left(\vec{\mathbf{F}}\right) = \sum_{j=0}^{\infty} a_j \cos\left(jE\right) + b_j \sin\left(jE\right), \tag{3.18}$$

and the independent variable of integration is shifted to eccentric anomaly, only the first two terms of the Fourier series remain,

$$\begin{aligned} J\left(\vec{\alpha}\right) &= \frac{1}{2\pi}\int_0^{2\pi} \left[\sum_{j=0}^{\infty} a_j \cos\left(jE\right) + b_j \sin\left(jE\right)\right]\left(1 - e\cos E\right) dE \\ &= a_0 - \frac{e}{2}a_1. \end{aligned} \tag{3.19}$$

By the definition of Fourier coefficients,

$$a_0 = \frac{1}{2\pi}\int_0^{2\pi} f\left(\vec{\mathbf{F}}\right) dE, \tag{3.20}$$

$$a_1 = \frac{1}{2\pi}\int_0^{2\pi} f\left(\vec{\mathbf{F}}\right) \cos\left(E\right) dE. \tag{3.21}$$

To evaluate Equation 3.15, we need the partial derivative $\frac{\partial J(\vec{\alpha})}{\partial \vec{\alpha}}$, which has the form

$$\frac{\partial J\left(\vec{\alpha}\right)}{\partial \vec{\alpha}} = \frac{\partial a_0}{\partial \vec{\alpha}} - \frac{e}{2}\frac{\partial a_1}{\partial \vec{\alpha}}. \tag{3.22}$$

This partial derivative can be evaluated numerically for most cost functions and may be evaluated analytically for certain simple cost functions. First, we consider the cost function $J(\vec{\alpha})$ representing the minimum of the norm of the acceleration vector for the targeting problem, which is the total velocity increment of the thrust over one orbit. We assume a negligible rate of mass loss such that this is the average thrust per orbit,

$$J\left(\vec{\alpha}\right) = \frac{1}{2\pi}\int_0^{2\pi}\sqrt{F_R^2+F_S^2+F_W^2}dM. \tag{3.23}$$

Equations 3.20 and 3.21 become

$$a_0 = \frac{1}{2\pi}\int_0^{2\pi}\sqrt{F_R^2+F_S^2+F_W^2}dE, \tag{3.24}$$

$$a_1 = \frac{1}{2\pi}\int_0^{2\pi}\sqrt{F_R^2+F_S^2+F_W^2}\cos\left(E\right)dE. \tag{3.25}$$

However, the the partial derivatives of these coefficients are difficult to evaluate analytically and are undefined in the zero thrust case,

$$\frac{\partial a_0}{\partial\vec{\alpha}} = \frac{1}{4\pi}\int_0^{2\pi}\frac{\frac{\partial}{\partial\vec{\alpha}}\left(F_R^2+F_S^2+F_W^2\right)}{\sqrt{F_R^2+F_S^2+F_W^2}}dE, \tag{3.26}$$

$$\frac{\partial a_0}{\partial\vec{\alpha}} = \frac{1}{4\pi}\int_0^{2\pi}\frac{\frac{\partial}{\partial\vec{\alpha}}\left(F_R^2+F_S^2+F_W^2\right)\cos\left(jE\right)}{\sqrt{F_R^2+F_S^2+F_W^2}}dE. \tag{3.27}$$

To avoid this problem, we consider a different cost function $J\left(\vec{\alpha}\right)$, the square of the norm, representing the minimum energy solution,

$$J\left(\vec{\alpha}\right) = \frac{1}{2\pi}\int_0^{2\pi}\left(F_R^2+F_S^2+F_W^2\right)dM. \tag{3.28}$$

This cost function allows us to find an upper bound on the velocity increment, ΔV, per unit time. For our control, the ΔV between two time periods, t_0 and $t_0 + \delta t$, is

$$\begin{aligned} \Delta V &= \int_{t_0}^{t_0+\delta t} \|\vec{u}(t)\| dt \\ &= \int_{t_0}^{t_0+\delta t} \sqrt{F_R^2 + F_S^2 + F_W^2} dt. \end{aligned} \tag{3.29}$$

From the Cauchy-Schwarz inequality [24],

$$\begin{aligned} \int_{t_0}^{t_0+\delta t} \sqrt{F_R^2 + F_S^2 + F_W^2} dt &\leq \sqrt{\int_{t_0}^{t_0+\delta t} \left(\sqrt{F_R^2 + F_S^2 + F_W^2}\right)^2 dt \cdot \int_{t_0}^{t_0+\delta t} dt} \\ &\leq \sqrt{\int_{t_0}^{t_0+\delta t} \left(F_R^2 + F_S^2 + F_W^2\right) dt \cdot \delta t}. \end{aligned} \tag{3.30}$$

Therefore, ΔV is bounded by

$$\Delta V \leq \sqrt{2\delta t} \sqrt{J\left(\vec{\alpha}\right)}. \tag{3.31}$$

The orthogonality conditions lead to a simple expression for Equation 3.20. To simplify Equation 3.21, we note that the square of each force vector component is a finite sum of products of two elements of $\vec{\alpha}$ and two sines or cosines of iE, where $i = 0, 1$, or 2. Using trigonometric identities, each product can be represented as a sum of sines and cosines of jE, where $j = 0, 1, 2, 3$, or 4. Thus the orthogonality conditons can be applied again,

$$a_0 = \frac{1}{2}\left(\vec{\alpha} \cdot \vec{\alpha} + \left(\alpha_0^R\right)^2 + \left(\alpha_0^S\right)^2 + \left(\alpha_0^W\right)^2\right), \tag{3.32}$$

$$\begin{aligned} a_1 &= 2\alpha_0^R\alpha_1^R + \alpha_1^R\alpha_2^R + 2\alpha_0^S\alpha_1^S + \alpha_1^S\alpha_2^S + \beta_1^S\beta_2^S + 2\alpha_0^W\alpha_1^W \\ &\quad + \alpha_1^W\alpha_2^W + \beta_1^W\beta_2^W. \end{aligned} \tag{3.33}$$

Now the partial derivative $\frac{\partial J(\vec{\alpha})}{\partial \vec{\alpha}}$ is straightforward to evaulate analytically,

$$\frac{\partial J\left(\vec{\alpha}\right)}{\partial \vec{\alpha}} = \vec{\alpha}\left(Q - \frac{1}{2}eZ\right), \tag{3.34}$$

where

$$Q = \begin{bmatrix} q_{4\times4} & & \mathbf{0} \\ & q_{5\times5} & \\ \mathbf{0} & & q_{5\times5} \end{bmatrix}_{14\times14}, \tag{3.35}$$

$$q_{4\times4} = \begin{bmatrix} 2 & & & \mathbf{0} \\ & 1 & & \\ & & 1 & \\ \mathbf{0} & & & 1 \end{bmatrix}, \; q_{5\times5} = \begin{bmatrix} 2 & & & & \mathbf{0} \\ & 1 & & & \\ & & 1 & & \\ & & & 1 & \\ \mathbf{0} & & & & 1 \end{bmatrix},$$

$$Z = \begin{bmatrix} z_{4\times4} & & \mathbf{0} \\ & z_{5\times5} & \\ \mathbf{0} & & z_{5\times5} \end{bmatrix}_{14\times14}, \tag{3.36}$$

$$z_{4\times4} = \begin{bmatrix} 0 & 2 & 0 & 0 \\ 2 & 0 & 1 & 0 \\ 0 & 1 & 0 & 0 \\ 0 & 0 & 0 & 0 \end{bmatrix}, \; z_{5\times5} = \begin{bmatrix} 0 & 2 & 0 & 0 & 0 \\ 2 & 0 & 1 & 0 & 0 \\ 0 & 1 & 0 & 0 & 0 \\ 0 & 0 & 0 & 0 & 1 \\ 0 & 0 & 0 & 1 & 0 \end{bmatrix}.$$

Equations 3.15 and 3.16 can now be solved to iteratively update $\vec{\alpha}$:

$$\delta\vec{\alpha} = -\left(Q - \frac{1}{2}eZ\right)^{-T}\Psi^T\lambda^T - \vec{\alpha_0}, \tag{3.37}$$

$$\lambda^T = \left[\Psi\left(Q - \frac{1}{2}eZ\right)^{-T}\Psi^T\right]^{-1}\left(\vec{x}\left(T;\vec{\alpha},\vec{x_0}\right) - \vec{x_f} - \Psi\vec{\alpha_0}\right). \tag{3.38}$$

The initial condition offset corrections described in Chapter 2 improve the accuracy of the targeting algorithm. We initialize the algorithm with zero thrust, then use the Fourier coefficients calculated in each iteration to correct the initial state of the subsequent iteration. Thus each integration of the averaged equations has a slightly different initial conditon which more closely approximates the average of the desired transfer trajectory. The initial condition of the j^{th} iteration is

$$\vec{x_0}(j) = \begin{bmatrix} a_0 + \overline{a}_p(j-1) \\ e_0 + \overline{e}_p(j-1) \\ i_0 + \overline{i}_p(j-1) \\ \Omega_0 + \overline{\Omega}_p(j-1) \\ \omega_0 + \overline{\omega}_p(j-1) \\ \epsilon_{10} + \overline{\epsilon_1}_p(j-1) \end{bmatrix}. \tag{3.39}$$

This method converges to a set of 14 Fourier coefficients that describes a control that solves the targeting problem in the averaged secular equations. The true trajectory under this control, as determined by the Newtonian equations, generally compares well to the averaged trajectory.

An example of the targeting methodology applied to a transfer in five orbital elements is shown below. Table 3.1 shows the initial and final states of the boundary value problem, between which the spacecraft must transfer. The targeting algorithm was initialized with the zero thrust case and terminated when the thrust coefficients changed by less than 0.1% between iterations. This occurred after twelve iterations. The final $\vec{\alpha}$ is shown in Table 3.2 and the transfer trajectory is shown in Figures 3.1 and 3.2.

The true spacecraft trajectory, as calculated by the Newtonian equations of motion, doesn't match the secular solution exactly due to the short period offsets between them. In solving these two-point boundary value problems, we solve only for the sec-

ular orbital elements, so precise agreeement with the Newtonian equation solutions is not expected.

Table 3.1: Initial and target states for 2PBVP targeting example

	Initial State	Final State
a (km)	6800	7000
e	0.2	0.25
i (deg.)	20	25
Ω (deg.)	20	25
ω (deg.)	20	25
M (deg.)	0	0

Table 3.2: Final force Fourier coefficients after twelve iterations for 2PBVP targeting example

Radial		Normal		Circumferential	
α_0^R	-174.069	α_0^S	-0.922	α_0^W	27.367
α_1^R	916.653	α_1^S	-1817.659	α_1^W	207.469
α_2^R	22.645	α_2^S	2.999	α_2^W	16.777
β_1^R	-43.777	β_1^S	-42.195	β_1^W	607.177
		β_2^S	402.234	β_2^W	47.261

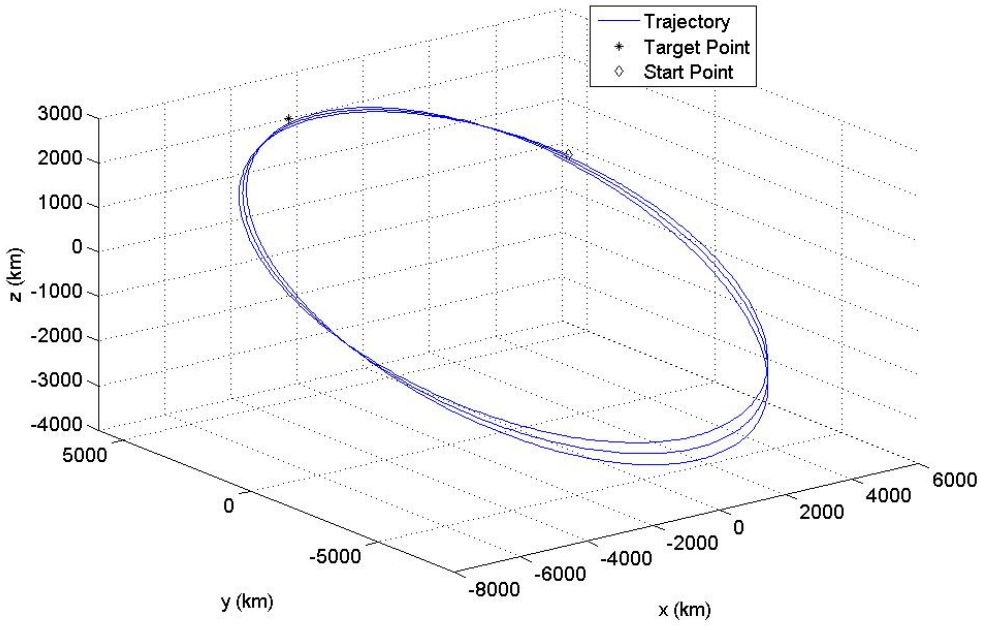

Figure 3.1: 3D trajectory after twelve iterations for 2PBVP targeting example

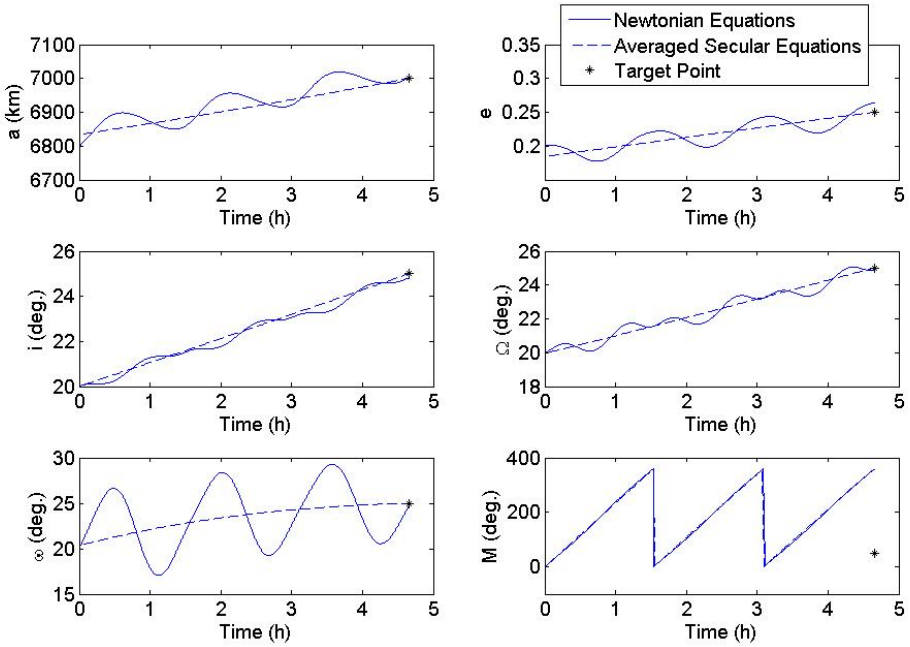

Figure 3.2: Orbital element trajectory after twelve iterations for 2PBVP targeting example

This method can also be used to solve more complex targeting problems involving sequences of two or more target states. A lengthy orbit transfer may be approached as a series of two-point boundary value problems and the optimal set of control coefficients may be calculated between each pair of states.

An example of this targeting through a series of states is shown below. The target points, shown in Table 3.3, approximately reflect the states of the SMART-1 spacecraft in the early days of its mission[1]. These states occur at fixed times over approximately 80 orbit periods.

Table 3.3: Target states for SMART-1 example

	Time (h)	a (km)	e	i (deg.)	Ω (deg.)	ω (deg.)	M (deg.)
Initial State	0	26433	0.671	6.915	160.315	194.821	3.136
Target 1	155.833	26825	0.662	6.907	158.793	197.752	3.138
Target 2	342.702	27815	0.640	6.871	157.153	200.66	3.128
Target 3	487.163	28713	0.622	6.861	156.084	202.442	3.142
Target 4	680.502	29745	0.604	6.838	154.886	204.387	3.143
Target 5	853.156	30235	0.598	6.848	153.996	205.839	3.142
Target 6	1017.363	31380	0.573	6.826	153.178	207.342	3.144

Starting with the given initial state and zero thrust, the vector $\vec{\alpha}$ was iteratively updated to converge on a control that drives the average trajectory to the first target point. The first target point was then used as the initial condition for the next two-point boundary value problem, and so on. The iterative algoirthm for each pair of states was terminated when the thrust coefficients changed by less than 0.1% between iterations, which happened after four to six iterations. Figures 3.3 and 3.4 show the final trajectory. The velocity increment for this orbit transfer is 1300.6 m/s.

[1]http://sci.esa.int/science-e/www/object/index.cfm?fobjectid=31517&farchive_objecttypeid=30&farchive_objectid=30930&fareaid_2=63

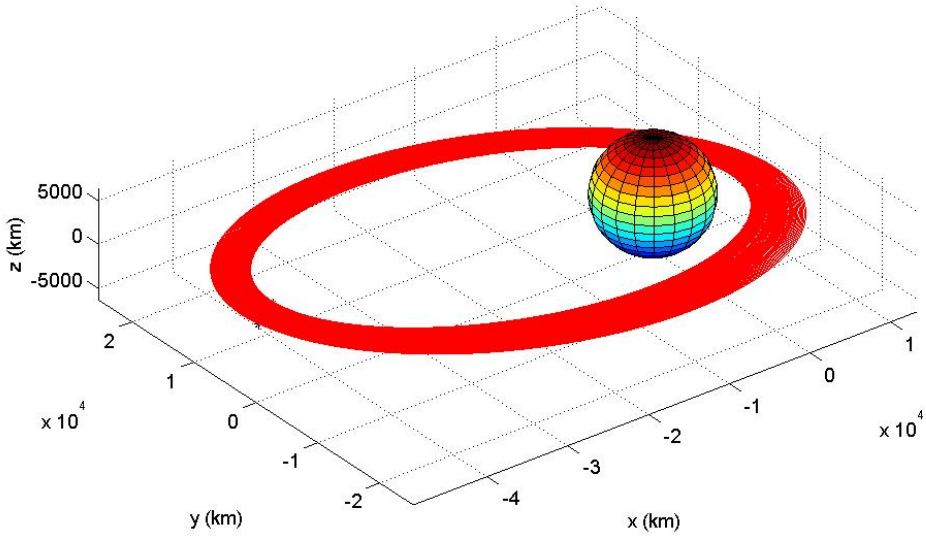

Figure 3.3: 3D trajectory calculated by 2PBVP method for SMART-1 targeting example

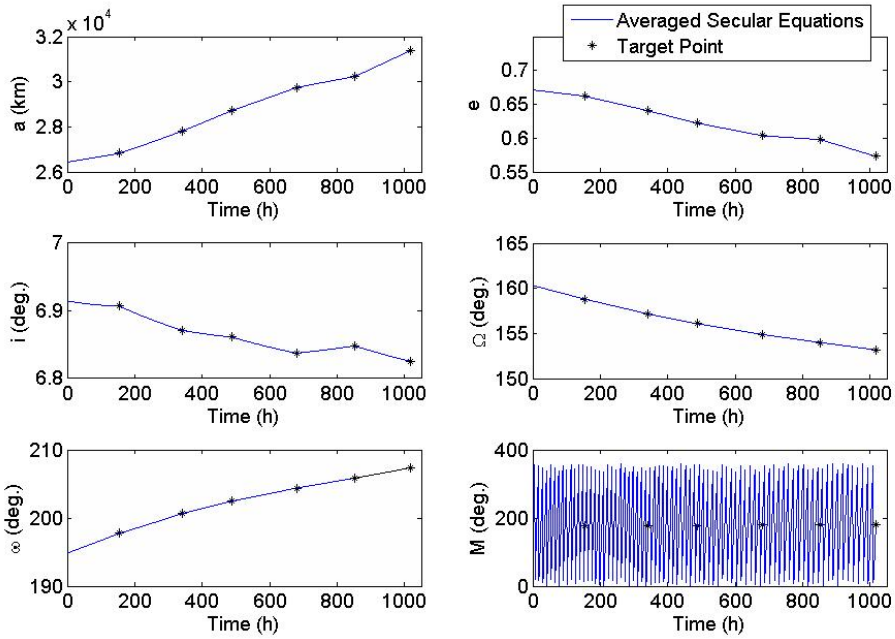

Figure 3.4: Orbital element trajectory calculated by 2PBVP method for SMART-1 targeting example

The average trajectory is continuous throughout the transfer; however, the true trajectory may have discontinuities at the intermediate target states due to short-period variations. Figure 3.5 is a detail view of the semi-major axis plot near the first target state, in which one of these discontinuities can be seen. In this example problem, we do not include corrections of short-period offsets in the initial conditions, which would also lead to discontinuities in the trajectory. In practice, these discontinuities would make it impossible to actually implement the trajectory, making this approach inappropriate for many applications.

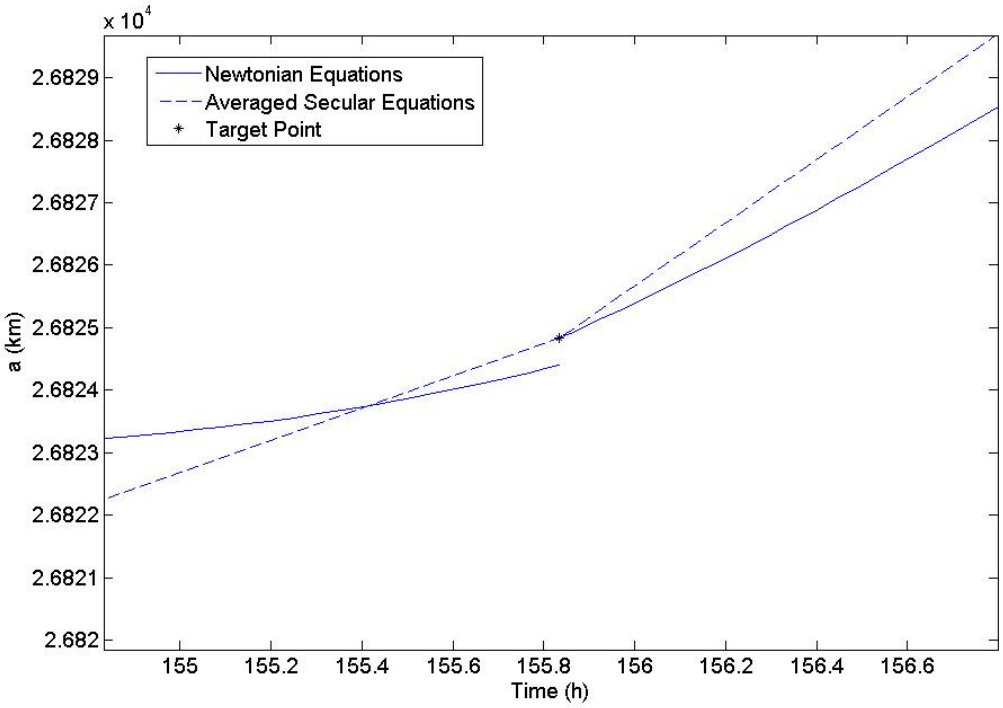

Figure 3.5: Detail of discontinuity in 2PBVP method for SMART-1 targeting example. This discontinuity in the true trajectory near the first target state is the result of initializing a new boundary value problem at each intermediate state.

In some cases, however, calculation of the precise trajectory through the target states is not necessary. In the early stages of mission planning, for example, the target points may represent general mission goals with some flexibility in the actual trajectory. This two-point boundary value method may be appropriate for these

applications.

3.2 Least-Squares Regression

In the second method for fitting sequences of orbital states, we use a least-squares regression approach for calculating the low-thrust trajectory. Here, we eschew precise targeting of the states to find a single control for the entire orbit transfer. We approach the problem using the averaged equations with a given initial state $\vec{x_0}$, a series of N intermediate target states $\vec{x} = [x(t_1), x(t_2,)..., x(t_N)]$, and a set of times associated with each target state $T = [t_1, t_2, ..., t_N]$. The equations of motion again have the form of Equation 3.1. To carry this out, we could use a cost function of the form

$$C\left(\vec{\alpha}\right) = \frac{1}{2}\sum_{i=1}^{N}\left[\vec{x}(\vec{\alpha}, t_i) - \vec{x}_i\right] \cdot \left[\vec{x}(\vec{\alpha}, t_i) - \vec{x}_i\right]. \tag{3.40}$$

To minimize $C\left(\vec{\alpha}\right)$, we would use the necessary condition

$$\frac{\partial C}{\partial \vec{\alpha}} = \sum_{i=1}^{N}\left[\vec{x}(\vec{\alpha}, t_i) - \vec{x}_i\right]\left(\frac{\partial \vec{x}}{\partial \vec{\alpha}}\right)_i = 0. \tag{3.41}$$

We would replace $\vec{x}(\vec{\alpha}, t_i)$ with its Taylor series approximation, Equation 3.4, and then solve Equation 3.41 for $\delta\vec{\alpha}$ to iteratively converge on a solution

$$\delta\vec{\alpha} = \left[\sum_{i=1}^{N}\left(\vec{x}_i - \vec{x}(\vec{\alpha_0}, t_i)\right)\left(\frac{\partial \vec{x}}{\partial \vec{\alpha}}\right)_i\right]\left[\sum_{i=1}^{N}\left(\frac{\partial \vec{x}}{\partial \vec{\alpha}}\right)_i^T\left(\frac{\partial \vec{x}}{\partial \vec{\alpha}}\right)_i\right]^{-1}. \tag{3.42}$$

However, the second bracketed term in Equation 3.42 is singular in most simulations. This is due to the fact that solutions are not unique, so more than one possible thrust profile may solve the problem. To resolve this issue, we add another constraint: a minimum-energy cost function $J\left(\vec{\alpha}\right)$ that must be minimized while solving

the least-squares targeting problem,

$$\overline{J} = J\left(\vec{\alpha}\right) + \sum_{i=1}^{N} \left[\vec{x}\left(\vec{\alpha}, t_i\right) - \vec{x_i}\right] w \left[\vec{x}\left(\vec{\alpha}, t_i\right) - \vec{x_i}\right]. \tag{3.43}$$

We minimize $J(\vec{\alpha})$, the minimum-energy cost funtion defined by Equation 3.28, while minimizing the least squares difference between $\vec{x}\left(\vec{\alpha}, t_i\right)$ and $\vec{x_i}$. We introduce the weighting matrix w, a 6×6 matrix of constants that can be independently selected to normalize numerical differences between variables or emphasize certain elements. The necessary conditions are

$$\frac{\partial \overline{J}}{\partial\left(\vec{\alpha}\right)} = [\mathbf{0}]_{14x1} = \frac{\partial J}{\partial \vec{\alpha}} + \sum_{i=1}^{N} \left[\vec{x}\left(\vec{\alpha}, t_i\right) - \vec{x_i}\right] w \left(\Psi\right)_i. \tag{3.44}$$

The matrix $\left(\frac{\partial \vec{x}}{\partial \vec{\alpha}}\right)_i = \left(\Psi\right)_i$ is calculated from Equation 3.14. The partial derivative for the cost function $J(\vec{\alpha})$ is evaluated by Equation 3.34.

To solve Equation 3.44, we replace $\vec{x}(\vec{\alpha}, t_i)$ with its Taylor series approximation, Equation 3.4, and iteratively update the thrust coefficient vector, $\vec{\alpha} = \vec{\alpha}_0 + \delta\vec{\alpha}$,

$$0 = \left(\vec{\alpha}_0 + \delta\vec{\alpha}\right)^T \left(Q - \frac{1}{2}eZ\right) + \sum_{i=1}^{N} \left[\vec{x}\left(\vec{\alpha}_0, t_i\right) + \Psi_i \delta\vec{\alpha} - \vec{x_i}\right] w \Psi_i, \tag{3.45}$$

$$\delta\vec{\alpha} = \left[-\vec{\alpha_0}^T \left(Q - \frac{1}{2}eZ\right) - \sum_{i=1}^{N} \left[\vec{x}\left(\vec{\alpha}_0, t_i\right) - \vec{x_i}\right] w \Psi_i\right] \left[Q - \frac{1}{2}eZ + \sum_{i=1}^{N} \Psi_i^T w \Psi_i\right]^{-1}. \tag{3.46}$$

Figures 3.6 and 3.7 show an example of this method applied to the same targeting problem as in Table 3.3. Beginning from a fixed initial state and with zero initial thrust, the averaged secular equations were integrated and Equation 3.46 was used to iteratively calculate the 14 thrust Fourier coefficients. The trajectory shown is the result after ten iterations of this least-squares targeting method, when the algorithm

was terminated because the coefficients changed by a maximum of 0.1% between iterations.

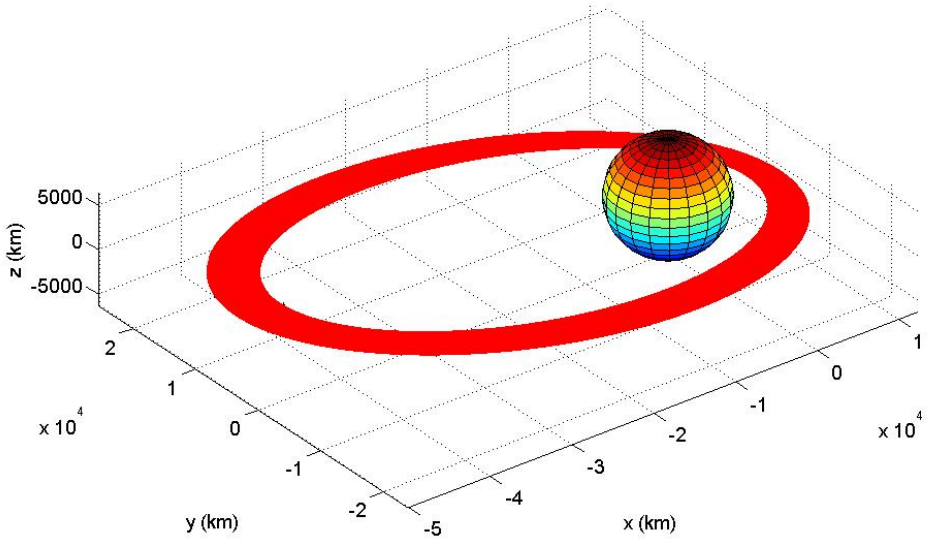

Figure 3.6: 3D trajectory calculated by least-squares method for SMART-1 targeting example

The velocity increment for this transfer is 410.3 m/s, less than half the value calculated by the previous approach. As shown in Figure 3.8, the overall magnitude of the thrust calculated by the least-squares method is less than that of the two-point boundary value method for most of the simulation time. Because the least-squares algorithm was not required to rigidly satisfy all the targeting criteria, it was able to find a significantly lower-cost solution to the problem.

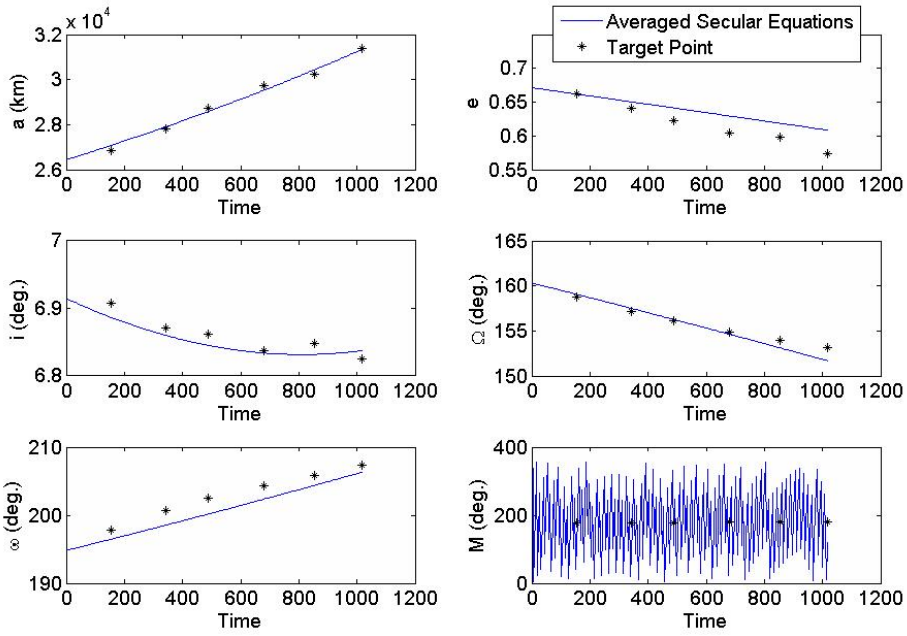

Figure 3.7: Orbital element trajectory calculated by least-squares method for SMART-1 targeting example

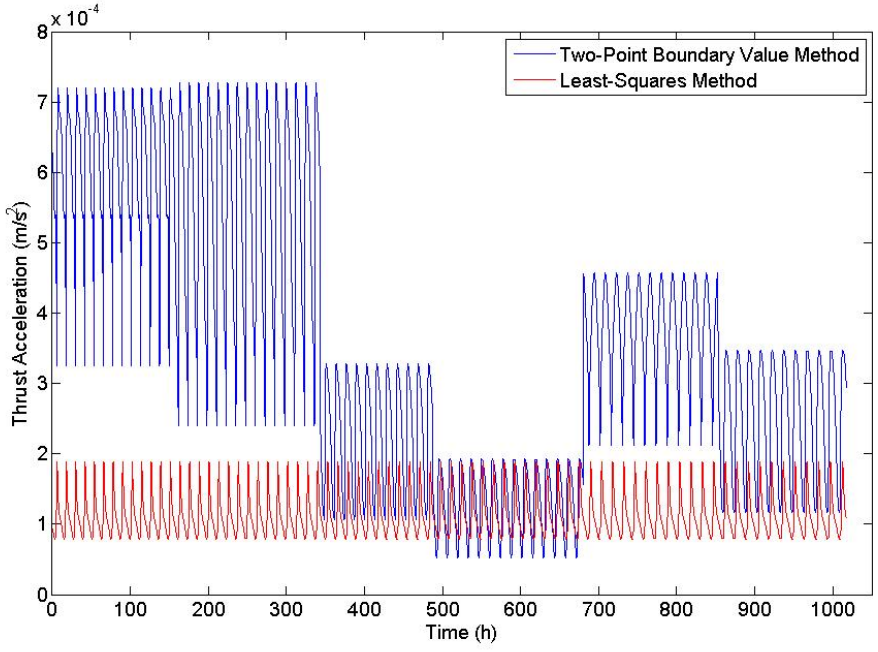

Figure 3.8: Comparison of thrust acceleration magnitudes for SMART-1 targeting example

The ΔV result from the least-squares approach is comparable to the actual SMART-1 spacecraft over the same interval. From launch through the final target state of this simulation, SMART-1 had a ΔV of 665 m/s over 72 days and 946 hours of thrust time[2]. This simulation does not include the first 30 days of the mission, during which the electric propulsion system was used discontinuously, but assumes continuous thrust over the remaining 42 days (1017 hours) without coast arcs.

Both the two-point boundary value method and the least-squares method are able to calculate trajectories that closely approach each of the target states. Table 3.4 shows the mean difference between the true and calculated average value of each orbital element over the six targets. The two-point boundary value method is very accurate, but requires a different control for each segment of the trajectory and includes discontinuities. The least-squares method is less accurate, but uses a single control. The relative accuracy of each variable in the least-squares method can be adjusted through the weighting parameter w in Equation 3.43; in this solution, mean anomaly was assigned a weighting value lower than the other orbital elements.

Table 3.4: Mean difference between calculated average state and target state for SMART-1 targeting example. The values shown are the average over the six target states of the difference between the target and the average trajectory.

	a (km)	e	i (deg.)	Ω (deg.)	ω (deg.)	M (deg.)
2PBVP	-0.2135e-3	3.0370e-9	-1.5588e-7	-5.8031e-7	8.5762e-7	3.4883e-4
LSQ	31.4609	0.0183	-0.0094	-0.3208	-1.6875	-56.4976

3.3 Targeting in the Non-Singular Equations

Targeting problems that involve near-circular or near-equatorial orbits can be solved using the nonsingular forms of the averaged secular equations given in Sections

[2]http://sci.esa.int/science-e/www/object/index.cfm?fobjectid=34361

2.6 and 2.7. In the case of circular orbits, Equations 2.81, 2.85, and 2.87 are most effective. The same targeting methods described in Sections 3.1 and 3.2 can be used with the alternate set of state variables $\vec{e}$, $\vec{h}$, and $\mathscr{E}$.

The equations of motion now have the form

$$\dot{\vec{x}} = \tilde{G}\left(\vec{x}\right)\tilde{\vec{\alpha}}, \tag{3.47}$$

where $\vec{x}$ is the 7×1 state vector of orbital elements, $\tilde{G}$ represents the nonsingular averaged secular equations, and $\tilde{\vec{\alpha}}$ is the 14×1 vector of redefined thrust Fourier coefficients given by Equations 2.79 and 2.80,

$$\vec{x} = \begin{bmatrix} \mathscr{E} \\ h_x \\ h_y \\ h_z \\ e_x \\ e_y \\ e_z \end{bmatrix} \quad \tilde{\vec{\alpha}} = \begin{bmatrix} \tilde{\alpha}_0^R \\ \tilde{\alpha}_1^R \\ \tilde{\alpha}_2^R \\ \tilde{\beta}_1^R \\ \tilde{\alpha}_0^S \\ \tilde{\alpha}_1^S \\ \tilde{\alpha}_2^S \\ \tilde{\beta}_1^S \\ \tilde{\beta}_2^S \\ \tilde{\alpha}_0^W \\ \tilde{\alpha}_1^W \\ \tilde{\alpha}_2^W \\ \tilde{\beta}_1^W \\ \tilde{\beta}_2^W \end{bmatrix}.$$

The vector $\tilde{\vec{\alpha}}$ is related to the vector $\vec{\alpha}$ by a matrix A,

$$\begin{aligned}\tilde{\vec{\alpha}} &= A\vec{\alpha} \\ &= \begin{bmatrix} A_{4\times4} & & \mathbf{0} \\ & A_{5\times5} & \\ \mathbf{0} & & A_{5\times5} \end{bmatrix}_{14\times14} \vec{\alpha}, \end{aligned} \tag{3.48}$$

where

$$A_{4\times4} = \begin{bmatrix} 1 & 0 & 0 & 0 \\ 0 & \cos\omega & 0 & -\sin\omega \\ 0 & 0 & \sin 2\omega & 0 \\ 0 & \sin\omega & 0 & \cos\omega \\ 0 & 0 & \sin 2\omega & 0 \end{bmatrix}, \tag{3.49}$$

$$A_{5\times5} = \begin{bmatrix} 1 & 0 & 0 & 0 & 0 \\ 0 & \cos\omega & 0 & -\sin\omega & 0 \\ 0 & 0 & \sin 2\omega & 0 & \cos 2\omega \\ 0 & \sin\omega & 0 & \cos\omega & 0 \\ 0 & 0 & \sin 2\omega & 0 & \cos 2\omega \end{bmatrix}. \tag{3.50}$$

To solve a two-point boundary value targeting problem, we follow the procedure described in Section 3.1, choosing a cost function $J(\vec{\alpha})$ to be minimized while satisfying the boundary conditions. The necessary conditions have the form of Equation 3.7. The matrix $\Psi = \frac{\partial \vec{x}}{\partial \vec{\alpha}}$ is found using the new equations of motion,

$$\frac{\partial}{\partial \vec{\alpha}}\left(\dot{\vec{x}}\right) = \vec{\alpha}\frac{\partial\left(\tilde{G}A\right)}{\partial \vec{x}}\Psi + \tilde{G}(\vec{x})\,A. \tag{3.51}$$

We ignore the $\vec{\alpha}\frac{\partial\left(\tilde{G}A\right)}{\partial \vec{x}}$ term, which is small compared to $\tilde{G}(\vec{x})\,A$, assuming that the

perturbing thrust coefficients are small. We can then integrate the equation

$$\dot{\Psi}(t) = \tilde{G}(\vec{x}(t))\, A, \tag{3.52}$$

$$\Psi(0) = 0, \tag{3.53}$$

to calculate $\Psi(t)$ and find the solution to the necessary conditions.

The rest of the two-point boundary value targeting problem takes the same form as in Section 3.1. Equations 3.37 and 3.38 can be solved with the new value of Ψ to iteratively update the thrust coefficient vector $\vec{\alpha}$ and converge on a solution to the targeting problem.

Figures 3.9, 3.10, and 3.11 show an example of this method. The initial state is an inclined, circular orbit with a radius of 6800 km; the target state is a circular orbit with a radius of 7000 km in the same plane. The targeting algorithm was terminated after 15 iterations, when the maximum change in the acceleration coefficients between iterations was less than 1%.

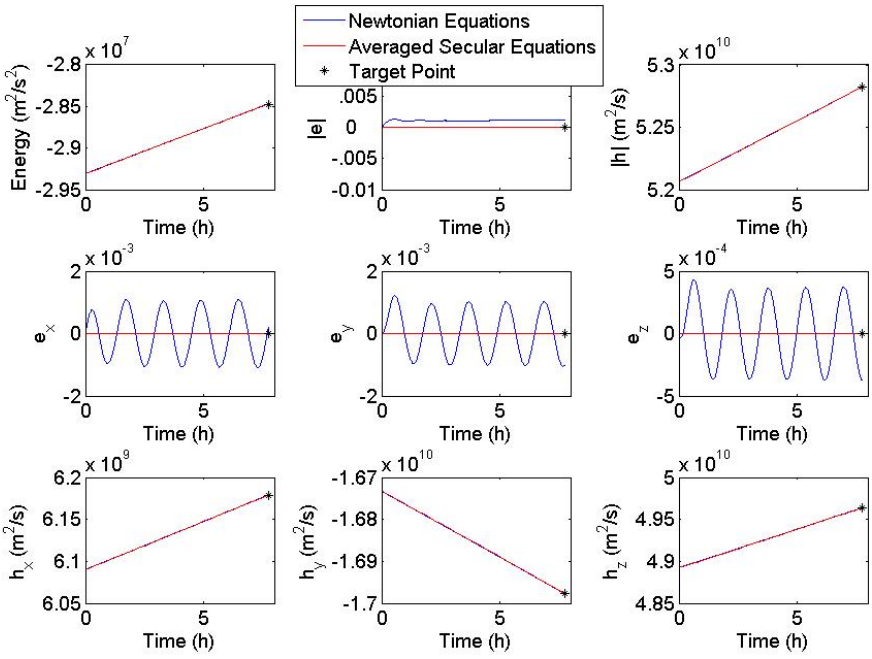

Figure 3.9: Alternate state variable trajectory for circular targeting example

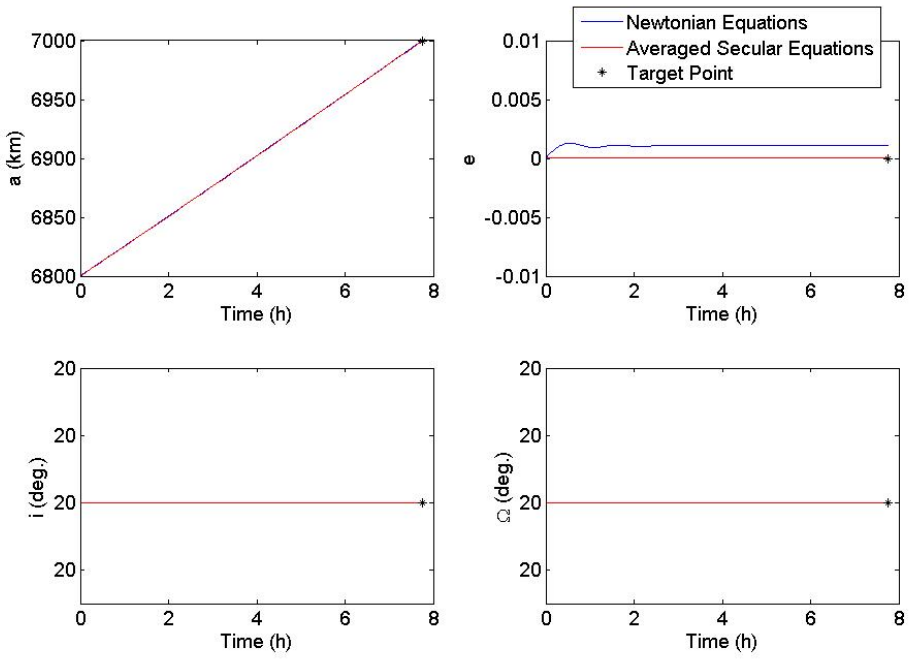

Figure 3.10: Classical orbital element trajectory for circular targeting example. The average trajectory was calculated using the secular equations for $\vec{E}$, $\vec{h}$, and $\mathscr{E}$, then converted to the classical orbital elements shown.

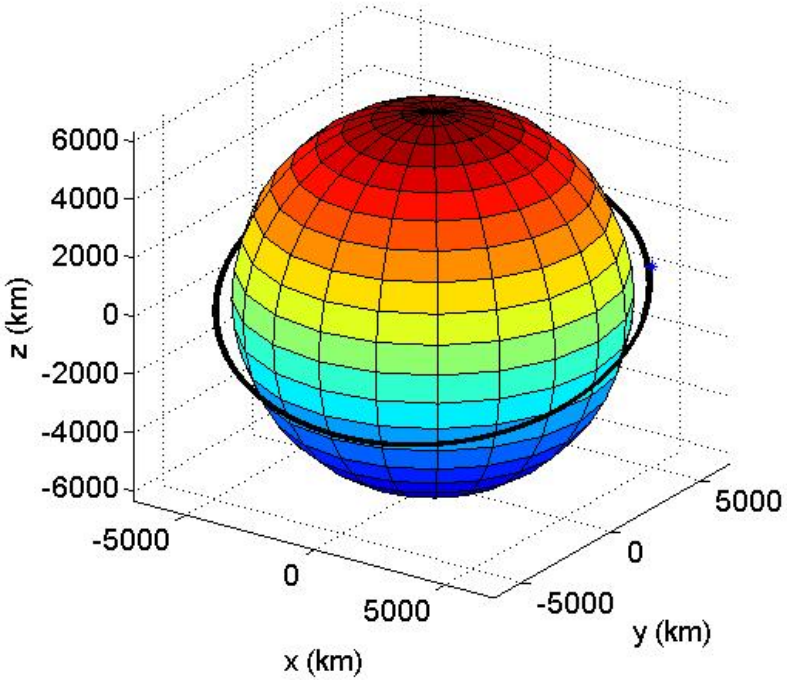

Figure 3.11: 3D trajectory for circular targeting example

3.4 Targeting in the Newtonian Equations

We may also use the Newtonian equations of motion (Equations 2.1 and 2.2) to solve targeting problems involving circular or near-circular orbits. By considering only the 14 acceleration Fourier coefficients that appear in the averaged secular equations, we reduce the dimensionality of the problem and significantly reduce the computational effort required to solve the full Newtonian targeting problem. The equations of motion have the form

$$\begin{aligned} \dot{\vec{x}} &= F_0(\vec{x}) + F_1(\vec{x})\,\vec{\alpha} \\ &= \begin{bmatrix} \vec{v} \\ \frac{-\mu}{r^3}\vec{r} \end{bmatrix} + \begin{bmatrix} 0 \\ \vec{G} \end{bmatrix} \vec{\alpha}. \end{aligned} \tag{3.54}$$

The state vector now contains the Cartesian position and velocity, while $\vec{G}$ contains the position unit vectors and the relevant Fourier series terms,

$$\vec{x} = \begin{bmatrix} \vec{r} \\ \vec{v} \end{bmatrix}_{6\times 1}, \quad \vec{G} = \left[\begin{array}{c|c|c|c|c} \hat{r} & \hat{r}\cos E & \hat{r}\cos 2E & \hat{r}\sin E & \ldots \end{array}\right]_{3\times 14}.$$

As in the targeting algorithms described above, solutions to Equation 3.54 are not unique. Therefore, we add an additional constraint, requiring that we choose the solution that minimizes a cost function $J = \frac{1}{2}\vec{\alpha}\cdot\vec{\alpha}$. Following the procedure described in Section 3.1, we find

$$\dot{\Psi} = \frac{\partial F_0}{\partial \vec{\alpha}} + \frac{\partial F_1}{\partial \vec{\alpha}}\vec{\alpha} + F_1. \tag{3.55}$$

The first and third terms of Equation 3.55 are simple analytical functions, but the second term is more difficult. Numerical simulations indicate that this term is not negligible; thus we cannot ignore it in the targeting algorithm and converge on a solution to the boundary value problem.

Lacking a convenient analytical form for $\frac{\partial F_1}{\partial \vec{\alpha}}$, we instead evaluate the matrix Ψ using numerical derivatives. We slightly increment each of the 14 Fourier coefficients in turn to find the columns of Ψ, using the standard formula

$$f'(x) = \frac{f(x+h) - f(x)}{h}. \tag{3.56}$$

In Sections 3.1 and 3.2, we initialized the targeting algorithms with zero thrust and they were able to converge on solutions. When we perform the targeting using the Newtonian equations with initially-circular orbits, the algorithm often requires a non-zero initial thrust vector in order to converge. We initialize the Fourier coefficients that appear in the secular equations of the transfer variables of interest with arbitrary values to speed the convergence.

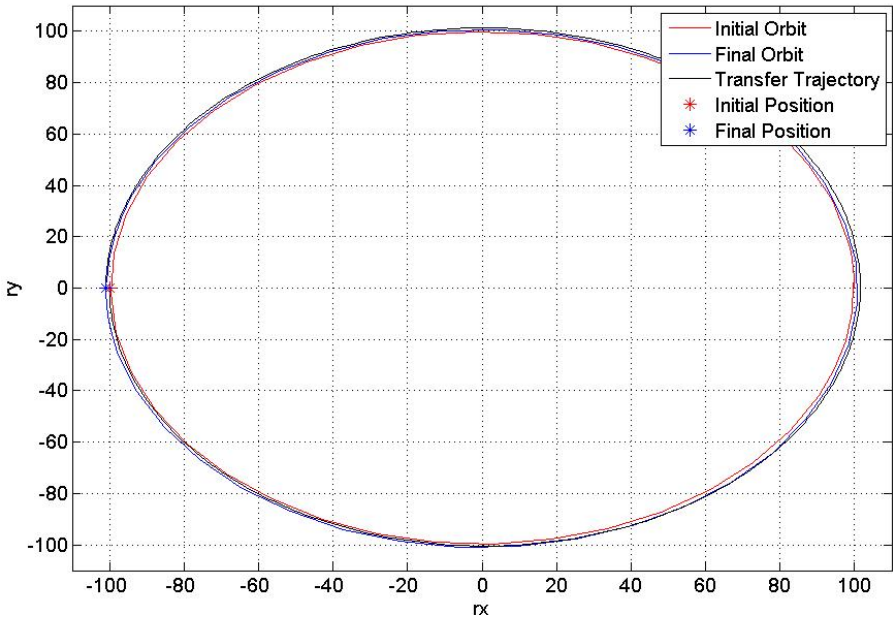

Figure 3.12: Trajectory calculated by Newtonian equations for one-orbit circular targeting example

Figure 3.12 shows an example of this targeting method. The semi-major axis of a circular orbit is increased by 1% over one orbit while keeping all other orbital elements

constant. The dimensions are normalized to a standard gravitational parameter $\mu = 1$. Due to the large fluctuations in the state vector over each orbit when integrating the Newtonian equations, multi-orbit problems have more difficulty converging with this method.

3.5 Error Analysis

The analytical methods developed in this dissertation include assumptions and approximations that can cause errors in calculating average trajectories and satisfying boundary conditions. Figure 2.11 shows an example of error in a trajectory calculated by the averaged equations compared to the same trajectory calculated by the Newtonian equations, even after correction of short period offsets. Table 3.4 shows another example of the mean errors in the boundary conditions of a multi-state targeting problem.

These errors are primarily caused by the averaging assumptions. In the derivation of the averaged secular equations, we assume that the thrust accelerations are small enough that the shape and size of the orbit does not change significantly from one revolution to the next. This assumption is never completely true, and the larger the thrust accelerations are, the less valid the first-order averaging becomes. The higher-order terms eliminated by the orthogonality still have a small influence on the average trajectory, and this effect may result in drift between the true and calculated average trajectories over many orbits.

Other errors may result from the use of Fourier series to model the thrust accelerations. In any function that contains jump discontinuities, for a finite number of terms, the Gibbs phenomenon causes the Fourier series approximation of the function near the jump to have large oscillations, which do not vanish as the number of terms approaches infinity [25]. This effect may not be significant in the analysis and targeting methods described in Chapters 2 and 3, as these include only the 0th, 1st,

and 2nd order coefficients of the Fourier series. However, it may affect the methods in Chapter 4, which use higher-order terms to re-shape the controls. Nonetheless, the errors associated with Fourier series are reasonably well understood and can usually be quantified.

In general, this analytical and targeting method involves some sources of error, which may not be as easily calculated as the errors in other purely computational approaches. The strengths of this method, however, are its efficiency and its identification of fundamental control parameters. In applications that require smaller, quantified errors, this approach could be used to initialize other numerical algorithms.

CHAPTER 4

Equivalent Average Trajectory Dynamics

Only 14 coefficients of the thrust acceleration Fourier series control the average trajectory dynamics of the low-thrust spacecraft. However, the other coefficients of order 3 and higher still affect the shape and frequency of the control itself. They may be set to zero, or they may be selected to shape the control into a more desirable form without altering the average trajectory.

In this chapter we explore several approaches for selecting these higher-order coefficients. First, they may be selected to reduce the fuel or energy cost of a transfer. An existence proof of this cost-reduction potential is developed.

The coefficients may also be selected to transform the control into a form that is more easily implemented by existing low-thrust engines. Current electric propulsion systems operate on a range of fixed throttle points, and minimal switching is preferred. Thus it is desirable to transform continuously-varying controls into step functions that produce equivalent average trajectory dynamics. In some cases, the magnitude of the total thrust acceleration within the step function can also be made constant, to mimic the design of a typical spacecraft with one gimbaled low-thrust engine.

4.1 Existence of Equivalent, Lower-Cost Control

In many cases, additional terms in the thrust acceleration Fourier series beyond the 14 key terms can reduce the total cost of the transfer without significantly altering the

trajectory. The following proves the existence of a lower-cost control for the quadratic cost function and all controls with nonzero values of α_2 or β_2.

The quadratic minimum energy cost function is given by Equation 3.28. If the thrust components F_R, F_S, and F_W represent the acceleration due only to the 14 key coefficients, this cost can be described by Equations 3.19, 3.32, and 3.33. For simplicity in this cost reduction calculation, we consider only the cosine series of one directional component of the thrust. This cost, based only on the key coefficients, is

$$J\left(\vec{\alpha}_3\right) = \frac{1}{2}\left[\vec{\alpha}_3 \cdot \vec{\alpha}_3 + \left(\alpha_0\right)^2 - e\left(2\alpha_0\alpha_1 + \alpha_1\alpha_2\right)\right], \tag{4.1}$$

where $\vec{\alpha}_3 = \left[\alpha_0\, \alpha_1\, \alpha_2\right]^T$.

If the Fourier series is extended up to order N, the cost becomes

$$J\left(\vec{\alpha}_N\right) = \frac{1}{2}\left[\vec{\alpha}_N \cdot \vec{\alpha}_N + \left(\alpha_0\right)^2 - e\left(2\alpha_0\alpha_1 + \alpha_1\alpha_2 + ... + \alpha_{N-1}\alpha_N\right)\right], \tag{4.2}$$

where $\vec{\alpha}_N = \left[\alpha_0 \ldots \alpha_N\right]^T$. The difference between the new cost function and the cost function for the key-element-only series is

$$\begin{aligned} \Delta J &= J\left(\vec{\alpha}_N\right) - J\left(\vec{\alpha}_3\right) \\ &= \frac{1}{2}\left[\left[\left(\alpha_3\right)^2 + \left(\alpha_4\right)^2 + ... + \left(\alpha_N\right)^2\right] - e\left(\alpha_2\alpha_3 + \alpha_3\alpha_4 + ... + \alpha_{N-1}\alpha_N\right)\right] \end{aligned} \tag{4.3}$$

If the additional terms are to reduce the energy of the transfer, we must have $\Delta J < 0$. One method for this is term-by-term selection of the additional Fourier coefficients. Given a nonzero value of α_2, we can choose α_3 such that

$$\alpha_3^2 - e\alpha_2\alpha_3 < 0. \tag{4.4}$$

That is,

$$0 < |\alpha_3| < e\,|\alpha_2|\,, \tag{4.5}$$

where ϵ is defined such that $0 < \epsilon < 1$. Then $\alpha_3 = e\epsilon\alpha_2$. Continuing in this manner, we can choose α_n such that

$$\alpha_n = (e\epsilon)^{n-2}\,\alpha_2, \tag{4.6}$$

where $n = 1...N$, so that each term further reduces ΔJ. Now, let $N \to \infty$ and define J'

$$J' \;=\; \alpha_2^2 + 2\Delta J. \tag{4.7}$$

Substituting Equations 4.3 and 4.6, we can simplify the expression

$$\begin{aligned} J' &= \sum_{j=0}^{\infty} \left[\alpha_{j+2}^2 - e\alpha_{j+2}\alpha_{j+3}\right] \\ &= \sum_{j=0}^{\infty} \left[(e\epsilon)^{2j} - \frac{(e\epsilon)^{2j+2}}{\epsilon}\right] \alpha_2^2 \\ &= \frac{\alpha_2^2}{1-(e\epsilon)^2}\left[1 - e^2\epsilon\right], \end{aligned} \tag{4.8}$$

where the final simplification is based on the fact that for any $w < 1$,

$$\sum_{j=0}^{\infty} w^j = \frac{1}{1-w}. \tag{4.9}$$

We can now solve Equation 4.7 to find the total reduction in transfer energy for a

given choice of ϵ and infinite additional terms in the Fourier series,

$$\Delta J = -\frac{1}{2}\alpha_2^2 \frac{e^2}{1-(e\epsilon)^2}(1-\epsilon). \tag{4.10}$$

Thus a lower-cost control exists for all controls with $\alpha_2 \neq 0$. This method can be extended to select terms of the full sine and cosine series of each directional component of the force, assuming α_2^R, β_1^R, α_2^S, β_2^S, α_2^W, and β_2^W are nonzero.

In practice, this method generally results in very small reductions in total energy cost. Other methods may be developed to improve or optimize the coefficient selection methodology for greater cost reductions.

4.2 Coefficient Selection for Constant Thrust Arcs

The higher-order thrust acceleration Fourier coefficients may also be used to shape a control function for improved implementation. We begin with a set of 14 control coefficients that accomplish an orbital transfer of interest. These coefficients may be the average solution to a targeting problem found by one of the methods in Chapter 3. Without additional terms, this control can be realized as a time-varying thrust acceleration.

By adding higher-order terms, we can change the control to a series of constant thrust arcs, which are easier for low-thrust engines to implement, without altering the average trajectory dynamics. In most cases we can uniquely solve for a set of thrust acceleration amplitudes and on/off times that produce a trajectory that is equivalent to the original orbit transfer.

There are many possible ways to perform these shaping transformations. As the number of degrees of freedom increase, the shape solution becomes more useful for implementation, but the problem complexity increases. Table 4.1 summarizes the shape transformations that are considered in this chapter.

Table 4.1: Control shaping overview

Control Shape	Degrees of Freedom	Coefficients
One Step	3 (per thrust direction)	α_0, α_1, β_1
Two Steps	5 (per thrust direction)	α_0, α_1, α_2, β_1, β_2
Three Constant-Magnitude Steps (planar)	10	α_0^R, α_1^R, α_2^R, β_1^R, (β_2^R), α_0^S, α_1^S, α_2^S, β_1^S, β_2^S
Four Constant-Magnitude Steps (3D)	14	all

4.3 Equivalent Control Function: One Step

As a simple case for an initial analysis, we choose a function shape with only one step per orbit. We begin by considering the step function pictured in Figure 4.1.

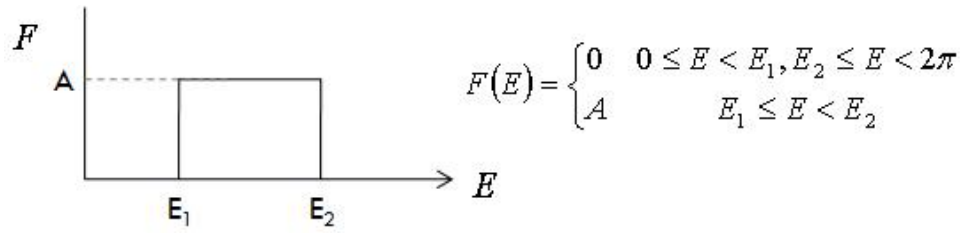

Figure 4.1: One-step circumferential acceleration

This function is defined by three parameters: A, E_1, and E_2, or equivalently, A,

$\Delta E = E_2 - E_1$, and $\overline{E} = \frac{E_1+E_2}{2}$. The Fourier series for this function is defined by

$$F = \sum_{k=0}^{\infty} \alpha_k \cos(kE) + \beta_k \sin(kE), \tag{4.11}$$

$$\alpha_0 = \frac{1}{2\pi} \int_{E_1}^{E_2} A dE, \tag{4.12}$$

$$\alpha_k = \frac{1}{\pi} \int_{E_1}^{E_2} A \cos(kE)\, dE, \tag{4.13}$$

$$\beta_k = \frac{1}{\pi} \int_{E_1}^{E_2} A \sin(kE)\, dE. \tag{4.14}$$

The 0th, 1st, and 2nd order coefficients are fixed by the targeting requirements. For simplicity in this initial analysis, we consider only the 0th and 1st order coefficients in a single-direction force,

$$\alpha_0 = \frac{1}{2\pi} \int_{E_1}^{E_2} A dE = \frac{A}{2\pi} \Delta E, \tag{4.15}$$

$$\alpha_1 = \frac{1}{\pi} \int_{E_1}^{E_2} A \cos(kE)\, dE = \frac{2A}{\pi} \cos\overline{E} \sin\left(\frac{\Delta E}{2}\right), \tag{4.16}$$

$$\beta_1 = \frac{1}{\pi} \int_{E_1}^{E_2} A \sin(kE)\, dE = \frac{2A}{\pi} \sin\overline{E} \sin\left(\frac{\Delta E}{2}\right). \tag{4.17}$$

We can re-write these equations

$$\overline{E} = \tan^{-1}\left(\frac{\beta_1}{\alpha_1}\right), \tag{4.18}$$

$$\alpha_1^2 + \beta_1^2 = \left(\frac{2A}{\pi}\right)^2 \sin^2\left(\frac{\Delta E}{2}\right), \tag{4.19}$$

$$\alpha_0 = \frac{A}{2\pi} \Delta E, \tag{4.20}$$

and find that Equations 4.19 and 4.20 lead to the equation

$$\Delta E - \frac{4\alpha_0}{\sqrt{\alpha_1^2 + \beta_1^2}} \sin\left(\frac{\Delta E}{2}\right) = 0. \tag{4.21}$$

Equation 4.21 is plotted in Figure 4.2 for various values of the coefficient $c = -\frac{4\alpha_0}{\sqrt{\alpha_1^2+\beta_1^2}}$. For a solution to exist, c must be less than approximately -2.

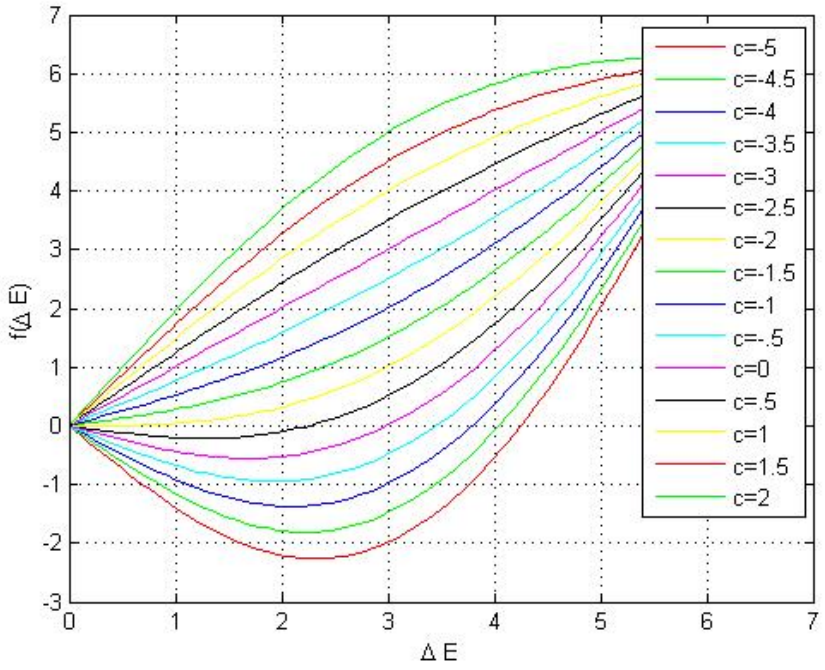

Figure 4.2: Equation 4.21, plotted for a range of values of c

Assuming the values of α_0, α_1, and β_1 from the targeting control are such that $c < -2$, we can solve for A, ΔE, and $\overline{E}$ and use these values in Equations 4.12-4.14 to generate higher-order coefficients for the force Fourier series.

Figures 4.3 and 4.4 show an example of this method. In this example, the Fourier coefficients for the original circumferential thrust acceleration were chosen to make $c < -2$ and the resulting trajectory was determined using both the Newtonian equations of motion and averaged secular equations (plotted in blue and red, respectively). Then, the above approach was used to re-calculate Fourier coefficients from order 2

to 100 and the resulting trajectories were again determined using both the Newtonian and averaged secular equations (plotted in black and green, respectively). As shown in Figure 4.3, the two different controls lead to the same trajectory.

This method is effective, but its applicability is limited by the $c < -2$ restriction. Also, the significant coefficients α_2 and β_2 are neglected, which may cause disparities between the trajectories due to the original and transformed controls, particularly over long time spans. (This re-calculating of α_2 and β_2 causes the difference between the red and green plots in Figure 4.3).

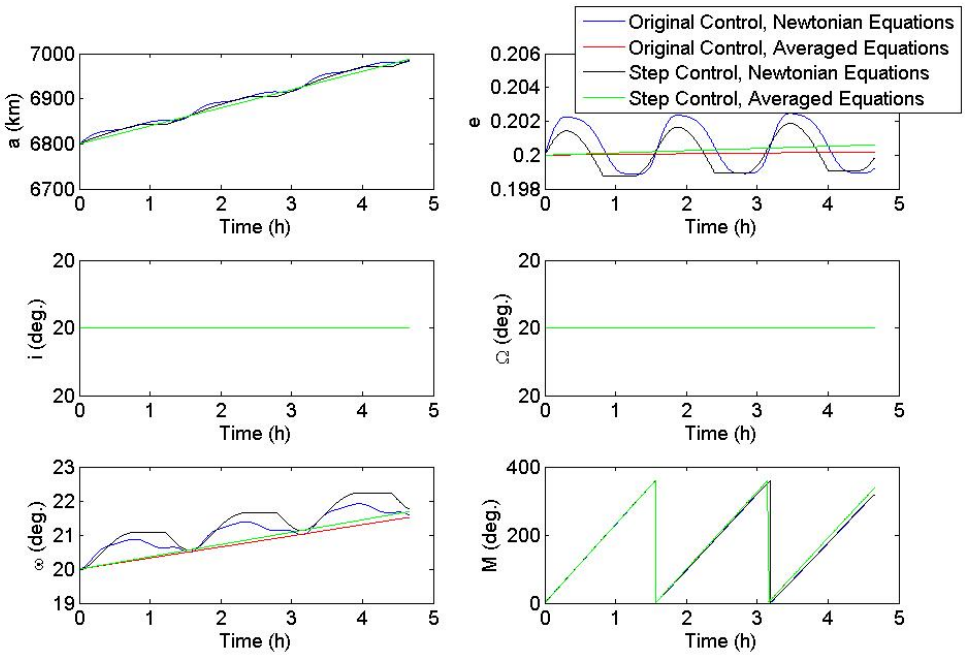

Figure 4.3: Orbital element trajectories due to "equivalent" initial and one-step controls, circumferential thrust only

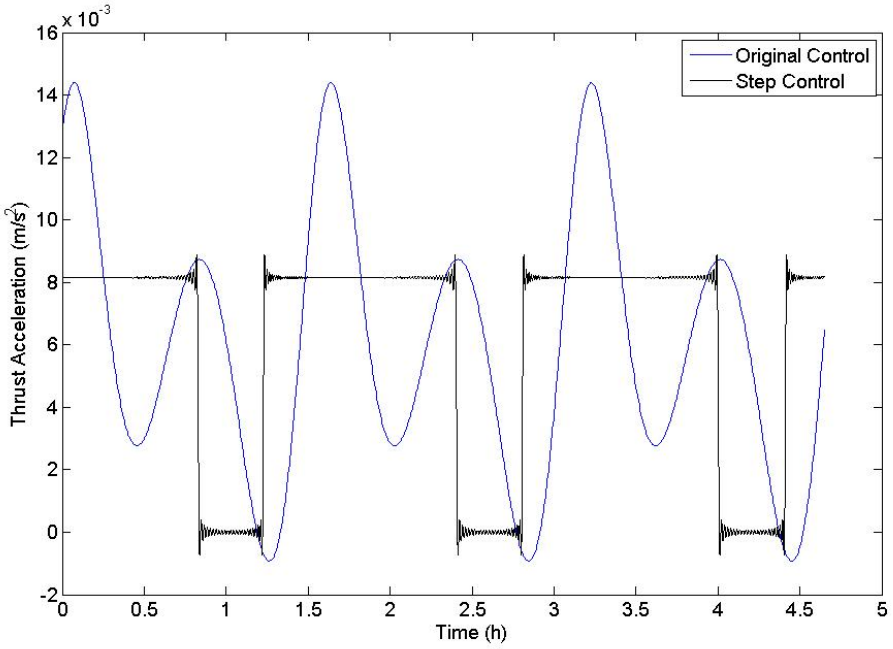

Figure 4.4: Initial, continuously-varying circumferential thrust acceleration and its "equivalent" one-step acceleration

4.4 Equivalent Control Function: Two Steps

To avoid the limitations and inaccuracies of the one-step approach, we consider a step function shape with five defining parameters, to match the maximum number of significant coefficients in each of the force directions. The function in Figure 4.5 is defined by A, E_1, E_2, E_3, and E_4 or, equivalently, A, $\Delta E_1 = E_2 - E_1$, $\overline{E}_1 = \frac{E_1+E_2}{2}$, $\Delta E_2 = E_4 - E_3$, $\overline{E}_2 = \frac{E_3+E_2}{4}$.

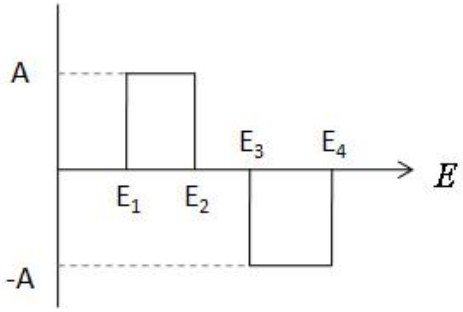

Figure 4.5: Two steps of same magnitude (opposite sign) and different duration

As above, the 0th, 1st, and 2nd order Fourier coefficients for this function are fixed by the original control,

$$\alpha_0 = \frac{A}{2\pi}\left(\Delta E_1 - \Delta E_2\right), \tag{4.22}$$

$$\alpha_1 = \frac{2A}{\pi}\left(\cos\overline{E}_1 \sin\frac{\Delta E_1}{2} - \cos\overline{E}_2 \sin\frac{\Delta E_2}{2}\right), \tag{4.23}$$

$$\beta_1 = \frac{2A}{\pi}\left(\sin\overline{E}_1 \sin\frac{\Delta E_1}{2} - \sin\overline{E}_2 \sin\frac{\Delta E_2}{2}\right), \tag{4.24}$$

$$\alpha_2 = = \frac{A}{\pi}\left(\cos 2\overline{E}_1 \sin\Delta E_1 - \cos 2\overline{E}_2 \sin\Delta E_2\right), \tag{4.25}$$

$$\beta_2 = \frac{A}{\pi}\left(\sin 2\overline{E}_1 \sin\Delta E_1 - \sin 2\overline{E}_2 \sin\Delta E_2\right). \tag{4.26}$$

By definition, there are several constraints on the angles, which can be used to find constraints between the coefficients and the amplitude,

$$0 \leq \Delta E_i \leq 2\pi, \tag{4.27}$$

$$0 \leq \overline{E}_i \leq 2\pi, \tag{4.28}$$

$$-2\pi \leq \Delta E_1 - \Delta E_2 \leq 2\pi, \tag{4.29}$$

where $i = 1, 2$. From these, and allowing A to be positive or negative, the coefficients are limited by

$$-|A| \leq \alpha_0 \leq |A|, \tag{4.30}$$

$$-|A| \leq \frac{\pi\alpha_1}{4} \leq |A|, \tag{4.31}$$

$$-|A| \leq \frac{\pi\beta_1}{4} \leq |A|, \tag{4.32}$$

$$-|A| \leq \frac{\pi\alpha_2}{2} \leq |A|, \tag{4.33}$$

$$-|A| \leq \frac{\pi\beta_2}{2} \leq |A|. \tag{4.34}$$

These relations dictate a minimum magnitude of A in order for real solutions to

exist. To solve Equations 4.22-4.26 using a numerical method, a useful starting guess is $A = \max\{\alpha_0, \frac{\pi\alpha_1}{4}, \frac{\pi\beta_1}{4}, \frac{\pi\alpha_2}{2}, \frac{\pi\beta_2}{2}\}$ or $A = \min\{\alpha_0, \frac{\pi\alpha_1}{4}, \frac{\pi\beta_1}{4}, \frac{\pi\alpha_2}{2}, \frac{\pi\beta_2}{2}\}$, whichever is largest in magnitude.

As the magnitude of A increases beyond this minimum, the relative sizes of the pulses must decrease, according to Equation 4.22. The relations

$$\begin{aligned}
\alpha_1^2 + \beta_1^2 &= \left(\frac{2A}{\pi}\right)^2 \left[\sin^2\frac{\Delta E_1}{2} + \sin^2\frac{\Delta E_2}{2}\right. \\
&\quad \left. -2\cos\left(\overline{E}_1 - \overline{E}_2\right)\sin\frac{\Delta E_1}{2}\sin\frac{\Delta E_2}{2}\right], \qquad (4.35) \\
\alpha_2^2 + \beta_2^2 &= \left(\frac{A}{\pi}\right)^2 \left[\sin^2\Delta E_1 + \sin^2\Delta E_2\right. \\
&\quad \left. -2\cos 2\left(\overline{E}_1 - \overline{E}_2\right)\sin\frac{\Delta E_1}{2}\sin\frac{\Delta E_2}{2}\right] \qquad (4.36)
\end{aligned}$$

may also be useful in choosing initial guesses for the unknown parameters.

Figures 4.6 - 4.8 show an example of this method. The initial control was the solution to a targeting problem in which the out-of-plane orbital elements were changed over three revolutions by thrust in the normal direction only. Matlab's fsolve function was used to solve Equations 4.22 - 4.26, initialized with guesses based on the relations described above. The coefficients of the step control were then calculated up to order 100.

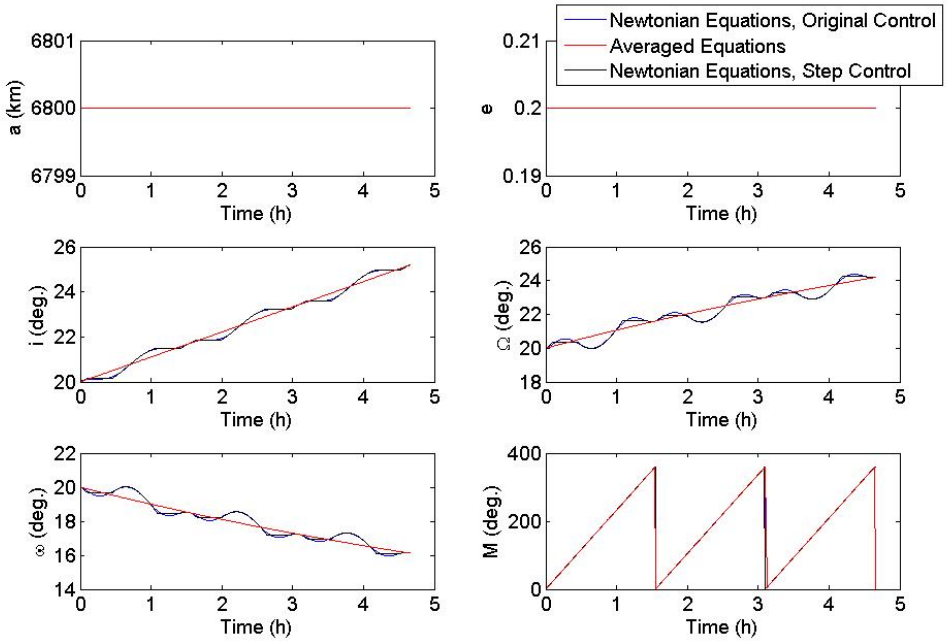

Figure 4.6: Orbital element trajectories due to "equivalent" inital and two-step controls, normal thrust only

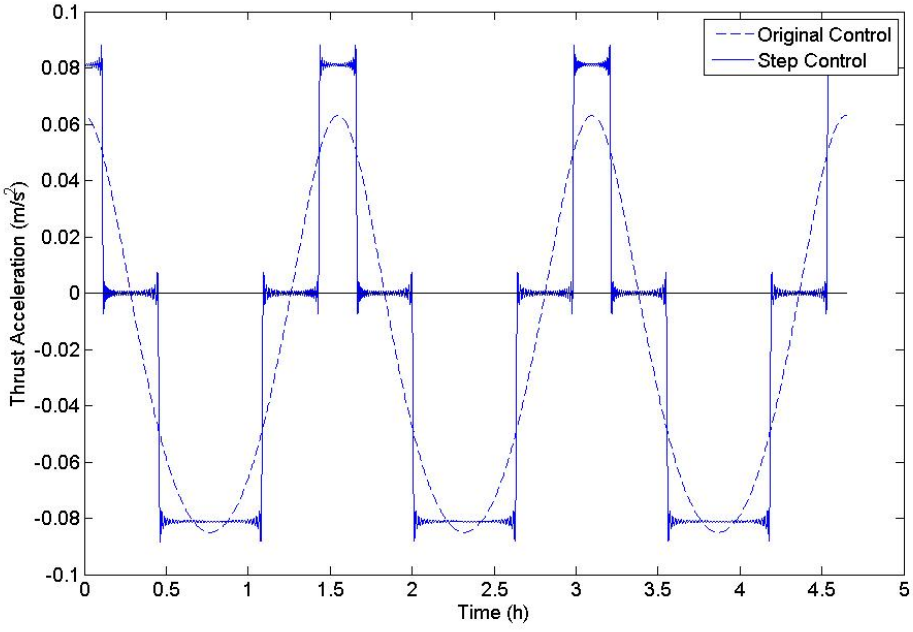

Figure 4.7: Initial, continuously-varying normal thrust acceleration and its "equivalent" two-step acceleration, plotted versus time

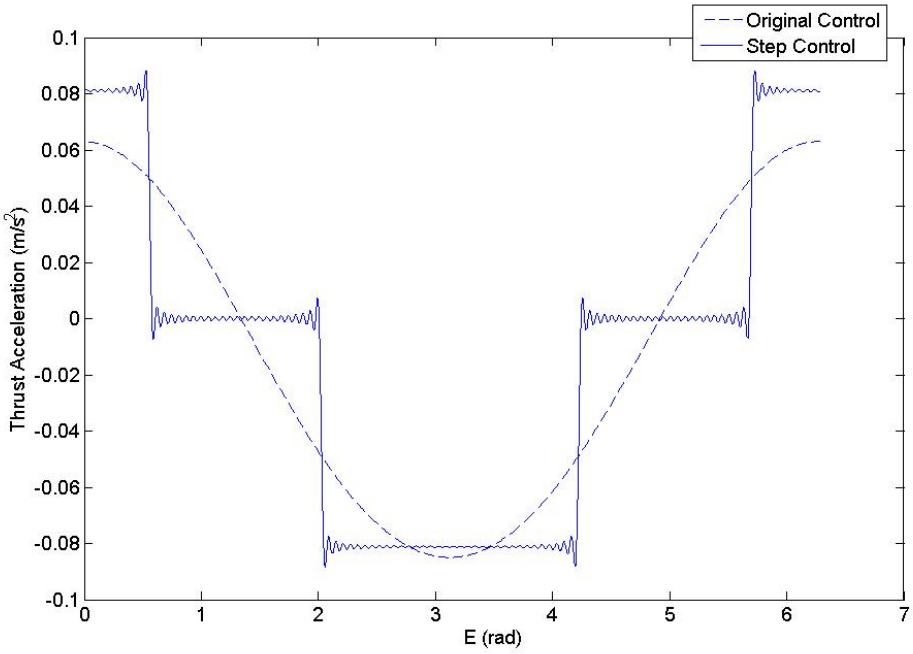

Figure 4.8: Initial, continuously-varying normal thrust acceleration and its "equivalent" two-step acceleration, plotted versus eccentric anomaly

This approach transforms the control into an "equivalent" step control. The velocity increment, ΔV, for the orbit transfer with the original control was 834.5 m/s. The ΔV for the transfer with the step control was 761.1 m/s, an 8.8% decrease.

Solutions have been found to exist for most cases when the initial control is the solution to a targeting problem. In some cases, multiple solutions for A, $\overline{E}_{1,2}$, and $\Delta E_{1,2}$ can be found, although these different solution sets usually describe the same step function. For example, in the single-direction thrust case shown above, two sets of solutions were found for the parameters of the step function. These two solutions are shown in Table 4.2. Both sets lead to the same values for the Fourier coefficients; thus they describe the same step control.

Figures 4.9 - 4.12 show another example of this method. In this example, the initial control was the solution to a targeting problem in which all six orbital elements were changed over three revolutions. Each directional component of the control was then transformed into a two-step control with equivalent average trajectory dynamics.

Table 4.2: Two sets of solutions that describe the same two-step control in the normal thrust example above

	Solution 1	Solution 2
$A(m/s^2)$	0.0811	0.0811
$\overline{E}_1(deg.)$	41.2071	0.8144
$\overline{E}_1(deg.)$	136.9942	179.0149
$\Delta E_1(deg.)$	149.6394	65.5979
$\Delta E_2(deg.)$	210.0291	125.9820

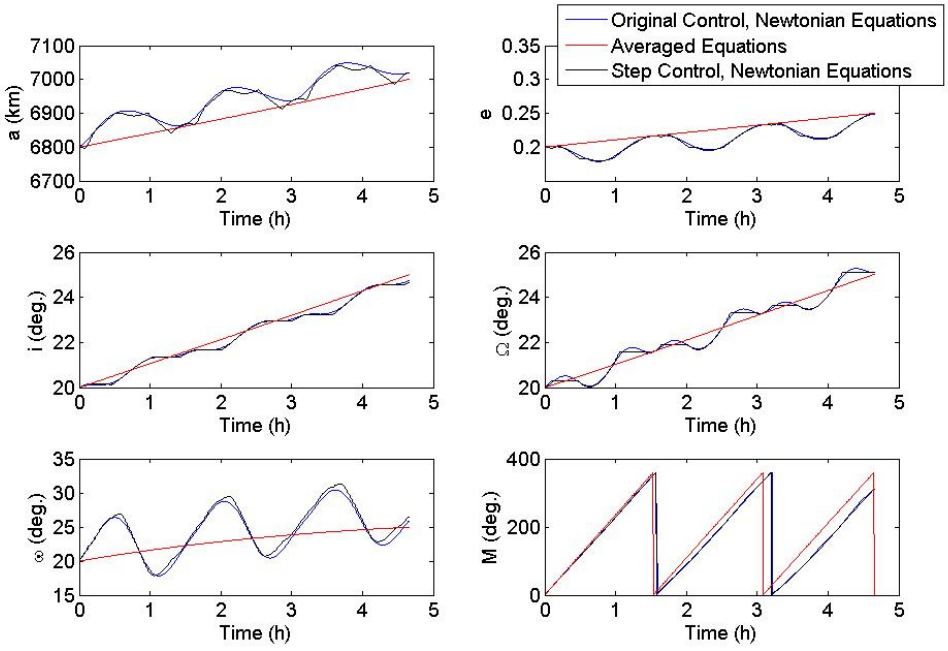

Figure 4.9: Orbital element trajectories due to "equivalent" inital and two-step controls, 3D thrust

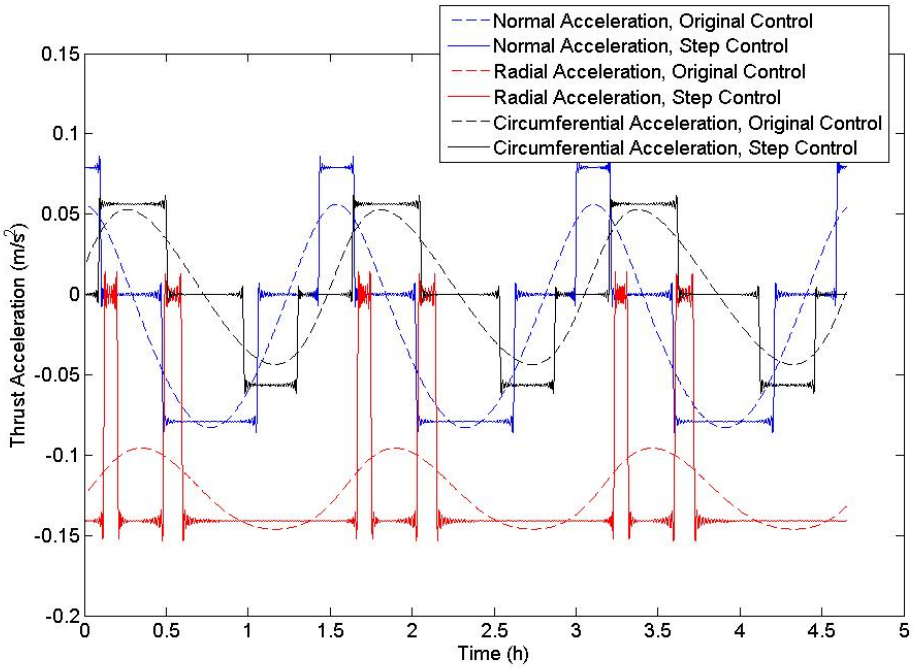

Figure 4.10: Initial, continuously-varying 3D thrust acceleration and its "equivalent" two-step acceleration, plotted versus time

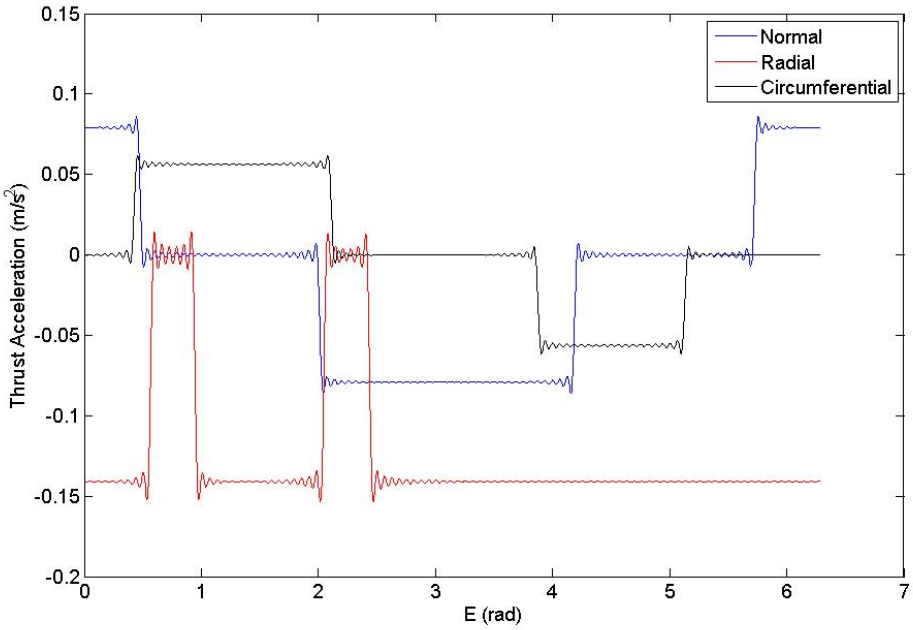

Figure 4.11: Initial, continuously-varying normal 3D acceleration and its "equivalent" two-step acceleration, plotted versus eccentric anomaly

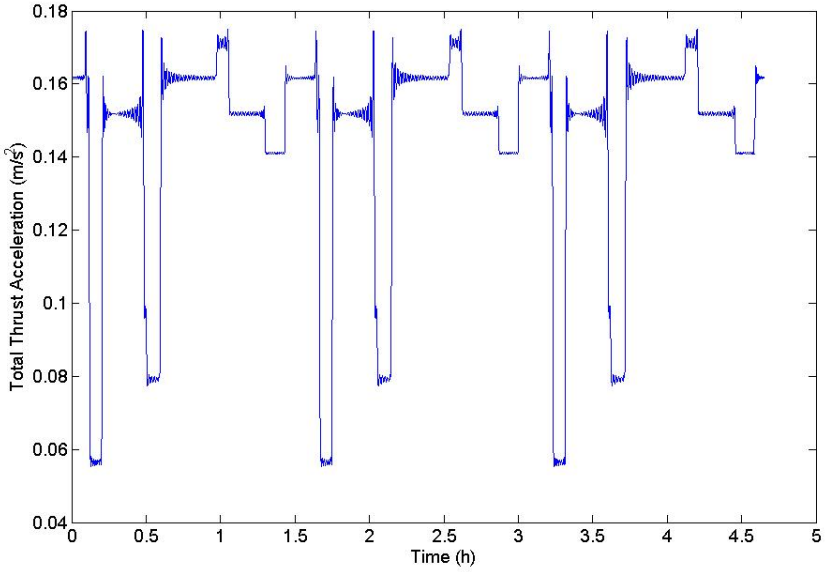

Figure 4.12: Total thrust acceleration of 3D thrust example. This plot shows the total thrust acceleration, $\sqrt{F_W^2 + F_R^2 + F_S^2}$, after each directional component was transformed into a two-step control. If one engine were to implement this control profile, considerable throttling would still be required.

This approach effectively transforms each directional component of the control into an "equivalent" step control. The velocity increment, ΔV, for the orbit transfer with the original control was 2320.6 m/s. The ΔV for the transfer with the step control was 2436.5 m/s, a 5% increase. Simulations indicate that transformation to a step control in this manner usually results in a decrease or small increase in ΔV.

4.5 Constant-Magnitude Control

These transformations to equivalent controls are motivated by the operational profiles of low-thrust propulsion systems. The method described in the previous section transforms each directional component of the control to a step function, which is a valuable improvement, but does not consider the relations between the directional components. As shown in Figure 4.12, this can result in a lot of switching for the spacecraft engine, which must change its thrust direction and magnitude at each

increment.

A more applicable approach should consider the control for all thrust directions simultaneously. We consider a control made up of three steps of constant magnitude, as pictured in Figure 4.13. The direction of the force, λ, stays constant throughout the step, but may be different for each step. To simplify the calculations, we consider the case of planar thrust only, as shown in Figure 4.14.

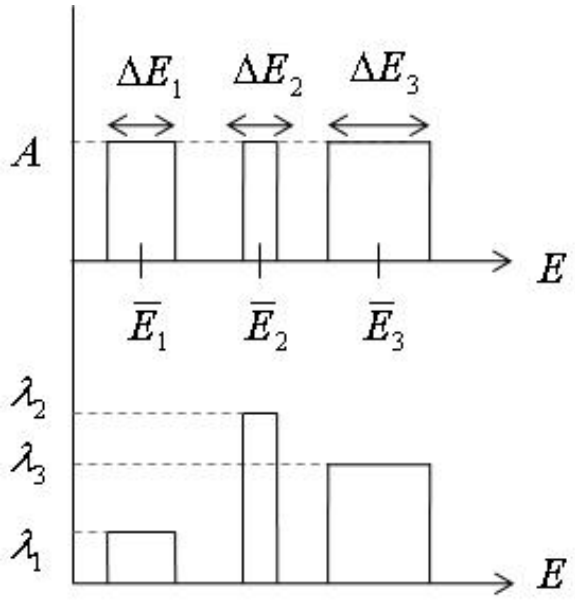

Figure 4.13: Constant-magnitude planar acceleration profile

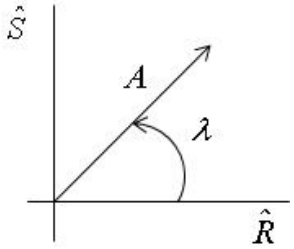

Figure 4.14: Planar acceleration angle definition

This thrust acceleration profile has 10 unknown parameters: A, $\overline{E}_1$, $\overline{E}_2$, $\overline{E}_3$, ΔE_1, ΔE_2, ΔE_3, λ_1, λ_2, and λ_3.

Using the definitions of Fourier coefficients, we can write equations for the nine key acceleration coefficients in terms of these unknown parameters (the tenth coefficient,

α_2^R, does not appear in the averaged equations, so we set it to zero). We solve for the unknowns, then use them to calculate higher-order Fourier coefficients to transform the control into step form,

$$\alpha_0^R = \frac{A}{2\pi}\sum_{i=1}^{3}\left(\cos\left(\lambda_i\right)\Delta E_i\right), \tag{4.37}$$

$$\alpha_k^R = \frac{2A}{k\pi}\sum_{i=1}^{3}\left(\cos\left(\lambda_i\right)\cos\left(k\overline{E}_i\right)\sin\left(\frac{k\Delta E_i}{2}\right)\right), \tag{4.38}$$

$$\beta_k^R = \frac{2A}{k\pi}\sum_{i=1}^{3}\left(\cos\left(\lambda_i\right)\sin\left(k\overline{E}_i\right)\sin\left(\frac{k\Delta E_i}{2}\right)\right), \tag{4.39}$$

$$\alpha_0^S = \frac{A}{2\pi}\sum_{i=1}^{3}\left(\sin\left(\lambda_i\right)\Delta E_i\right), \tag{4.40}$$

$$\alpha_k^S = \frac{2A}{k\pi}\sum_{i=1}^{3}\left(\sin\left(\lambda_i\right)\cos\left(k\overline{E}_i\right)\sin\left(\frac{k\Delta E_i}{2}\right)\right), \tag{4.41}$$

$$\beta_k^S = \frac{2A}{k\pi}\sum_{i=1}^{3}\left(\sin\left(\lambda_i\right)\sin\left(k\overline{E}_i\right)\sin\left(\frac{k\Delta E_i}{2}\right)\right), \tag{4.42}$$

An example of this method is shown below. The initial control was the solution to a targeting problem in which semi-major axis was increased and eccentricity was decreased over three orbits while the other orbital elements were held constant. Table 4.3 shows the parameters of the solution step function. Figures 4.15 - 4.17 show the implementation of this solution.

Table 4.3: Parameters of example constant-magnitude planar step function

$A\ (m/s^2)$	0.1062	$\Delta E_2\ (deg.)$	59.8
$\overline{E}_1\ (deg.)$	114.3	$\Delta E_3\ (deg.)$	62.1
$\overline{E}_2\ (deg.)$	247.8	$\lambda_1\ (deg.)$	167.3
$\overline{E}_3\ (deg.)$	337.4	$\lambda_2\ (deg.)$	185.6
$\Delta E_1\ (deg.)$	181.8	$\lambda_3\ (deg.)$	186.7

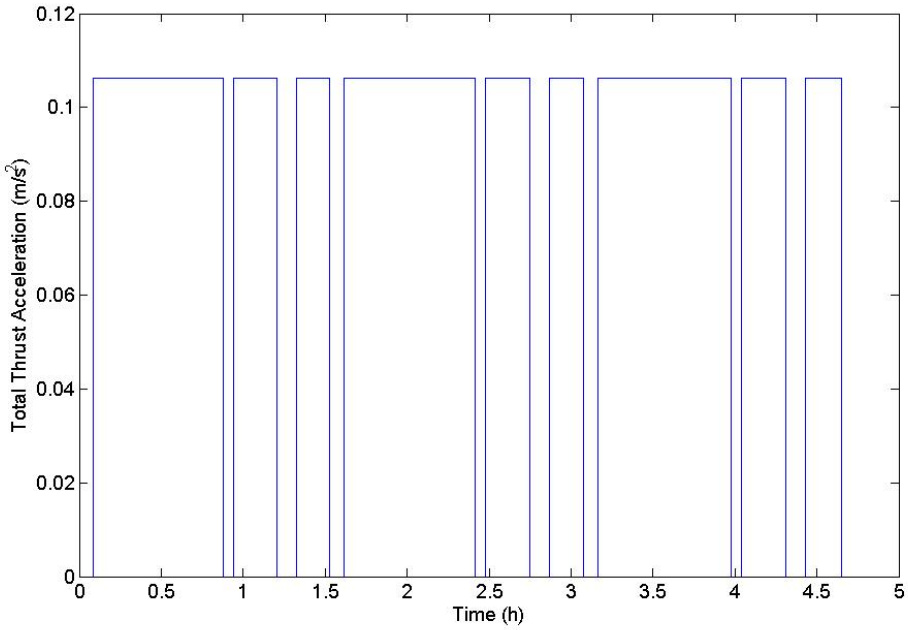

Figure 4.15: Thrust acceleration profile based on step parameters

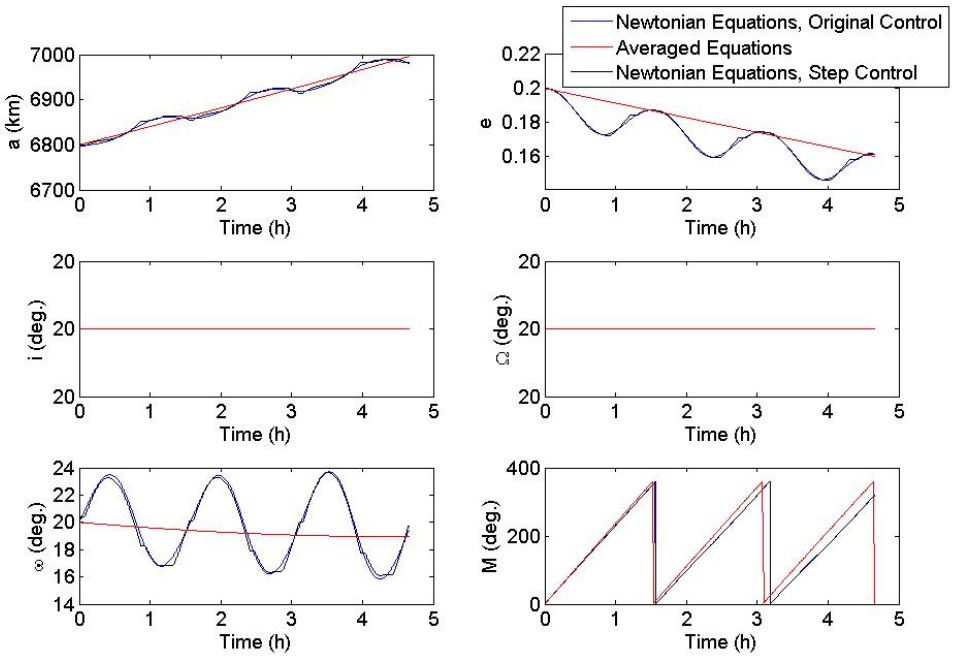

Figure 4.16: Orbital element trajectories due to "equivalent" inital and planar constant-magnitude step control

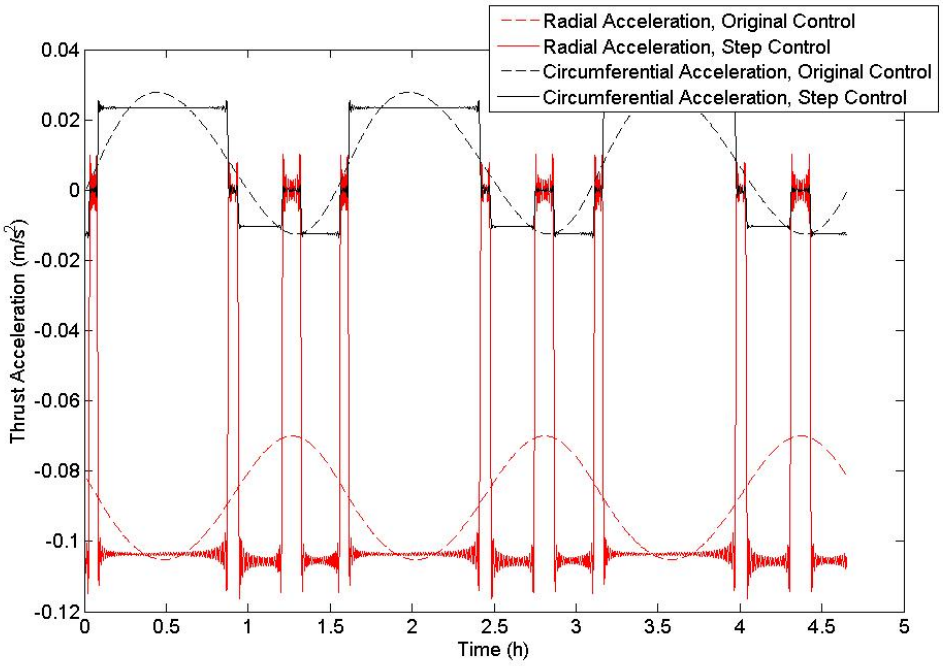

Figure 4.17: Initial, continuously-varying planar thrust acceleration and its "equivalent" planar constant-magnitude acceleration, plotted versus time

The velocity increment, ΔV, for the orbit transfer with the original control was 1503.8 m/s. The ΔV for the transfer with the constant-magnitude step control was 1515.6 m/s, a 0.79% increase.

To make this method fully general, out-of-plane thrust acceleration should be included. This would require a step control defined by 14 parameters with a single acceleration magnitude and variable thrust direction in three dimensions. Any function shape that meets these criteria could be used. For example, four steps of the same magnitude and duration and different angles, as shown in Figure 4.18, could be defined by the 14 parameters A, E_1, E_2, E_3, E_4, ΔE, λ_1, λ_2, λ_3, λ_4, ϕ_1, ϕ_2, ϕ_3, and ϕ_4.

To shape the original control into this form, we would write the equations for the 14 key coefficients in terms of these 14 unknown parameters, solve for the unknowns, then use them to calculate higher-order Fourier coefficients of the thrust acceleration.

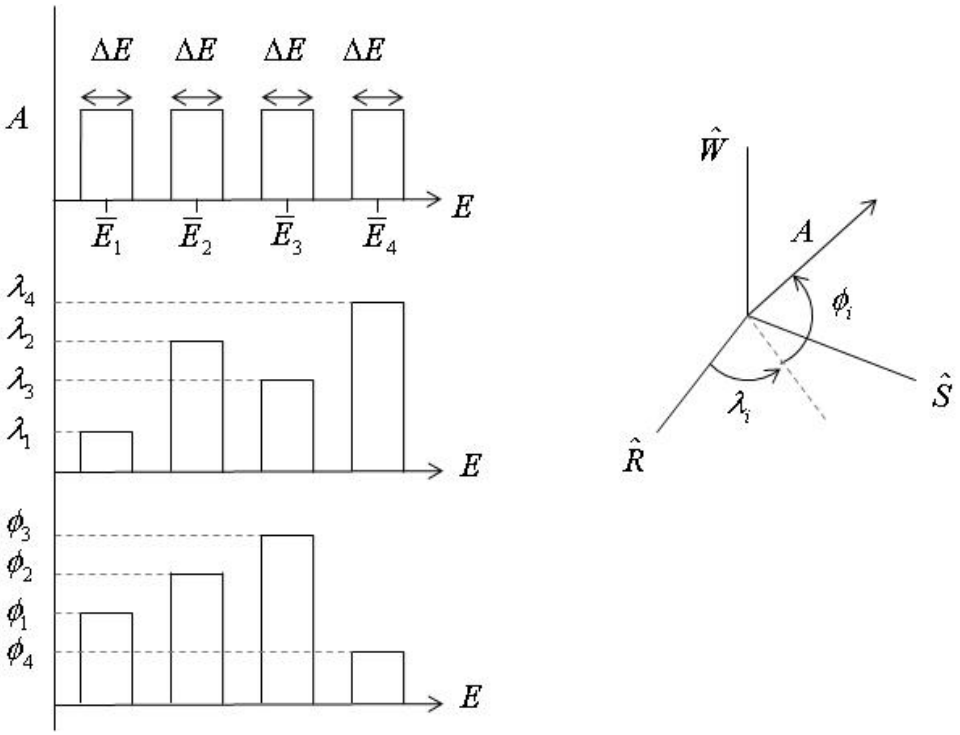

Figure 4.18: Four steps of constant magnitude and duration, varying direction in 3D

The equations for the 14 coefficients are

$$\alpha_0^R = \frac{A}{2\pi}\sum_{i=1}^{4}\left(\cos\left(\phi_i\right)\cos\left(\lambda_i\right)\Delta E\right), \tag{4.43}$$

$$\alpha_k^R = \frac{2A}{k\pi}\sum_{i=1}^{4}\left(\cos\left(\phi_i\right)\cos\left(\lambda_i\right)\cos\left(k\overline{E}_i\right)\sin\left(\frac{k\Delta E}{2}\right)\right), \tag{4.44}$$

$$\beta_k^R = \frac{2A}{k\pi}\sum_{i=1}^{4}\left(\cos\left(\phi_i\right)\cos\left(\lambda_i\right)\sin\left(k\overline{E}_i\right)\sin\left(\frac{k\Delta E}{2}\right)\right), \tag{4.45}$$

$$\alpha_0^W = \frac{A}{2\pi}\sum_{i=1}^{4}\left(\sin\left(\phi_i\right)\Delta E\right), \tag{4.46}$$

$$\alpha_k^W = \frac{2A}{k\pi}\sum_{i=1}^{4}\left(\sin\left(\phi_i\right)\cos\left(k\overline{E}_i\right)\sin\left(\frac{k\Delta E}{2}\right)\right), \tag{4.47}$$

$$\beta_k^W = \frac{2A}{k\pi}\sum_{i=1}^{4}\left(\sin\left(\phi_i\right)\sin\left(k\overline{E}_i\right)\sin\left(\frac{k\Delta E}{2}\right)\right), \tag{4.48}$$

$$\alpha_0^S = \frac{A}{2\pi}\sum_{i=1}^{4}\left(\cos\left(\phi_i\right)\sin\left(\lambda_i\right)\Delta E\right), \tag{4.49}$$

$$\alpha_k^S = \frac{2A}{k\pi}\sum_{i=1}^{4}\left(\cos\left(\phi_i\right)\sin\left(\lambda_i\right)\cos\left(k\overline{E}_i\right)\sin\left(\frac{k\Delta E}{2}\right)\right), \tag{4.50}$$

$$\beta_k^S = \frac{2A}{k\pi}\sum_{i=1}^{4}\left(\cos\left(\phi_i\right)\sin\left(\lambda_i\right)\sin\left(k\overline{E}_i\right)\sin\left(\frac{k\Delta E}{2}\right)\right), \tag{4.51}$$

where $k = 1, 2$ and $\beta_2^R = 0$.

An example of a control shaped in this manner is shown in Table 4.4 and Figures 4.19 - 4.22. With this control shape, it is common for solutions to Equations 4.43 - 4.51 to exist that do not describe the intended shape. In this example, the solution $\Delta E = -175.3757°$ is not a realistic value for the width of the thrust intervals, which leads to overlap of the intervals and changes in the total acceleration magnitude. It is difficult to find solutions in which this overlap and thrust variation does not occur.

Nonetheless, solutions of this type may still be useful. Despite the changes in thrust magnitude, these solutions still require less switching than the separate-direction model described in Section 4.4. In many cases, operators may actually prefer to switch between a few throttle levels and keep the thruster running constantly, rather than repeatedly shutting down and restarting.

Table 4.4: Parameters of example 3D step function

$A\ (m/s^2)$	0.0948	$\lambda_2\ (deg.)$	1.3510
$\overline{E}_1\ (deg.)$	11.7876	$\lambda_3\ (deg.)$	7.9511
$\overline{E}_2\ (deg.)$	155.9458	$\lambda_4\ (deg.)$	79.1455
$\overline{E}_3\ (deg.)$	271.8353	$\phi_1\ (deg.)$	10.4828
$\overline{E}_4\ (deg.)$	348.7416	$\phi_2\ (deg.)$	29.6743
$\Delta E\ (deg.)$	-175.3757	$\phi_3\ (deg.)$	21.2180
$\lambda_1\ (deg.)$	-41.4604	$\phi_4\ (deg.)$	-64.6803

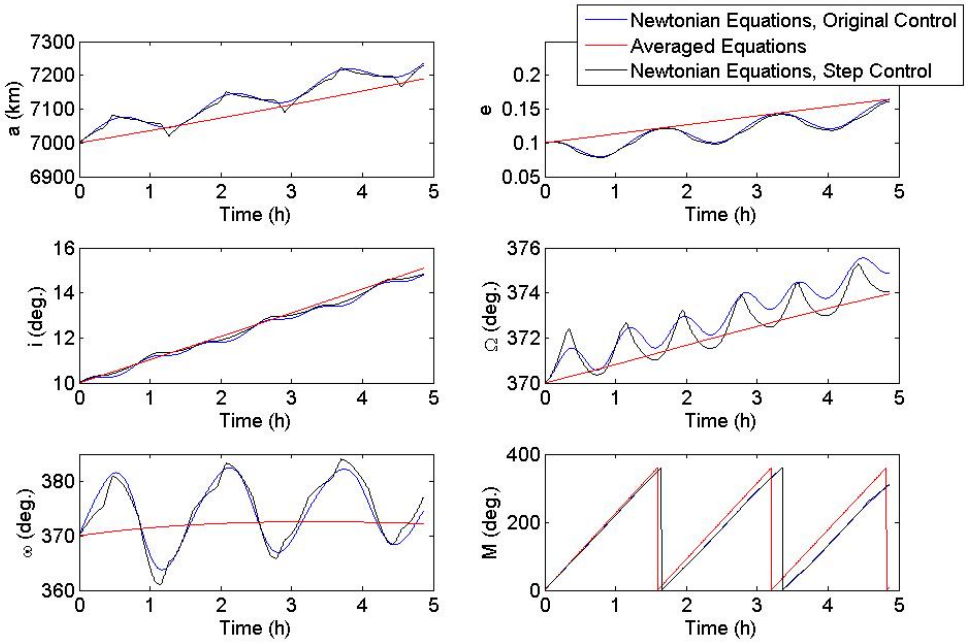

Figure 4.19: Orbital element trajectories due to "equivalent" inital and 3D step control

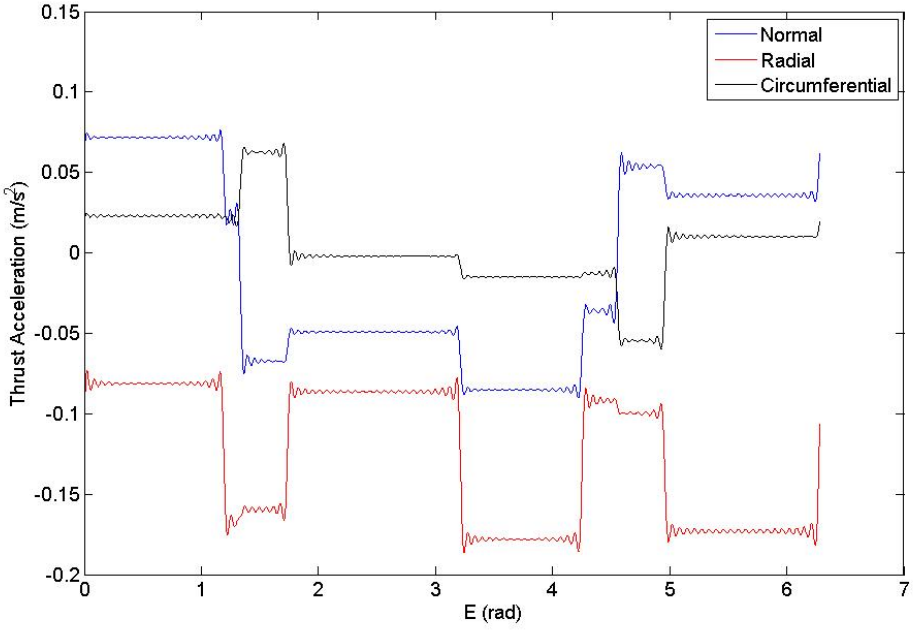

Figure 4.20: Initial, continuously-varying planar thrust acceleration and its "equivalent" 3D acceleration components, plotted versus eccentric anomaly

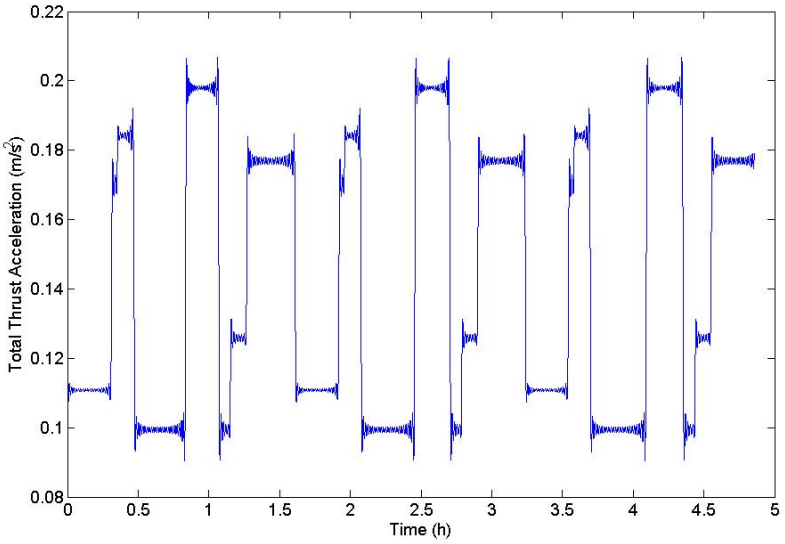

Figure 4.21: Total thrust acceleration of 3D step control example

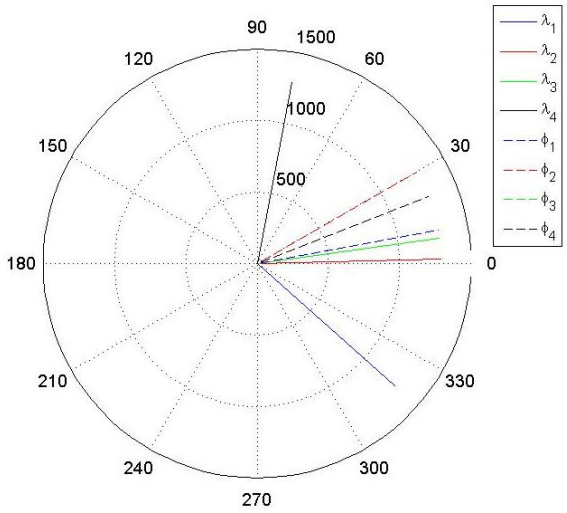

Figure 4.22: Polar plot of acceleration components for 3D step control example

4.6 Impulsive Controls

This approach can also be used to model the dynamics of spacecraft with impulsive controls. An impulsive change in velocity may be approximated as a step function, as shown in Figure 4.1, where ΔE approaches zero. Thus the function to be modeled by a Fourier series has the shape shown in Figure 4.23. This function can be described

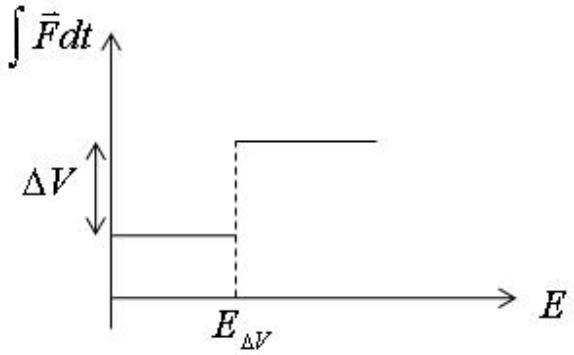

Figure 4.23: Impulsive control

by the delta function,

$$F(E) = \Delta V \delta (E - E_{\Delta V}) . \tag{4.52}$$

The Fourier series for this function can be found with Equations A.1 - A.4. For a function with n impulses, the Fourier coefficients are

$$\alpha_0 = \frac{1}{2\pi} \sum_{i=1}^{n} \Delta V_i, \tag{4.53}$$

$$\alpha_k = \frac{1}{\pi} \sum_{i=1}^{n} \Delta V_i \cos (k E_{\Delta V_i}) , \tag{4.54}$$

$$\beta_k = \frac{1}{\pi} \sum_{i=1}^{n} \Delta V_i \sin (k E_{\Delta V_i}) . \tag{4.55}$$

Figures 4.24 and 4.25 show an example of this type of control. From its initial orbit, the spacecraft undergoes a ΔV in the circumferential direction of 50 m/s at $E_{\Delta V} = \frac{\pi}{4}$.

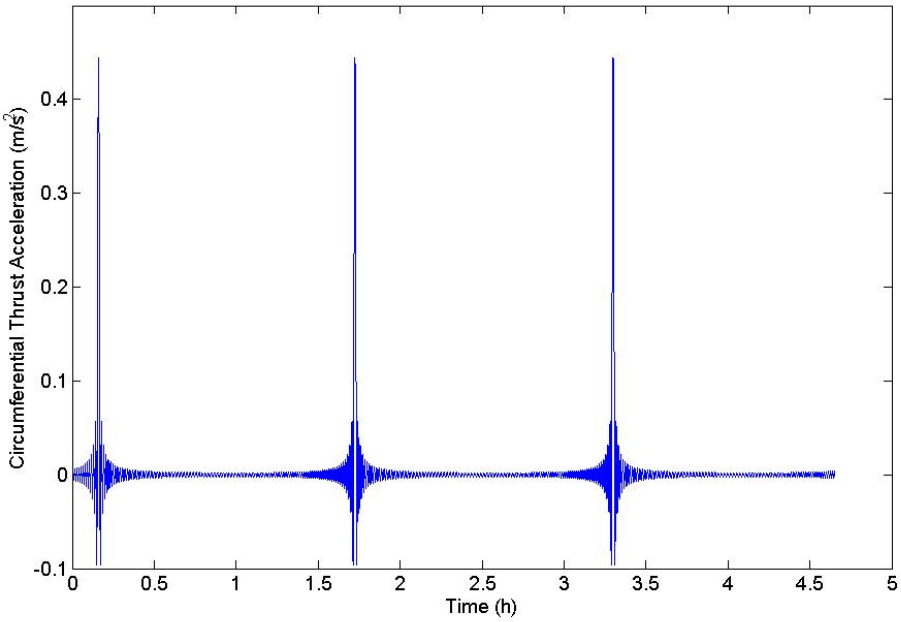

Figure 4.24: Fourier series for impulsive thrust acceleration, evaluated up to 100 terms

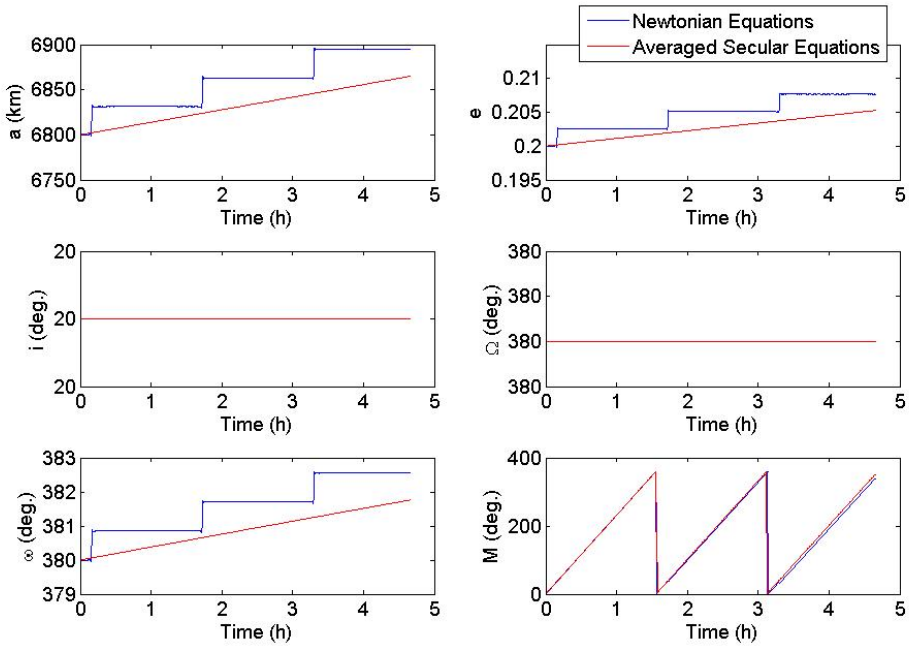

Figure 4.25: Orbital element trajectory due to impulsive control

Equations 4.53 - 4.55 have a specific structure that may be useful for determining whether an unfamiliar spacecraft has performed an impulsive maneuver. Given two or more state observations of a spacecraft, we can use one of the targeting methods in Chapter 3 to determine the 14 coefficients of the average control that connects them. We can then evaluate the ratios

$$\frac{\beta_1^{(R,W,S)}}{\alpha_1^{(R,W,S)}} = \tan E_{\Delta V}, \tag{4.56}$$

$$\frac{\beta_2^{(R,W,S)}}{\alpha_2^{(R,W,S)}} = \tan 2E_{\Delta V}, \tag{4.57}$$

and solve for $E_{\Delta V}$. If these result in the same value for $E_{\Delta V}$, we can conclude that the spacecraft performed one impulsive maneuver with a ΔV given by Equation 4.53.

We can also shape a time-varying control into an impulsive control using an approach similar to the methods described in the previous sections. If we consider each thrust direction separately, as in Section 4.4, the impulsive control in each direction must have five degrees of freedom. We choose the control shape shown in Figure 4.26.

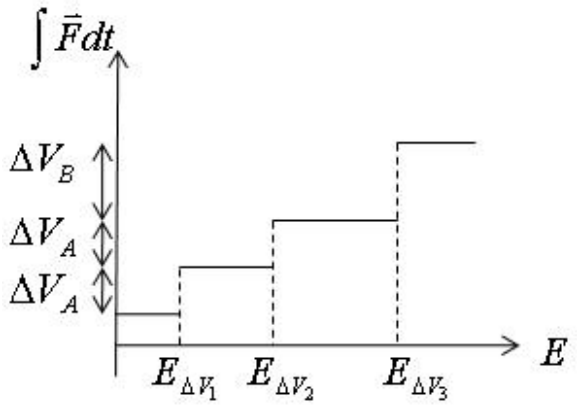

Figure 4.26: Three impulses, two of which have the same ΔV

We solve Equations 4.53 - 4.55 with $k = 1, 2$ for the unknowns, ΔV_A, ΔV_B, $E_{\Delta V_1}$, $E_{\Delta V_2}$, and $E_{\Delta V_3}$, then calculate the Fourier coefficients from order 3 to 100. The resulting control and trajectory are shown in Figures 4.27 - 4.29. The ΔV of the original trajectory is 285.9 m/s; the transformed ΔV is 858.7 m/s.

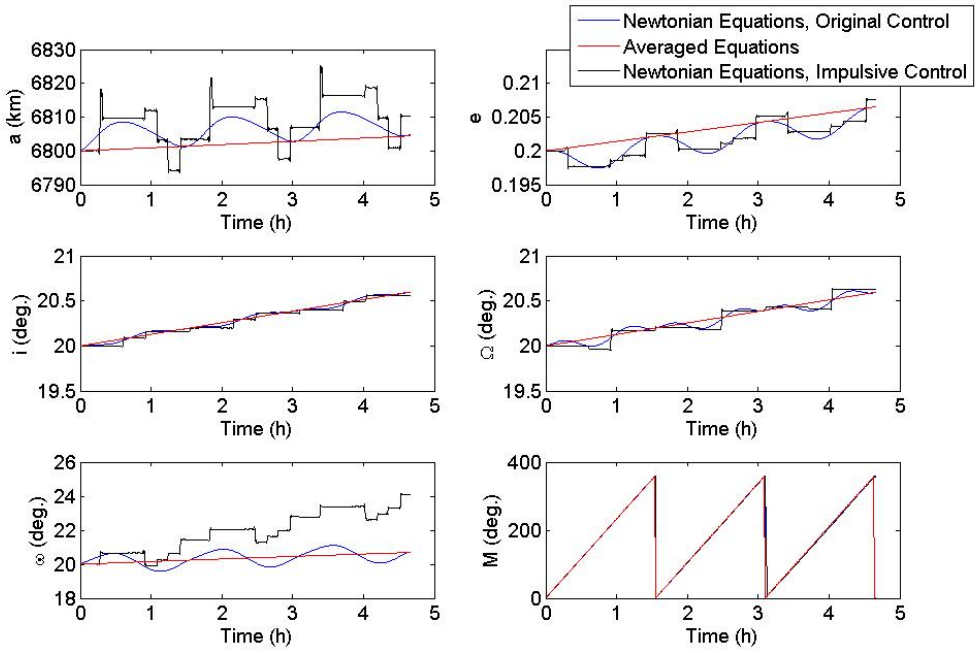

Figure 4.27: Orbital element trajectories due to "equivalent" initial and impulsive controls

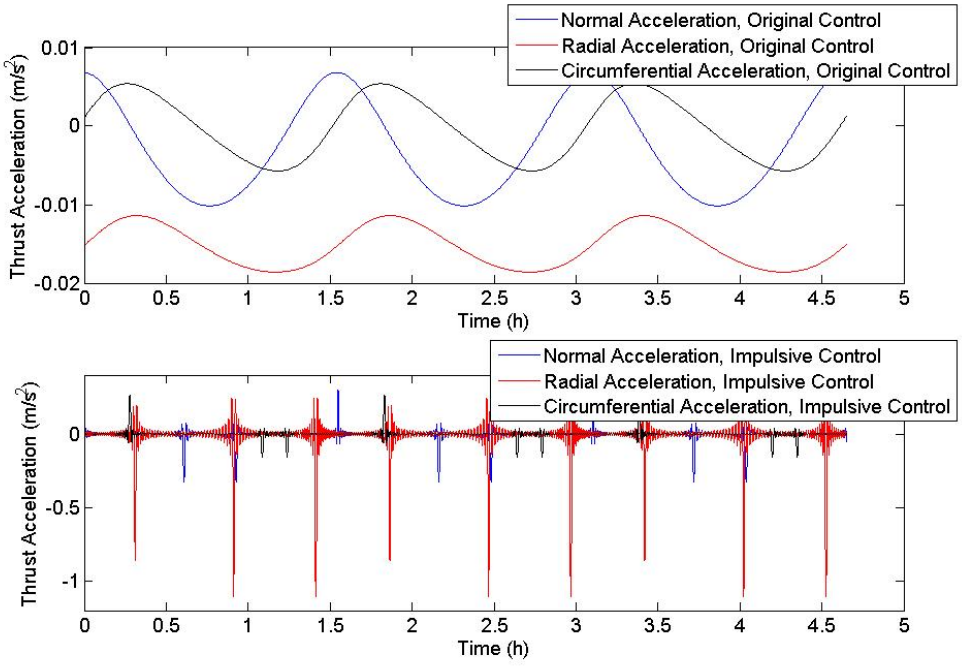

Figure 4.28: Initial, continuously-varying planar thrust acceleration and its "equivalent" impulsive acceleration, plotted versus time

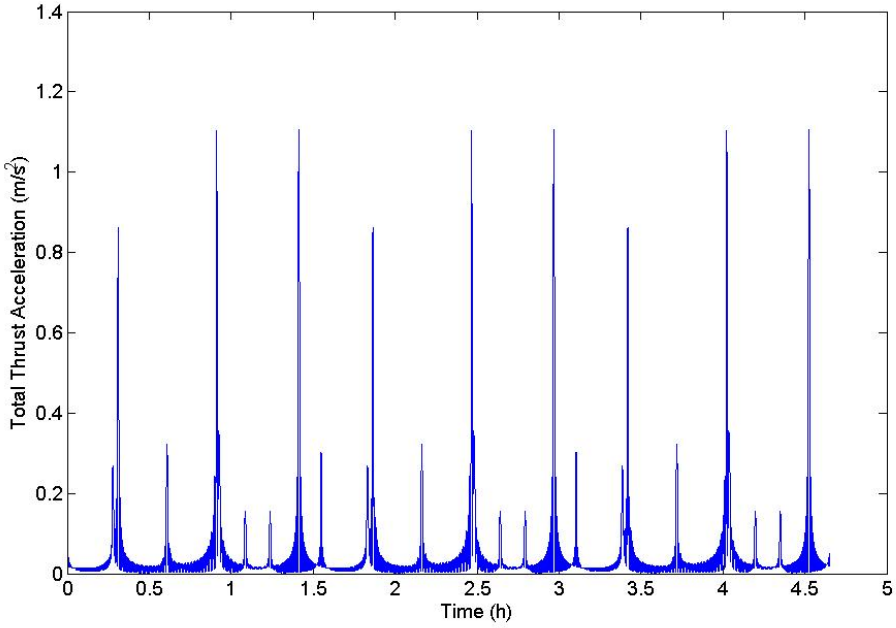

Figure 4.29: Total impulsive thrust acceleration. This plot shows the total thrust acceleration, $\sqrt{F_W^2 + F_R^2 + F_S^2}$, after each directional component was transformed into an impulsive control.

In general, an equivalent impulsive trajectory can only be found if the original control coefficients are relatively small. In these simulations, with low Earth orbit initial conditions, the control coefficients had to be less than approximately 100 km/h^2 (0.0077 m/s^2) in magnitude in order for the extended Fourier series to describe an impulsive function and for the averaged equations to accurately determine the trajectory.

Although this limits the applicability of this approach, the ability to represent impulsive ΔV dynamics with the averaged secular equations is still useful for comparing low-thrust results with traditional impulsive controls.

CHAPTER 5

Applications

Trajectory analysis using the reduced Fourier coefficients has several potential fields of application, including mission design and space situational awareness. The different methods described above for solving orbital targeting problems and calculating equivalent control laws have different strengths and weaknesses that make them appropriate, respectively, for these different applications.

The averaged secular equations can be used in low-thrust mission design to evaluate the control laws required for desired orbital trajectories. The solutions obtained from these equations are not, in themselves, optimal, but they satisfy the proposed targeting problem. Thus, they could serve as useful initial estimates for other optimization methods.

Using the averaged equations, mission planners can efficiently estimate the control laws for a large number of potential orbital paths, to compare the fuel costs and other trajectory characteristics. Once a baseline mission profile has been selected, these equations can be used to quickly determine the feasibility and cost of proposed deviations from the selected path.

Generally, the two-point boundary value targeting method is best suited for mission design applications. The precise agreement of the averaged trajectory with the target states is desirable, and discontinuities in the true trajectory may be inconsequential in the early mission planning stages, particularly if the solutions will later be used to initialize other optimization methods. When the target states represent flex-

ible objectives, rather than strict targets, the segmented solutions may help mission designers to shift the target states to lower-cost alternatives. The two-point boundary value method also converges fastest and doesn't require the user to define a weighting matrix, which can be subjective.

Space situational awareness (SSA) problems can also be solved using the averaged secular equations. Given a few discrete observations of a suspected low-thrust spacecraft, these equations can reconstruct its orbital path and identify the fundamental characteristics of the control law used. The parameters of an impulsive maneuver can be determined using Equations 4.53 - 4.55 as described in Section 4.6. If, instead, the spacecraft is found to have performed a low-thrust maneuver, observers could estimate the amount of fuel remaining and extrapolate to predict the future trajectory.

The least-squares targeting method is generally most appropriate for SSA problems. In these cases, precise agreement between the calculated and actual trajectory may be less important than simply finding a reasonable estimate for the thrust profile and fuel consumption. The SMART-1 example in Section 3.2 illustrates the process of reconstructing a trajectory from a few known states using this method. Another example of an SSA problem is shown below.

Table 5.1 shows a set of four states at which a hypothetical spacecraft has been observed over six days. The trajectory is approaching the orbit of the International Space Station. In this scenario, analysts would need to quickly characterize the spacecraft's propulsion system and control law and determine its future path.

Figures 5.1 - 5.3 show the results of the least-squares targeting in the averaged equations through this set of states, using the 14 critical control coefficients. The targeting alorithm was terminated after four iterations, when the coefficients changed by less than 0.1% between iterations. The mean difference between the average trajectory and the target states is shown in Table 5.2. In this simulation, the mean

Table 5.1: Target states for SSA example

	Time (h)	a (km)	e	i (deg.)	Ω (deg.)	ω (deg.)	M (deg.)
Initial State	0	6713.0	0.7842e-3	51.6	234.0	300.6	0
Target 1	28.94	6720.0	0.7841e-3	51.6	234.0	300.6	0.0974
Target 2	62.55	6728.2	0.7867e-3	51.6	234.0	300.3	0.2865
Target 3	90.15	6734.9	0.7936e-3	51.6	234.0	300.0	0.8480

anomaly was given a low weighting value in order to improve the accuracy of the other orbital elements.

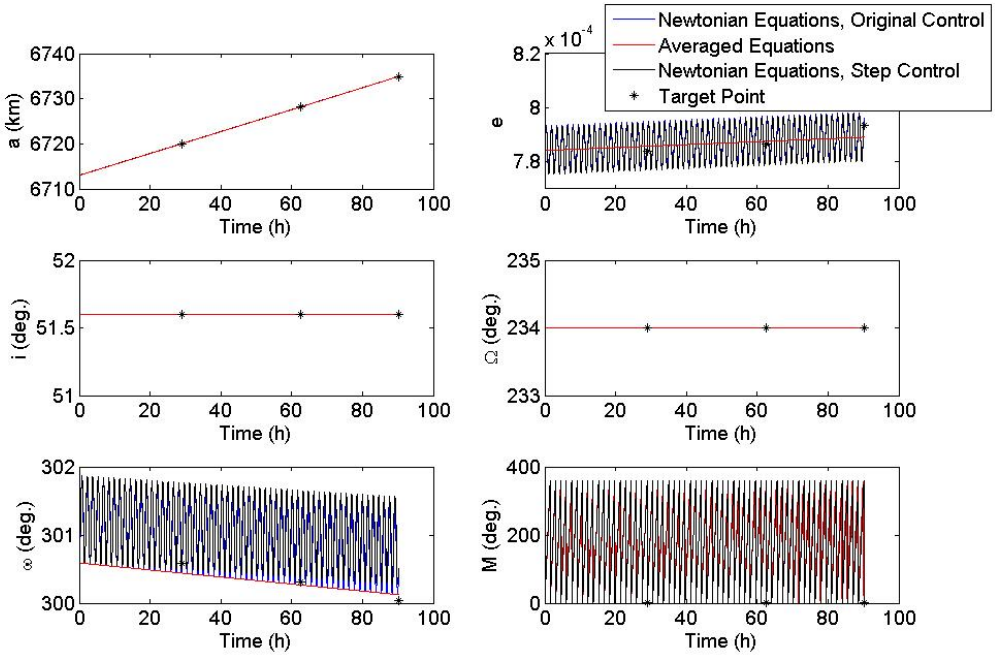

Figure 5.1: Orbital element trajectory calculated by least-squares method for SSA targeting example

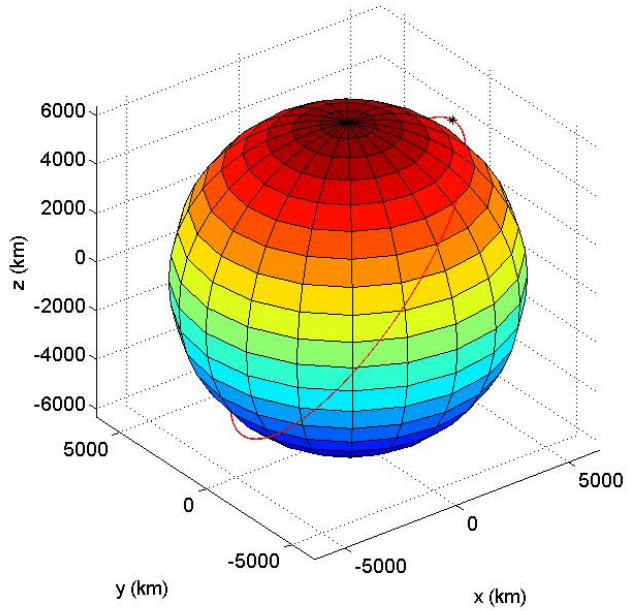

Figure 5.2: 3D trajectory calculated by least-squares method for SSA targeting example

Table 5.2: Mean difference between calculated average state and target state for SSA example

	a (km)	e	i (deg.)	Ω (deg.)	ω (deg.)	M (deg.)
LSQ	0.0306	-7.3654e-007	2.7486e-007	-7.9385e-004	-0.0368	27.7552

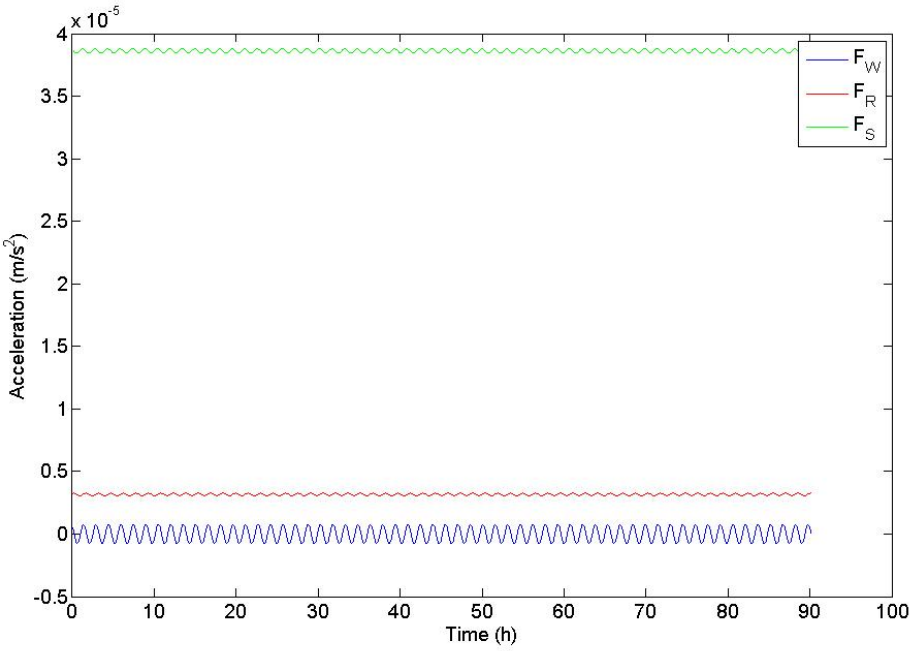

Figure 5.3: Thrust acceleration magnitude calculated by least-squares methods, 14 coefficients only

Figures 5.1 and 5.4 - 5.6 show the equivalent constant thrust arc implementation of this trajectory, using the two-step approach for the normal thrust direction, as described in Section 4.4, and the planar constant-magnitude approach for the radial and circumferential directions, as described in Section 4.5. The original ΔV for this trajectory was 12.5764 m/s; the ΔV for the trajectory with the equivalent step control, with Fourier series calculated up to order 100, was 12.5729 m/s.

The maximum total thrust acceleration for the step implementation was about 5.2e-5 m/s^2, which would require a thrust of about 20.8 mN for a 400 kg spacecraft. This is well within the thrust capability of existing electric propulsion systems, such as the NASA Solar Electric Propulsion Technology Application Readiness (NSTAR) electrostatic ion thruster used on the Deep Space 1 and Dawn missions.

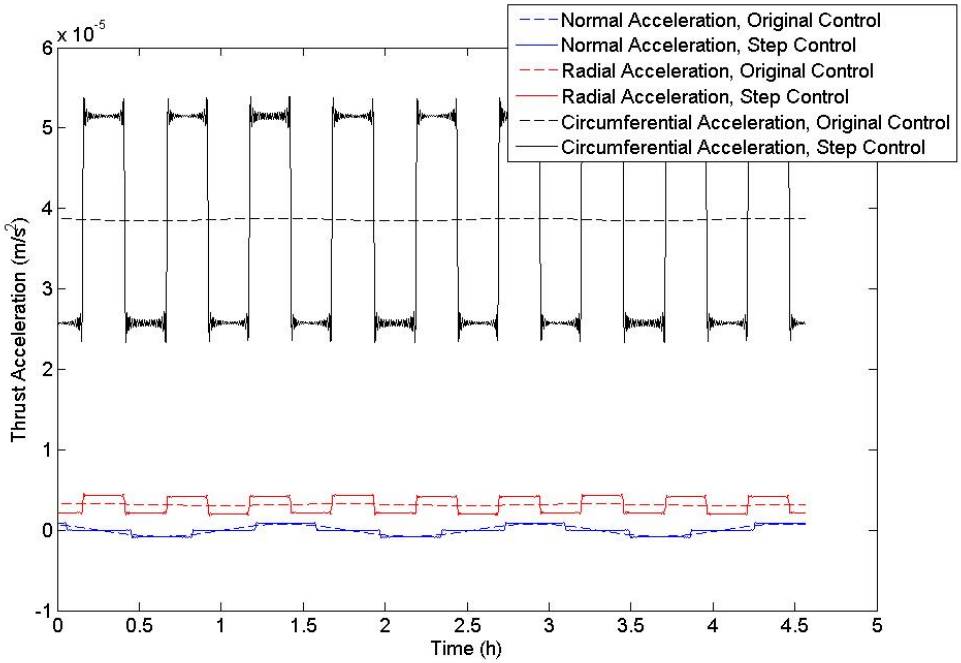

Figure 5.4: Equivalent step thrust acceleration for SSA example, plotted versus time. Only the first three orbits are plotted, so that the individual steps can be seen.

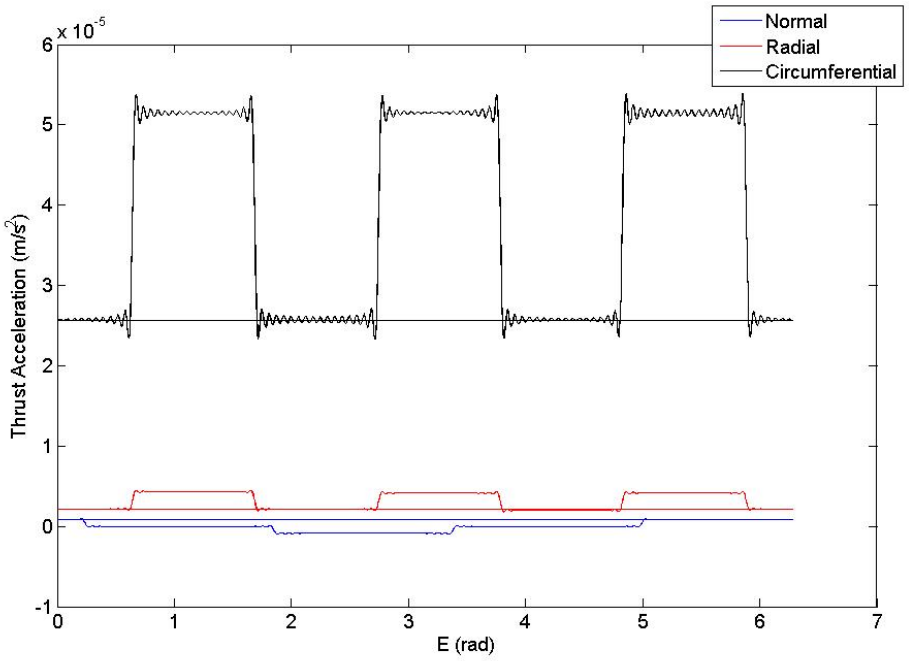

Figure 5.5: Equivalent step thrust acceleration for SSA example, plotted versus eccentric anomaly

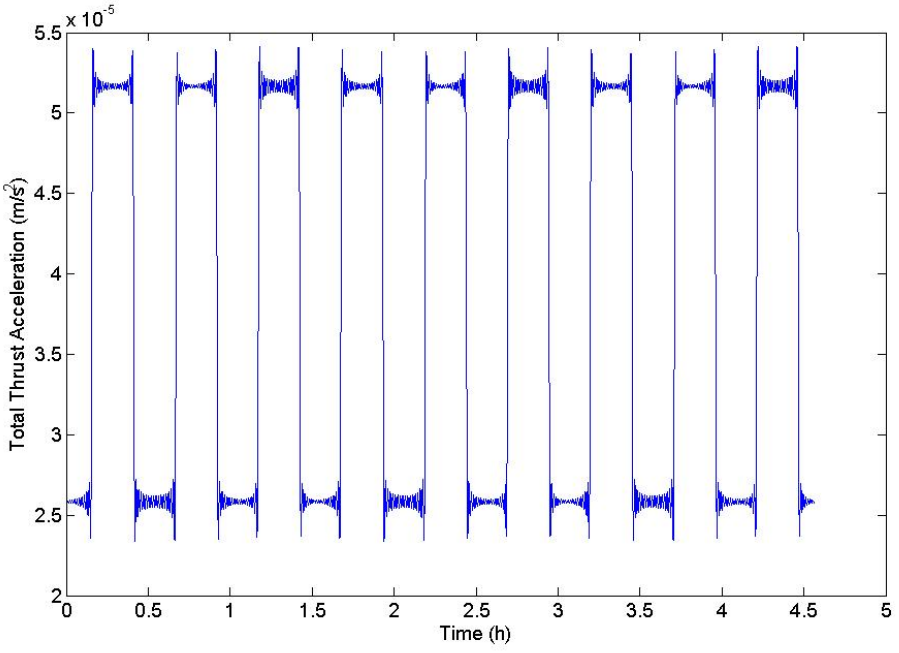

Figure 5.6: Total equivalent step thrust acceleration for SSA example, first three orbits

As low-thrust propulsion technology becomes increasingly popular, SSA for low-thrust spacecraft may become an area of increasing interest. Operators are more frequently using low-thrust propulsion to place satellites in orbit, creating more opportunities for collisions and radio frequency interference as these spacecraft travel slowly through altitude ranges. The averaged secular equations could provide analysts with a valuable tool for quickly and accurately assessing unknown low-thrust objects.

CHAPTER 6

Conclusions

A novel method was developed to efficiently evaluate the trajectory dynamics resulting from low-thrust propulsion. The thrust acceleration vector components were represented as Fourier series in eccentric anomaly, then Gauss's variational equations were averaged over one orbit and simplified by the orthogonality conditions. The resulting secular equations were a function of 14 of the thrust Fourier coefficients, regardless of the order of the original Fourier series. Thus, a general thrust profile was reduced to a set of only 14 parameters. Unlike many special-case solutions, this analytical method is not limited to constant-magnitude or constant-direction thrust.

The averaged variational equations in the 14 coefficients were shown to accurately determine spiral trajectories resulting from continuous or discontinuous low-thrust propulsion over many orbits, as compared with numerical integration of the full Newtonian equations of motion. Offsets of the averaged trajectory due to initial conditions were corrected by addition of an averaged periodic term. Singularities of the Gauss equations were addressed with alternate state variables and reference frames.

Orbital targeting problems were solved using the averaged equations. Two methods, a two-point boundary value method and a least-squares method, were developed for calculating averaged trajectories for single- or multi-orbit transfers through a finite number of orbital states. The two-point boundary value method generally results in closer agreement between the average trajectory and the target states, however it requires implementation of a new thrust vector for each interval. The calculated

trajectory may have discontinuities due to short-period offsets of the true trajectory from the averaged, so this method may not be suitable for applications that require precise targeting. The least-squares method generally calculates controls with lower dynamic fidelity, but provides a continuous trajectory.

A time-varying, low-thrust control can be transformed into various other types of controls by selection of Fourier coefficients that do not affect the fundamental dynamics. The transformed controls lead to spacecraft trajectories with equivalent average trajectory dynamics. These transformations can reduce the energy cost of an orbit transfer. They can also reduce the amount of throttling required by the low-thrust engine, by shaping the control into a step function. In some cases, the magnitude of the steps may be set constant, such that the control is simply a set of on/off times and thrust directions. Numerical examples have shown that transformation to equivalent step controls can increase or decrease the velocity increment required for a given orbit transfer.

6.1 Future Work

Future work in this area could focus on many interesting applications of the averaged secular equations, particularily in control optimization and shaping. The cost reduction method described in Section 4.1 is just one example of a method that uses the Fourier coefficient representation of a low-thrust control to reduce the energy cost of an orbit transfer. Other methods can likely be developed to further reduce costs.

Likewise, the methods described in Sections 4.3 - 4.5 show several ways that a control can be shaped into a form with improved implementation properties. These shaping methods can also increase or decrease the velocity increment of an orbit transfer. Methods for consistent, simultaneous cost reduction and control shaping have not yet been developed.

This dissertation describes two key developments that bracket the problem of

simultaneous control optimization and shaping. First, the output of any optimization routine can be defined by a set of key coefficients that accurately describe the average trajectory dynamics. Second, any general orbital targeting problem can be solved as a two-point boundary value problem and the solution can be transformed into a series of constant thrust arcs.

These two approaches might be combined into a complete method to optimize an average trajectory using a realistic control cost. First, a targeting boundary value problem could be solved as a constrained minimization problem, as described in Section 3.1. This results in a minimum fundamental average solution: the set of 14 control coefficient that meet the targeting objectives on average while minimizing the cost function. This solution can then be driven to a minimum implementable average solution – a control with constant thrust arcs that further minimizes the cost function – by selection of higher-order Fourier coefficients.

For any continuous thrust vehicle, the minimum-fuel optimal control usually consists of thrusting at the maximum allowable rate while appropriately orienting the thrust vector. The process of selecting the minimum-energy key coefficients and mapping them into the equivalent constant thrust arcs should then produce similar results. Future work could compare this method to known optimal low-thrust solutions for specific problems to evaulate this agreement.

APPENDIX

APPENDIX A

Fourier Series

According to Fourier's theorem, every piecewise-smooth function $f(\theta)$ with a finite number of jump discontinuities on the interval $(0, L)$ can be represented by a Fourier series,

$$f(\theta) \sim \sum_{k=0}^{\infty} \left[a_k \cos\left(\frac{2\pi k\theta}{L}\right) + b_k \sin\left(\frac{2\pi k\theta}{L}\right) \right]. \tag{A.1}$$

Where the periodic extension of the function is continuous, the Fourier series converges to the periodic extension of $f(\theta)$. Where jump discontinuities exist, the Fourier series converges to the average of the two limits [25]. The Fourier coefficients are given by

$$a_0 = \frac{1}{L} \int_0^L f(\theta)\, d\theta, \tag{A.2}$$

$$a_k = \frac{2}{L} \int_0^L f(\theta) \cos\left(\frac{k\pi\theta}{L}\right) d\theta, \tag{A.3}$$

$$b_k = \frac{2}{L} \int_0^L f(\theta) \sin\left(\frac{k\pi\theta}{L}\right) d\theta. \tag{A.4}$$

Nearly all physical systems meet the conditions of piecewise-smoothness and jump discontinuities. Thus, this representation can be applied to general low-thrust spacecraft controls that can be physically implemented.

BIBLIOGRAPHY

BIBLIOGRAPHY

[1] G. Forbes, "The trajectory of a powered rocket in space," *Journal of the British Interplanetary Society*, vol. 9, no. 2, pp. 75–79, 1950.

[2] T. Tsu, "Interplanetary travel by solar sail," *Journal of the American Rocket Society*, vol. 29, pp. 422–427, 1959.

[3] G. Pinkham, "Reference solution for low thrust trajectories," *Journal of the American Rocket Society*, vol. 32, no. 5, pp. 775–776, 1962.

[4] A. Petropoulos and J. Longuski, "Shape-based algorithm for automated design of low-thrust, gravity-assist trajectories," *Journal of Spacecraft and Rockets*, vol. 41, no. 5, pp. 787–796, 2004.

[5] H. Tsien, "Take-off from satellite orbit," *Journal of the American Rocket Society*, vol. 23, no. 4, pp. 233–236, 1953.

[6] R. Battin, *An Introduction to the Mathematics and Methods of Astrodynamics*. New York: AIAA Education Series, AIAA, 1959.

[7] J. Prussing and V. Coverstone-Carroll, "Constant radial thrust acceleration redux," *Journal of Guidance, Control, and Dynamics*, vol. 21, no. 3, pp. 516–518, 1998.

[8] N. Markopoulos, "Explicit, near-optimal guidance for power-limited escape from a circular orbit," in *AIAA Guidance, Navigation and Control Conference*, (San Diego, CA), July 1996.

[9] D. Lawden, "Optimal intermediate-thrust arcs in a gravitational field," *Astronautica Acta*, vol. 8, pp. 106–123, 1962.

[10] R. Bishop and D. Azimov, "Analytical space trajectories for extremal motion with low-thrust exhaust-modulated propulsion," *Journal of Spacecraft and Rockets*, vol. 38, no. 6, pp. 897–903, 2001.

[11] J. Marec and N. Vinh, "Optimal low-thrust, limited power transfers between arbitrary elliptical orbits," *Acta Astronautica*, vol. 4, pp. 511–540, 1977.

[12] C. Kluever and S. Oleson, "Direct approach for computing near-optimal low-thrust earth-orbit transfers," *Journal of Spacecraft and Rockets*, vol. 35, no. 4, pp. 897–903, 1998.

[13] C. Kluever, "Simple guidance scheme for low-thrust orbit transfers," *Journal of Guidance, Control, and Dynamics*, vol. 21, no. 6, pp. 1015–1017, 1998.

[14] C. Kluever, "Low-thrust orbit transfer guidance using an inverse dynamics approach," *Journal of Guidance, Control, and Dynamics*, vol. 18, no. 1, pp. 187–189, 1995.

[15] C. Kluever and D. O'Shaughnessy, "Trajectory-tracking guidance law for low-thrust earth-orbit transfers," *Journal of Guidance, Control, and Dynamics*, vol. 23, no. 4, pp. 754–756, 2000.

[16] M. Ilgen, "Low thrust otv guidance using lyapunov optimal feedback control techniques," in *AIAA/AAS Astrodynamics Specialist Conference*, (Victoria, BC, Canada), August 1993, AAS Paper 93-680.

[17] P. Gurfil, "Nonlinear feedback control of low-thrust orbital transfer in a central graviational field," *Acta Astronautica*, vol. 60, no. 8-9, pp. 631–648, 2007.

[18] A. Petropoulos, "Some analytic integrals of the averaged variational equations for a thrusting spacecraft," *IPN Progress Report 42-150*, pp. 1–29, 2002.

[19] T. Edelbaum, "Optimum power-limited orbit transfer in strong gravity fields," *AIAA Journal*, vol. 3, no. 5, pp. 921–925, 1965.

[20] Y. Gao, "Near-optimal very low-thrust earth-orbit transfers and guidance schemes," *Journal of Guidance, Control, and Dynamics*, vol. 30, no. 2, pp. 529–539, 2007.

[21] Y. Gao, "Low-thrust nonlinear guidance by tracking mean orbital elements," *Journal of Guidance, Control, and Dynamics*, vol. 31, no. 4, pp. 1103–1110, 2008.

[22] J. Danby, *Fundamentals of Celestial Mechanics*. Richmond, Virginia: 2nd ed. 5th printing, Willmann-Bell, 2003.

[23] W. Smart, *Celestial Mechanics*. London: Longmans, Green and Co., 1953.

[24] E. Gustafson and D. Scheeres, "Optimal timing of control-law updates for unstable systems with continuous control," *Journal of Guidance, Control, and Dynamics*, vol. 32, no. 3, pp. 878–887, 2009.

[25] R. Haberman, *Applied Partial Differential Equations with Fourier Series and Boundary Value Problems*. Upper Saddle River, New Jersey: 4th ed., Pearson Prentice Hall, 2004.